KINETIC ANALYSES OF POTENTIAL FORMATION IN PLASMA FLOW ALONG OPEN MAGNETIC FIELDS TO A WALL

KUNIHIRO SATO

Abstract

The problem of the potential formation in a quasistationary plasma flowing along open magnetic fields to a wall is treated using a kinetic description for the motion of particles. Influences of spatial variation of magnetic field strength, ionization of neutral gas, existence of energetic electrons, and secondary electron emission on potential formation are investigated theoretically. Universal properties of the quasistationary plasma flow are demonstrated.

In chapter 1, historical survey of theoretical works related to this thesis, and the purpose and scope of this work are described.

In chapter 2, the plasma-sheath equation for a collisionless plasma generated in a divergent open magnetic field is formulated. Outside the sheath, an analytic solution of this equation is obtained. The ion distribution function, the wall potential, and the energy and particle flux are explicitly calculated. The plasma-sheath equation is also solved numerically for various profiles of the magnetic field.

In chapter 3, effects of an expanding magnetic field on the plasma presheath are investigated numerically. It is shown that potential drop in the presheath is remarkably increased by applying an expanding magnetic field. An effect of a nonuniform magnetic field on the sheath formation is also discussed.

In chapter 4, the electrostatic potential in a collisionless plasma flowing out through the magnetic throat is analyzed under the condition of no particle source in a plasma. A

monotonically falling potential is found to build up due to nonuniformity of the magnetic field only if the generalized Bohm criterion is marginally satisfied at the magnetic throat. A potential profile is strongly dependent upon the particle density of electrons trapped in the open region.

In chapter 5, development of the steady-state potential in a two-electron-temperature plasma in contact with the wall is investigated in order to clarify contribution of energetic electrons to the sheath and presheath formation. The double layer structure is found to be set up in the plasma due to self-consistent separation of two electron species.

In chapter 6, the electrostatic sheath and the heat flow of a two-electron-temperature plasma in the presence of secondary electron emission are investigated. It is shown that the space-charge effect of hot electrons affects to suppress secondary electron emission, if the hot- to cold-electron temperature ratio is of the order of 10.

In chapter 7, the main results of this thesis are summarized. The problems left in this thesis are also mentioned.

Acknowledgement

I would like to acknowledge Professor Ryohei Itatani for his continuing guidance and encouragement from the beginning of my research on plasma physics and controlled nuclear fusion research at Department of Electronics, Faculty of Engineering, Kyoto University.

I wish to express my gratitude to Professor Hiromu Momota of National Institute for Fusion Science (NIFS) who has draw my attention to the problem of plasma flow in open magnetic fields and has helped me with valuable advice and useful suggestions.

I am indebted to Professor Fujio Miyawaki for his helpful supports and continuous encouragement since my appointment to Department of Electrical Engineering, Himeji Institute of Technology. It is a pleasure to thank to Professor Tadatsugu Hatori of NIFS, Professor Tadao Uyama and Professor Yasutomo Ohguchi for their constant encouragements.

Thanks are due to many plasma physicists with whom I have discussed this problem. Among them, I should like especially to thank Dr. T. Takizuka and Dr. M. Shimada of Japan Atomic Energy Research Institute at Naka, Professor N. Ohyabu of NIFS and Dr. S. Ishiguro of Tohoku University for their fruitful and pleasant discussions and criticisms. I was favored to have stimulating and valuable discussions with Dr. L. C. Steinhauer of STI Optronics Inc. on the investigation of Chapter 4.

I would like to extend my appreciation to Professor Noriyoshi Sato of Tohoku Uni-

versity and Professor Shuichi Takamura of Nagoya University for their interests in this work and important suggestions.

I am also grateful to Y. Ishikawa, H. Kuwagaki, Y. Ikeda and H. Katayama for their considerable assistance in computer programming and numerical calculations.

Contents

CHAPTER

Papers published in connection with the present thesis

CHAPTER

2 *Sheath and Presheath in a Collisionless Open-Field Plasma*
K. Sato, F. Miyawaki, and W. Fukui
Phys. Fluids B 1, 725 (1989).

3 *Effects of a Nonuniform Open Magnetic Field on the Plasma Presheath*
K. Sato and F. Miyawaki
Phys. Fluids B 3, 1963 (1991).

4 *Electrostatic Potential in a Collisionless Plasma Flow near the Magnetic Throat*
K. Sato, H. Katayama, and F. Miyawaki
J. Phys. Soc. Jpn. 61, 3034 (1992).

Potential Formation in a Plasma Flowing out through the Magnetic Throat
K. Sato, H. Katayama, and F. Miyawaki
submitted to Phys. Fluids B.

5 *Formation of Presheath and Current-Free Double Layer in a Two-Electron-Temperature Plasma*
K. Sato and F. Miyawaki
Phys. Fluids B 4, 1247 (1992).

6 *Sheath and Heat Flow of a Two-Electron-Temperature Plasma in the Presence of Electron Emission*
K. Sato and F. Miyawaki
J. Phys. Soc. Jpn. 61, 1453 (1992).

CHAPTER 1

Introduction

Formation of the electrostatic potential in a plasma flowing to a wall, one of the oldest problem in plasma physics, is important for nearly all plasma applications ; A plasma must be bounded by some confining structure, e.g., a limiter or the wall of the vacuum vessel. Since edge plasmas in fusion devices, for instance, are of growing interest, it is increasingly important. Nevertheless, because of its inherent difficulty it has only been solved in some special cases. The analysis is complicated not only by the effects involved at the boundary but also by strong inhomogeneity, which requires a kinetic treatment.

The problem of calculating the characteristics of a plasma flowing along a spatially varying magnetic field arises in a number of plasma configurations for fusion research. Potential along magnetic field lines in the region bounded by a wall becomes an issue when we approach the subject of the axial thermal transport of electrons in mirror machines [1,2] or the subject of the plasma flow in the open-field line region of field-reversed configurations [3]. Knowledge of the potential variation as well as the ion particle and energy fluxes to the wall is important in the theory of divertors and limiters

of closed devices like stellerators or tokamaks [4,5]. Moreover, knowledge of the potential variation along an expanding magnetic field is the key to knowing parameters of a plasma for design of a direct energy convertor and for evaluation of its efficiency [6,7]. In the presence of a divergent open magnetic field, ions are accelerated toward the wall and their density drops accordingly. Therefore, spatial variation of the magnetic field provides a potential formation mechanism. The expanding magnetic field will be available not only for enlargement of the potential drop along field lines but also for stabilization of the sheath potential.

On the other hand, a plasma with energetic electrons is produced due to strong fields of radio frequency waves in various laboratory devices, e.g., in scrape-off layer of tokamak [8,9] or in the open end region of the tandem mirror [10]. The appearance of energetic electrons is predicted to have dramatic effects on the potential formation in the plasma because the potential profile is closely associated with the electrons distribution. Hotter electrons also induce significant emission of secondary electrons, which can lead to marked reduction of the sheath potential and enhancement of the heat flow to walls. Thus, an admixture of the energetic electrons and the secondary electron emission from the wall are of interest in the study of potential formation and plasma transport.

In this thesis, we theoretically examine the behavior of a plasma flowing to a wall in the presence of a nonuniform magnetic field, an energetic electron population, or the secondary electron emission. The following sections present historical survey of theoretical works that describe the behavior of a plasma in contact with a wall, and describe the purpose and scope of this work.

1.1 SURVEY OF THE THEORY OF A PLASMA IN CONTACT WITH A WALL

This survey is restricted to theoretical investigations of potential formation in a plasma bounded by absorbing walls. Progress of the theoretical treatment of this problem has been made by a number of workers over many years. One of the earliest kinetic analysis of the potential in a bounded collisionless plasma was performed by Langmuir [11] and Tonks and Langmuir [12] in context of discharge plasmas about six decades ago. Their famous model is characterized by the free fall of ions originating from ionization of cold neutrals. Tonks and Langmuir introduced the subdivision in separate plasma and sheath regions with two scales of the Debye length λ_D and system length L, and solved the plasma equation in cylindrical and in plane geometry by series expansion. Over the years there have been a number of refinements to this early work [12-38].

The explicit formulation and clear interpretation of the sheath condition is due to Bohm [13]. Bohm suggested that there may be a small electric field in the plasma that accelerates ions up to and beyond the acoustic velocity before they enter the sheath. A decade later, Harrison and Thompson [14] more thoroughly solved the Tonks and Langmuir plasma equation in plane geometry and derived a generalized kinetic formulation of Bohm's sheath criterion valid under rather general conditions [15,16,17]. The validity of the generalized Bohm criterion for the case of low velocity ions located at the plasma-sheath boundary was subsequently discussed by Hall [18,19].

Caruso and Cavaliere [20] reinvestigated the plane problem with emphasis on a sys-

tematic two-scale formalism. Unfortunately, the separation of length scales makes matching one solution to the other impossible. The plasma-sheath equation was then solved numerically by Parker [21] for radial variations of the potential in a plasma column and Self [22] for potential variations along the axis of a plasma column with finite λ_D/L avoiding the subdivision in plasma and sheath regions. Self also obtained numerical solutions to the asymptotic problem $\lambda_D/L \to 0$ in various geometries [23]. Woods [24] and Kino and Shaw [25] showed that a simple fluid approach is suitable to describe basic features of the system with reasonable agreement. This provides a basis for numerous subsequent investigations accounting for various additional effects.

The first model to include warm ions in the quasineutral plasma region is due to Hu and Ziering [26], who assume that the distribution of ions incident at the plasma-sheath boundary is an accelerated cutoff Maxwellian. Emmert *et al.* [27] extended the model of Hu and Ziering, allowing for a general ion distribution function. The ion source distribution function is chosen such that the ion distribution is Maxwellian in the absence of any electric fields. They solve the resulting integrodifferential plasma-sheath equation numerically for small but finite values of λ_D/L. An analytic solution of the quasineutral integral plasma equation is also provided, which compared well the numerical solutions for small λ_D/L in the plasma region.

Bissell and Johnson [28] have developed an analytic model of the plasma region based upon a Maxwellian ion source function. This choice of source function, for a constant potential, leads to an ion distribution function that is singular at zero velocity. The generalized Bohm criterion is used as the boundary condition at the plasma-sheath

boundary. In a later paper, Bissell [29] showed that the model of Emmert *et al.* satisfies the generalized Bohm criterion at the boundary. Scheuer and Emmert [30] analytically solved for the quasineutral potential profile with a Maxwellian ion source function without applying the generalized Bohm criterion as a boundary condition. The solutions are shown to obey this criterion within numerical error. Bissell *et al.* [31] presented a detailed discussion of the source models and a comparison with fluid theories, and Scheuer and Emmert [32] also showed applicability of the fluid equation to the presheath for collisionless plasmas with a source of warm ions.

Riemann [33,34,35] and Berg *et al.* [36] discussed the basic features of the plasma-sheath transition and their relation to the Bohm criterion using a zero-Debye-length model. It is shown that the generalized Bohm criterion is marginally satisfied if the electric field is singular at the sheath edge, as it is in the models of Bissell and Johnson, and Scheuer and Emmert. Riemann also points out that the field singularity at the boundary is a direct consequence of the source region. Schwager and Birdsall [37] and Procassini *et al.* [38] used a fully kinetic particle-in-cell model to self-consistently determine the steady-state potential profiles in a collisionless bounded plasma. The results of the potential drops obtained from the simulations are compared well to those from the theories. In these investigations the ion kinetics is governed by ionization of neutrals.

A collision dominated plasma is usually described in terms of diffusion and mobility. The effects of charge exchange collisions or Coulomb collisions on the presheath have been treated by many workers [39-50]. Persson [39] and Self and Ewald [40] has treated the problem of a weakly ionized plasma, in which the dominant process is charge exchange

collisions. They use fluid equations to describe the ion motion and obtain solutions for the density and velocity of the ions as a function of position. Persson is the first to recognize the universal role of ion inertia for the presheath mechanism. A kinetic approach was used by Chekmarev [41], who take into account ion-neutral collisions by using Hamel's collision model. The first self-consistent kinetic analysis of a collisional presheath was presented by Riemann [42]. For a charge exchange model with cold neutrals based on the assumption of constant mean free path , Riemann was able to give the analytic solution of the plasma sheath transition including the ion distribution function and the self-consistent potential variation. Biehler *et al.* [45] extended the analysis to a charge exchange model with hot neutrals on the assumption of constant collision frequency. Scheuer and Emmert [46] treated ion collisions by using the BGK collision operator, and Koch and Hitchon [47] numerically investigated the effects of charge exchange collisions using more realistic collision model. These works showed that as the number of charge exchange collisions increases, the presheath potential drop also increases due to the role of ion inertia.

Particle simulation of transport in a bounded Coulomb collisional plasma was carried out by Takizuka *et al.* [48]. A particle-in-cell code has been coupled to a Monte Carlo binary particle model of Coulomb collisions : This code provides a fully kinetic self-consistent description of transport and potential formation in one spatial dimension and two velocity components. The dependence of plasma transport on Coulomb collisionality is investigated by varying collision frequency, and the limitations of the fluid description of collisional plasma transport are discussed. Several years later, Procassini

and Birdsall [49] reinvestigated transport in a bounded Coulomb collisional plasma using a simulation code based upon the same methodology, but increasing the number of particles per grid cell. Procassini and Birdsall [50] also combined particle-in-cell methods with charged/neutral interactions to calculate plasma transport through a high recycling divertor scrape-off layer in a tokamak.

In the models mentioned above, the plasma is either unmagnetized or the magnetic field is uniform and normal to the wall. The Lorenzt force in an oblique magnetic field or in a spatially varying magnetic field provides a mechanism of the presheath formation [51-59,64-66]. To evaluate transport to limiters or divertor plates of tokamaks, Chodura [51,52,53] accounted for field lines intersecting the wall at small angle, distinguishing a plasma presheath and a magnetic presheath. Beyond the Bohm criterion at the sheath boundary Chodura postulates a second condition of supersonic flow along magnetic field lines at the entrance of the magnetic presheath. DeWald and Bailey [54] used a particle-in-cell method for modeling a boundary plasma in which the magnetic field intersects the wall at an oblique angle.

Plasma flow along a nonuniform magnetic field to a wall remained unsolved until recently. Sato *et al.* [55] formulated the plasma-sheath equation for a collisionless plasma with a finite-temperature particle source in an expanding magnetic field. They analytically solve the plasma equation for a model magnetic field and explicitly express the potential profile, the potential at the sheath edge, and the wall potential as well as the particle and energy fluxes. Hussein and Emmert [56] numerically simulated the same problem solved by Sato *et al.* for a wider range of mirror ratios and compared their

simulation results with the analytical solutions. Hussein and Emmert also investigated the dependence of the presheath potential on the spatial distribution both of the particle source and of the magnetic field strength. In a later paper, Sato and Miyawaki [57] systematically investigated effects of an expanding magnetic field on the sheath and presheath formation by numerically solving the plasma equation. Sato and Miyawaki also check validity of their previous analysis [55] and simulation results obtained by Hussein and Emmert [56].

Hussein and Emmert [58] developed a kinetic code for simulation of plasma flow in the edge region of stellarators, considering divergent magnetic field lines and neutral gas recycling at the neutralizer plate. Hitchon *et al.* [59] numerically treated a stellarator divertor as a collisional presheath under the influence of a magnetic field, introducing a simplified model with a BGK collision term and the averaged magnetic moment.

Potential control along spatially varying magnetic flux tubes has been a main subject of mirror confinement. Although there have been several models to calculate the axial potential profile [60-63], the region considered in almost all works was restricted to the confinement region. Rognlien and Brengle [64] investigated the characteristics of a plasma flowing through a magnetic mirror, using the fluid code that solves four time-dependent moment equations. Rognlien and Brengle found the sonic transition of the plasma flow velocity at the mirror throat. Recently, Sato *et al.* [65,66] kinetically treated the problem of the potential formation in a collisionless quasistationary plasma flowing through the magnetic throat to a wall. Necessary conditions for the formation of stationary potential are derived on the assumption of no particle source in a plasma.

Sato *et al.* [66] also discuss possibility of potential control in the open region by the combination of an expanding magnetic field and the ECRH heating, illustrating numerical solutions to Poisson's equation.

Each of the preceding models assumes that the electron consists of only one component. Formation of double layer in a multi-component plasma, which is a physically interesting subject, has been studied extensively during the last two decades (see the reviews [67,68,69] and the references therein). The expansion of a two-electron-population plasma into vacuum has also been examined in connection with the expanding corona of a laser-produced plasma both experimentally and theoretically ; The development of a rarefaction shock in a plasma, which has a double layer structure, has been verified by a number of theoretical analyses [70-73]. The number of theoretical works on a plasma flow with different components of negative particles, however, is limited [15,73-78].

Boyd and Thompson [15] presented a modified form of the Bohm criterion in a plasma with negative ions. Itatani [74] discussed complex behaviors of the sheath of a plasma with negative ions, calculating structure of the sheath potential. The possibility of bifurcation of the potential at the plasma-sheath boundary is pointed out as one of the seasons of complexity of reactive plasmas. Takamura [75] analyzed the sheath potential and its structure for a plasma with an energetic electron population. The fluid equations are solved for a three component plasma by Schott [76] to describe the effect of energetic primary electrons on the whole boundary layer including the sheath region. Braithwaite and Allen [77] discussed the condition for the sheath formation in a plasma with negative ions for the special case of a spherical probe collecting cold ions. Recently, Sato and

Miyawaki [78] investigated development of the steady-state potential owing to ionization of neutral gas in a two-electron-temperature plasma using the Vlasov-Poisson equation. A stable stationary potential structure satisfying the Vlasov-Poisson equation is obtained over the whole range of plasma parameters. The current-free double layer is found to build up in a plasma both due to self-consistent separation of two electron species and due to ionization of cold neutrals.

One of practically important subjects to understand plasma-wall interactions in fusion research is the influence of secondary electron emission due to particle bombardment at the wall [79,82-85]. Electron injection from an emissive plane has also remarkable effects on potential development and plasma transport [80,81]. The space-charge effect of secondary electron was first discussed by Langmuir [11], and the effect of secondary electron emission on heat transport through the sheath was first described by Hobbs and Wesson [79]. Hobbs and Wesson show that a double sheath structure is formed in front of the wall under strong secondary electron emission so as to limit the coefficient of electron emission to a value smaller than unity. The situation for a hot electron-emitting boundary has been investigated by Shcherbinin [80] and Prewett and Allen [81].

Harbour and Harrison [82,83] analytically assessed the effects of secondary electron emission upon the plasma transport and upon the potential of the sheath at divertor target of a tokamak fusion reactor. Sizonenko [84] found the solution to the sheath equation corresponding to a negative charged sheath under strong secondary electron emission. The rate of plasma electron cooling due to contact with the wall was calculated. Franklin and Han [85] examined the beam-plasma instability due to secondary electron

emission using particle-in-cell simulations.

Recently, Ishiguro and Sato [86] investigated potential formation due to contact between an emissive plane electrode and collisionless plasma by using a one-dimensional particle-in-cell model. The structure and potential drop in the sheath are shown for a wide range of parameters of an injected electron beam. Sato and Miyawaki [87] investigated the heat flow of a two-electron-temperature plasma in the presence of electron emission. The hotter electron is found to form the negative space-charge layer, provided a hot- to cold-electron temperature ratio is larger than 10 ; This layer has the effect exhibiting secondary electron emission.

1.2 PURPOSE AND SCOPE OF THE PRESENT WORK

As mentioned in the historical survey, one important aspect of a plasma flowing to a wall that was not included in analyses published before the present series of works is spatial variation of the magnetic field : nonuniformity of the magnetic field provides the presheath mechanism through divergence of particle flux and conversion of kinetic energy perpendicular to field lines into parallel kinetic energy. Another aspect is existence of energetic electrons which has dramatic effects on the potential formation through self-consistent separation of two electron species and through induction of secondary electron emission. In the open region of practical confinement systems for fusion research, one needs to consider these aspects in order to describe the behavior of a plasma flowing to

a wall.

The present series of works have started with the purpose to verify characteristics of the potential formed in open field plasmas related to the controlled thermonuclear research. Influences of an expanding magnetic field, existence of energetic electrons, and/or secondary electron emission on the plasma flow are investigated on the base of the kinetic theory.

In chapter 2 and 3, sheath and presheath of a collisionless plasma originating in an expanding magnetic field are investigated by using both analytic and numerical approaches. In chapter 2, the integrodifferential plasma-sheath equation for a plasma with arbitrary ion temperature is formulated. Outside the sheath, this equation is solved analytically. In addition, the wall potential, energy and particle fluxes, and the ion distribution function are expressed explicitly. The condition for sheath formation is checked by applying the generalized Bohm criterion to the analytic solution. The plasma-sheath equation is also solved numerically for various profiles of the magnetic field.

In chapter 3, the dependence of the presheath potential profile on spatial variation of the magnetic field and the particle source is investigated by solving the plasma equation numerically. Numerical results are compared with the analytical solution obtained in chapter 2 in order to demonstrate justice of the analysis ; Accuracy of the simulation code developed by Hussein and Emmert [56] is also checked by comparing the numerical results with the simulation ones. Results for various spatial profiles both of the magnetic field strength and of the particle source are shown to discuss possibility of potential control by applying an expanding magnetic field. An effect of the nonuniform magnetic

field on the sheath formation is also discussed by using a calculated ion distribution function.

In chapter 4, the problem of quasistationary plasma flow through the magnetic throat to a wall is treated. Necessary conditions for formation of a monotonically falling static potential are derived under the assumption of no particle source in the plasma. Poisson's equation for model distribution functions is solved numerically to examine the potential formation due to nonuniformity of the magnetic field. The dependence of the potential profile on the trapped-electron distribution function is also investigated.

In chapter 5 and 6, characteristics of the electrostatic potential in a plasma with energetic electrons are described. In chapter 5, development of the static potential in a two-electron-temperature plasma is analyzed by a kinetic treatment. The potential structure is clarified, and the potential drop in a plasma is also evaluated. The characteristics of the current-free double layer analyzed in the present analysis are compared with those of the double layer experimentally observed by Hairapetian and Stenzel [88].

In chapter 6, the sheath equation of heat flow of a two-electron-temperature plasma in the presence of electron emission are solved in order to demonstrate the effects of electrons emitted from the wall. Enhancement of the heat flow due to the electron emission are discussed by comparing results under conditions of space-charge limitation with results in the absence of electron emission. In addition, the space-charge effect of hotter electrons to supress the secondary electron emission is described.

Finally, the concluding remarks and several subjects left in future are described in chapter 7.

REFERENCES

[1] L. S. Hall, Nucl. Fusion **17**, 681 (1977).

[2] G. D. Porter, Nucl. Fusion **22**, 1279 (1982).

[3] L. C. Steinhauer, Phys. Fluids **29**, 3379 (1986).

[4] P. C. Stangeby, in *Physics of Plasma-Wall Interaction in Controlled Fusion*, eds. D. E. Post and R. Behrisch (Plenum Press, New York, 1986) p. 41.

[5] P. C. Stangeby and G. M. McCracken, Nucl. Fusion **30**, 1225 (1990).

[6] R. W. Moir and W. L. Barr, Nucl. Fusion **13**, 35 (1973).

[7] H. Momota, A. Ishida, Y. Kohzaki, G. H. Miley, S. Ohi, M. Ohnishi, K. Yoshikawa, K. Sato, L. C. Steinhauer, Y. Tomita, and M. Tuszewski, Fusion Technol. **21**, 2307 (1992).

[8] Lipschultz, B. LaBombard, H. L. Manning, J. L. Terry, S. Knowlton, E. S. Marmar, M. Porkolab, J. Rice, Y. Takase, S. Texter, and A. Wan, Nucl. Fusion **26**, 1463 (1986).

[9] S. Takamura, A. Sato, Y. Shen, and T. Okuda, J. Nucl. Mater. **149**, 212 (1987).

[10] K. Kurihara, T. Saito, Y. Kiwamoto, and S. Miyoshi, J. Phys. Soc. Jpn. **58**, 3453 (1989).

[11] I. Langmuir, Phys. Rev. **33**, 954 (1929).

[12] L. Tonks and I. Langmuir, Phys. Rev. **34**, 876 (1929).

[13] D. Bohm , in *The Characteristics of Electrical Discharges in Magnetic Fields*, eds. A. Guthrie and R. K. Wakerling (McGraw-Hill, New York, 1949) p.77.

[14] E. R. Harrison and W. B. Thompson, Proc. Phys. Soc. London **74**, 145 (1959).

[15] R. L. F. Boyd and J. B. Thompson, Proc. R. Soc. A **252**, 102 (1959).

[16] B. Bertotti and A. Cavaliere, Nuovo Cimento **35**, 1244 (1965).

[17] J. E. Allen, J. Phys. D : Appl. Phys. **9**, 2331 (1976).

[18] L. S. Hall, Phys. Fluids **4**, 388 (1961).

[19] L. S. Hall, Proc. Phys. Soc. **80**, 3309 (1962).

[20] A. Caruso and A. Cavaliere, Nuovo Cimento **26**, 1389 (1962).

[21] J. V. Parker, Phys. Fluids **6**, 1657 (1963).

[22] S. A. Self, Phys. Fluids **6**, 1762 (1963).

[23] S. A. Self, J. Appl. Phys. **36**, 456 (1965).

[24] L. C. Woods, J. Fluid Mech. **23**, 315 (1965).

[25] G. Kino and E. W. Shaw, Phys. Fluids **9**, 587 (1966).

[26] P. N. Hu and S. Ziering, Phys. Fluids **9**, 2168 (1966).

[27] G. A. Emmert, R. M. Wieland, A. T. Mense, and J. N. Davidson, Phys. Fluids **23**, 803 (1980).

[28] R. C. Bissell and P. C. Johnson, Phys. Fluids **30**, 779 (1987).

[29] R. C. Bissell, Phys. Fluids **30**, 2264 (1987).

[30] J. T. Scheuer and G. A. Emmert, Phys. Fluids **31**, 3645 (1988).

[31] R. C. Bissell, P. C. Johnson, and P. C. Stangeby, Phys. Fluids B **1**, 1133 (1989).

[32] J. T. Scheuer and G. A. Emmert, Phys. Fluids B **2**, 445 (1990).

[33] K.-U. Riemann, J. Phys. D : Appl. Phys. **24**, 493 (1991).

[34] K.-U. Riemann, Phys. Fluids B **3**, 3331 (1991).

[35] K.-U. Riemann, Phys. Fluids B **1**, 961 (1989).

[36] H.-P. van den Berg, K.-U. Riemann, and G. Ecker, Phys. Fluids B **3**, 838 (1991).

[37] L. A. Schwager and C. K. Birdsall, Phys. Fluids B **2**, 1057 (1990).

[38] R. J. Procassini, C. K. Birdsall, and E. C. Morse, Phys. Fluids B **2**, 3191 (1990).

[39] K. B. Persson, Phys. Fluids **5**, 1625 (1962).

[40] S. A. Self and H N Ewald, Phys. Fluids **9**, 2486 (1966).

[41] I. B. Chekmarev, Sov. Phys.-Tech. Phys. **17**, 207 (1972).

[42] K.-U. Riemann, Phys. Fluids **24**, 2163 (1981).

[43] I. B. Chekmarev, E. M. Skylyaroba, and E. N. Kolesnikova, Beitr. Plasmaphys. **23**, 411 (1983).

[44] G. L. Main, Phys. Fluids **30**, 1800 (1987).

[45] S. Biehler, G. Ecker, and K-U Riemann, Phys. Fluids **31**, 1999 (1988).

[46] J. T. Scheuer and G. A. Emmert, Phys. Fluids **31**, 1748 (1988).

[47] D. J. Koch and W. N. Hitchon, Phys. Fluids B **1**, 2239 (1989).

[48] T. Takizuka, K. Tani, M. Azumi, and K. Shimizu, J. Nucl. Mater. **128 & 129**, 104 (1984).

[49] R. J. Procassini and C. K. Birdsall, Phys. Fluids B **3**, 1876 (1991).

[50] R. J. Procassini, C. K. Birdsall, and B. I. Cohen, Nucl. Fusion **30**, 2329 (1990).

[51] R. Chodura, Phys. Fluids **25**, 1628 (1982).

[52] R. Chodura, in *Physics of Plasma-Wall Interaction in Controlled Fusion*, eds. D. E. Post and R. Behrisch (Plenum Press, New York, 1986) p. 99.

[53] R. Chodura, Contr. Plasma Phys. **28**, 303 (1988).

[54] A. B. DeWald and A. W. Bailey, Phys. Fluids **30**, 267 (1987).

[55] K. Sato, F. Miyawaki, and W. Fukui, Phys. Fluids B **1**, 725 (1989).

[56] M. A. Hussein and G. A. Emmert, Phys. Fluids B **2**, 218 (1990).

[57] K. Sato and F. Miyawaki, Phys. Fluids B **3**, 1963 (1991).

[58] M. A. Hussein and G. A. Emmert, Nucl. Fusion **29**, 1721 (1989).

[59] W. N. G. Hitchon, D. J. Kock, and W. D. D'haeseleer, Nucl. Fusion **29**, 1675 (1989).

[60] K. Sato, Nucl. Fusion **23**, 25 (1983).

[61] R. H. Cohen, Nucl. Fusion **21**, 209 (1981).

[62] R. H. Cohen, Phys. Fluids **26**, 2774 (1983).

[63] I. Katanuma, Y. Kiwamoto, K. Ishii, and S. Miyoshi, Phys. Fluids **29**, 4138 (1986).

[64] T. D. Rognlien and T. A. Brengle, Phys. Fluids **24**, 871 (1981).

[65] K. Sato, H. Katayama, and F. Miyawaki, J. Phys. Soc. Jpn. **61**, 3034 (1992).

[66] K. Sato, H. Katayama, and F. Miyawaki, submitted to Phys. Fluids B.

[67] J. E. Allen, Plasma Phys. Controlled Fusion **27**, 1343 (1985).

[68] M. A. Raadu and J. J. Rasmussen, Astrophys. Space Sci. **144**, 43 (1988).

[69] M. A. Raadu, Phys. Res. **178**, 25 (1989).

[70] B. Bezzerides, D. W. Forslund, and E. L. Lundman, Phys. Fluids **21**, 2180 (1978).

[71] L. M. Wickens, J. E. Allen, and P. T. Rumsby, Phys. Rev. Lett. **41**, 243 (1978).

[72] J. Denavit, Phys. Fluids **22**, 1384 (1979).

[73] M. A. True, J. R. Albritton, and E. A. Williams, Phys. Fluids B **24**, 1885 (1981).

[74] R. Itatani, *Proc. 11th Symp. on ISIAT* (Tokyo, 1987), p.189.

[75] S. Takamura, Phys. Lett. A **133**, 312 (1988).

[76] L. Schott, Phys. Fluids **30**, 1795 (1987).

[77] N. St. J. Braithwaite and J. E. Allen, J. Phys. D : Appl. Phys. **21**, 1733 (1988).

[78] K. Sato and F. Miyawaki, Phys. Fluids B **4**, 1247 (1992).

[79] G. D. Hobbs and J. A. Wesson, Plasma Phys. **9**, 85 (1967).

[80] P. P. Shcherbinin, Sov. Phys. Tech. Phys. **17**, 1941 (1973).

[81] P. D. Prewett and J. E. Allen, Proc. R. Soc. A **348**, 435 (1976).

[82] P. J. Harbour and F. A. Harrison, J. Nucl. Mater. **76 & 77**, 513 (1978).

[83] P. J. Harbour and F. A. Harrison , Nucl. Fusion **19**, 695 (1976).

[84] V. L. Sizonenko, Sov. Phys. Tech. Phys. **26**, 1345 (1981).

[85] R. N. Franklin and W. E. Han, Plasma Phys. Controlled Fusion **30**, 771 (1987).

[86] S. Ishiguro and N. Sato, J. Phys. Soc. Jpn. **60**, 2218 (1991).

[87] K. Sato and F. Miyawaki, J. Phys. Soc. Jpn., **61**, 1453 (1992).

[88] G. Hairapetian and R. L. Stenzel, Phys. Rev. Lett. **65**, 175 (1990).

CHAPTER 2

Potential Formation in a Collisionless Plasma Produced in an Open Magnetic Field

2.1 INTRODUCTION

The problem of the potential formation in an open-field plasma is important for research on magnetically confined plasmas because it determines characteristics of the boundary layer. Potential along field lines in an open magnetic field becomes an issue when we approach the subject of the axial thermal transport of electrons in mirror machines [1] or the subject of the plasma flow in the open-field line region of field-reversed configurations [2]. This problem is also of interest in connection with the interaction of the plasma with the divertor collector plate in closed systems [3,4].

The first kinetic analysis of the potential near a plasma boundary was given by Tonks and Langmuir in the context of discharge plasmas [5]. They formulated the plasma-sheath equation and within the limit of small Debye length they obtained a solution to the plasma equation in series form for various geometries. Over the years

there have been a number of refinements to their work [6-10]. An analytic solution to the plasma equation in plane geometry was presented by Harrison and Thompson. In the early analyses a collisionless plasma with a cold-ion source was assumed. Emmert *et al.* [9] improved the early works by considering a finite-temperature ion source and by introducing no approximation with respect to the Debye length. Recently, by solving the plasma equation for the case of a Maxwellian particle source, which differs from the particle source given by Emmert *et al.*, Bissell and Johnson [10] indicated that the choice of a source function should be a considerable influence on the results. These previous investigations, however, are restricted to the case of unmagnetized plasmas or to the case of plasmas magnetized by a uniform field.

In this chapter, we investigate formation of a presheath and a sheath along field lines in a nonuniform open magnetic field using both analytic and numerical approaches. We consider a collisionless plasma in an axisymmetric magnetic field that expands to walls with a monotonically decreasing axial profile. The expression by Emmert *et al.* for the ion source function and the Boltzmann law for the electrons are used to derive the plasma-sheath equation for the potential in the open magnetic field. Since the potential in the steady state is expected to have a monotonic profile, we can adopt a function of the potential instead of that of the axial coordinate to express the spatial variation of the magnetic field. This enables us to carry out an analysis along the lines of that performed by Emmert *et al.*. We present results calculated from the analytical solution to show the dependence of the potential on the magnetic field profile, and also derive explicit formulas for the wall potential, for energy and particle fluxes, and for the ion

distribution function by making use of the analytic solution. The generalized Bohm criterion is applied to the solution to make sure of the sheath formation [6,11-14]. It is shown that the solution of the plasma equation always satisfies this criterion when the magnetic field has a monotonically decreasing axial profile. We also discuss the generalized Bohm criterion in the case of a monotonically increasing magnetic field. The integrodifferential equation is solved numerically for various profiles of the magnetic field.

The content of this chapter is as follows. The integrodifferential form of the plasma-sheath equation for the potential in an open magnetic field is formulated in Sec. 2.2. The solution obtained from the quasineutral approximation is described and results calculated from the analytical solution are presented in Sec. 2.3. In Sec. 2.4 the condition for the sheath formation is discussed. The analytical solution is compared with the numerical solution of the plasma-sheath equation in Sec. 2.5. The conclusions are given in Sec. 2.6.

2.2 PLASMA-SHEATH EQUATION

We consider an axisymmetric magnetic field that is also symmetric about $x = 0$ and decreases monotonically for $x > 0$ as shown in Fig. 2.1. The walls at $x = \pm L$ are assumed to be perfectly absorbing and electrically floating. The potential $\phi(x)$ in the steady state is expected to drop monotonically in the axial direction for $x > 0$ and the value at $x = 0$, ϕ_0, is defined as zero. The subscript 0 denotes the value at $x = 0$

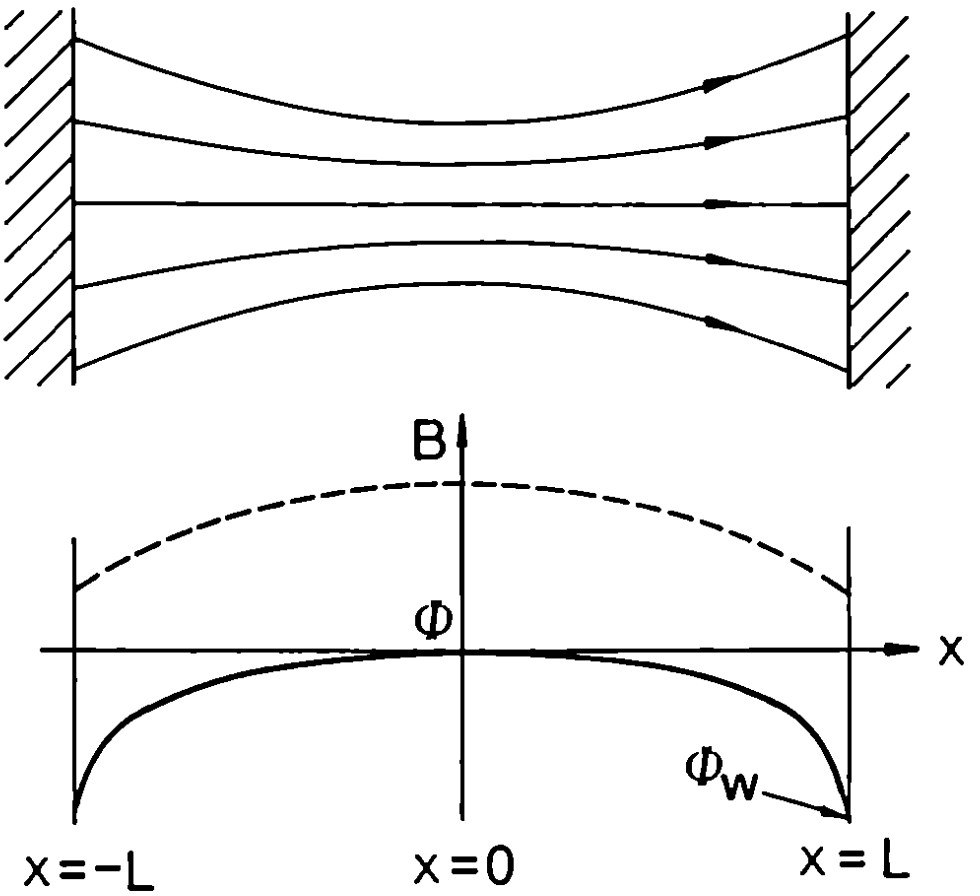

FIG. 2.1. The geometry of the model and axial profiles of the potential and of the magnetic field strength.

throughout this chapter. The ion's constant of motion is the energy

$$\varepsilon = \frac{1}{2}M(v_{\parallel}^2 + v_{\perp}^2) + q\phi(x) \ , \tag{2.1}$$

where M is the mass, q is the charge, and $v_{\perp}$ and $v_{\parallel}$ are the perpendicular and parallel components of the velocity. The magnetic moment,

$$\mu = \frac{1}{2}Mv_{\perp}^2/B(x) \ , \tag{2.2}$$

is taken as a constant of motion, like ε, where $B(x)$ is the magnetic field strength at the point x. Considering the plasma near the axis, we neglect radial dependence and also integrate out the gyromotion.

The kinetic equation in the phase space (x, ε, μ) is simply described by

$$\sigma v_{\parallel}(x, \varepsilon, \mu)\frac{\partial f(x, \varepsilon, \mu)}{\partial x} = S(x, \varepsilon, \mu) \ , \tag{2.3}$$

where

$$v_{\parallel}(x, \varepsilon, \mu) = \left\{2\left[\varepsilon - \mu B(x) - q\phi(x)\right]/M\right\}^{1/2} \ , \tag{2.4}$$

$\sigma(= \pm 1)$ denotes the direction of the ion motion, $f(x, \varepsilon, \mu, \sigma)$ is the ion distribution function, and $S(x, \varepsilon, \mu)$ is the distribution function of the ion source. Here, we assume symmetry about $x = 0$, that is, $S(x, \varepsilon, \mu) = S(-x, \varepsilon, \mu)$ and $\phi(x, \varepsilon, \mu) = \phi(-x, \varepsilon, \mu)$. The boundary conditions of the distribution function are $f(-L, \varepsilon, \mu, +1) = 0$ and $f(L, \varepsilon, \mu, -1) = 0$.

All ions originating in the magnetic field are accelerated toward the walls by the monotonically decreasing effective potential $\mu B(x)+q\phi(x)$. The $\varepsilon-\mu$ space is separated into two regions, the reflected region and the passing region. Any ion originating in the region such that $\varepsilon < \mu B_0$ cannot reach the center of the plasma. When $\sigma = -1$ and $x > 0$ or when $\sigma = 1$ and $x < 0$, ions in this region are reflected at the turning point, $x_t(\varepsilon,\mu)$, determined from

$$\varepsilon - \mu B(x_t) - q\phi(x_t) = 0 \,. \tag{2.5}$$

All ions originating in the region such that $\varepsilon > \mu B_0$ pass through the plasma along the field lines without a change in direction of the motion. Integrating Eq. (2.3) along the trajectory of a particle on the boundary conditions, we obtain the distribution function $f(x,\varepsilon,\mu,\sigma)$. The sum of $f(x,\varepsilon,\mu,+1)$ and $f(x,\varepsilon,\mu,-1)$ in each region of the $\varepsilon-\mu$ space can be written as

$$\sum_\sigma f(x,\varepsilon,\mu,\sigma) = 2\int_0^L dx' \frac{S(x',\varepsilon,\mu)}{v_\parallel(x',\varepsilon,\mu)} \,, \qquad \varepsilon > \mu B_0 \,, \tag{2.6a}$$

$$\sum_\sigma f(x,\varepsilon,\mu,\sigma) = 2\int_{x_t(\varepsilon,\mu)}^L dx' \frac{S(x',\varepsilon,\mu)}{v_\parallel(x',\varepsilon,\mu)} \,, \qquad \varepsilon < \mu B_0 \,, \tag{2.6b}$$

where x' is the point at which ions originate. It is seen that although $f(x,\varepsilon,\mu,+1)$ and $f(x,\varepsilon,\mu,-1)$ are dependent on the coordinate x, their sum becomes independent of x under the assumption of the symmetry of the system about $x = 0$.

The ion density $n_i(x)$ is obtained by integrating $f(x,\varepsilon,\mu,\sigma)$ over the $\varepsilon-\mu$ space by using the Jacobian, $\partial(v_\perp^2, v_\parallel)/\partial(\varepsilon,\mu) = 2B/(M^2 v_\parallel)$;

$$n_i(x) = \frac{2\pi B(x)}{M^2}\sum_\sigma \int d\varepsilon \int d\mu \frac{f(x,\varepsilon,\mu,\sigma)}{v_\parallel(x,\varepsilon,\mu)} \,. \tag{2.7}$$

Substituting Eqs. (2.6a) and (2.6b) into Eq. (2.7), we obtain

$$\begin{aligned} n_i(x) = \frac{4\pi B(x)}{M^2}\Bigg(& \int_0^\infty d\varepsilon \int_0^{\varepsilon/B_0} d\mu \frac{1}{v_\parallel(x,\varepsilon,\mu)} \int_0^L dx' \frac{S(x',\varepsilon,\mu)}{v_\parallel(x',\varepsilon,\mu)} \\ & + \int_{q\phi(x)}^0 d\varepsilon \int_0^{[\varepsilon-q\phi(x)]/B(x)} d\mu \frac{1}{v_\parallel(x,\varepsilon,\mu)} \int_{x_1(\varepsilon,\mu)}^L dx' \frac{S(x',\varepsilon,\mu)}{v_\parallel(x',\varepsilon,\mu)} \\ & + \int_0^\infty d\varepsilon \int_{\varepsilon/B_0}^{[\varepsilon-q\phi(x)]/B(x)} d\mu \frac{1}{v_\parallel(x,\varepsilon,\mu)} \int_{x_1(\varepsilon,\mu)}^L dx' \frac{S(x',\varepsilon,\mu)}{v_\parallel(x',\varepsilon,\mu)} \Bigg) \,. \end{aligned} \tag{2.8}$$

Separating the area of integration with respect to x' into two sections, $0 \le x' < x$ and $x \le x' \le L$, one can interchange the order of integration in Eq. (2.8) with the aid of Eqs. (2.1) and (2.2). The integration over one section has a form very similar to that over another section, and then the integration over the whole section can be written as

$$n_i(x) = \frac{4\pi B(x)}{M^2}\int_0^L dx' \int_{\varepsilon_s}^\infty d\varepsilon \int_0^{(\varepsilon-\varepsilon_s)/B_s} d\mu \frac{1}{v_\parallel(x,\varepsilon,\mu)} \frac{S(x',\varepsilon,\mu)}{v_\parallel(x',\varepsilon,\mu)} \,, \tag{2.9}$$

where $\varepsilon_s = q\phi(x')$ and $B_s = B(x')$ for $x' < x$, and $\varepsilon_s = q\phi(x)$ and $B_s = B(x)$ for $x' \ge x$.

To calculate the density, we must describe the ion source. In this work we use the same expression for the ion source chosen by Emmert *et al.* [9]:

$$S(x,\varepsilon,\mu) =< \sigma v > n_0 n_n h(x) \frac{M^2}{4\pi(kT_i)^2} v_{\parallel}(x,\varepsilon,\mu) \exp\left(\frac{-[\varepsilon - q\phi(x)]}{kT_i}\right) , \quad (2.10)$$

where $< \sigma v >$is the ionization rate coefficient, n_0 is the electron density at the midpoint, n_n is the neutral atom density, k is Boltzmann's constant, and T_i is the ion temperature. The factor $h(x)$ expresses the spatial variation of the ionization rate.

By substituting Eq. (2.10) into Eq. (2.9) and carrying out the integration over the $\varepsilon - \mu$ space, the ion density is given in the integral form

$$n_i(x) =< \sigma v > n_0 n_n \left(\frac{\pi M}{2kT_i}\right)^{1/2} \int_0^L dx' I(x,x') h(x') , \quad (2.11)$$

where

$$I(x,x') = \exp\left(\frac{q\phi(x') - q\phi(x)}{kT_i}\right) \mathrm{erfc}\left[\left(\frac{q\phi(x') - q\phi(x)}{kT_i}\right)^{1/2}\right]$$

$$- \left(\frac{B(x') - B(x)}{B(x')}\right)^{1/2} \exp\left(\frac{B(x')}{B(x') - B(x)} \frac{q\phi(x') - q\phi(x)}{kT_i}\right)$$

$$\times \mathrm{erfc}\left[\left(\frac{B(x')}{B(x') - B(x)} \frac{q\phi(x') - q\phi(x)}{kT_i}\right)^{1/2}\right] , \quad x' < x ,$$

$$I(x,x') = \exp\left(\frac{q\phi(x') - q\phi(x)}{kT_i}\right) , \quad x' > x ,$$

and $\mathrm{erfc}(x)$ is the complementary error function :

$$\mathrm{erfc}(x) = \int_0^x \exp(-t^2)dt \ .$$

This expression is the same form as the expression obtained by Emmert *et al.* except for the second term of $I(x, x')$ for $x' < x$ that comes from the spatial variation of the magnetic field. It should be noted that the second term of $I(x, x')$ is independent of the absolute value of the magnetic field strength, $B(x)$ and $B(x')$, but is dependent on the ratio $B(x)/B(x')$. The integrand $I(x, x')$ for $x > x'$ becomes independent of the magnetic field when the ion source is given by Eq. (2.10).

In order to have a steady-state solution, we must introduce processes that cause electrons to scatter in velocity space. To simplify the analysis, we use the Boltzmann law for electrons on the assumption that these processes are so strong that they cause the electrons to scatter during a period of time shorter than the transit time of ions,

$$n_e(x) = n_0 \exp\left(e\phi(x)/kT_e\right) \ , \tag{2.12}$$

where T_e is the electron temperature and $-e$ is the electron charge. If the processes are not sufficiently strong, the electron distribution function differs from the Maxwellian, especially near the loss boundary in velocity space, and it is affected by the variation of the magnetic field.

Substituting Eqs. (2.11) and (2.12) into Poisson's equation, we obtain the integrod-ifferential equation

$$\lambda_{D0}^2 \frac{e}{kT_e}\frac{d^2\phi}{dx^2} = \exp\left(\frac{e\phi(x)}{kT_e}\right) - \frac{q}{e} < \sigma v > n_n \left(\frac{\pi M}{2kT_i}\right)^{1/2} \int_0^L dx' I(x,x') h(x') \ , \tag{2.13}$$

where λ_{D0} is the Debye length at $x = 0$ described by $\lambda_{D0}^2 = \epsilon_0 kT_e/n_0 e^2$. Equation (2.13) is the plasma-sheath equation for the ion source given by Eq. (2.10), which determines the potential along field lines both in the presheath and the sheath regions.

2.3 ANALYTIC SOLUTION OF THE PLASMA EQUATION

In its complete form the plasma-sheath equation is too complicated to carry out the analysis, but it can, fortunately, be simplified in the plasma by dropping the second derivative term. The scale length for potential variation in the plasma is expected to be the same order of the plasma length L, whereas inside the sheath it is comparable with the Debye length. Then, as long as the plasma dimension is large compared with the Debye length, the solution obtained from Eq. (2.13) is approximated by the one obtained from the quasi-neutral approximation, $Zn_i = n_e$, which is called the plasma equation. The two solutions differ by the order of λ_{D0}^2/L^2 and the solution to Eq. (2.13) satisfies charge neutrality to the same order.

It is convenient to simplify the expressions by introducing the dimensionless variables

$$s = x/L \ , \quad Z = q/e \ , \quad \tau = T_e/T_i \ ,$$

$$\Psi = -e\phi/kT_e\ , \qquad R = B_0/B\ , \tag{2.14}$$

where the mirror ratio $R(s)$ is the ratio of the magnetic field strength at the midpoint to the local value at the normalized axial coordinate s. On the assumption of the monotonically varying potential, both the mirror ratio and the spatial variation of Ψ the particle source can be expressed by the function of Ψ because the coordinate s can be expressed by a single-valued function of Ψ. Making use of the dimensionless variables, we can write the plasma equation as

$$\exp(-\Psi) = Z < \sigma v > n_n L \left(\frac{\pi M}{2kT_i}\right)^{1/2} \int_0^1 ds' G(\Psi(s), \Psi(s'))h(\Psi(s'))\ , \tag{2.15}$$

where

$$G(\Psi, \Psi') = \exp[Z\tau(\Psi - \Psi')]\mathrm{erfc}[Z\tau(\Psi - \Psi')^{1/2}]$$
$$- \left(\frac{R(\Psi) - R(\Psi')}{R(\Psi)}\right)^{1/2} \exp\left(\frac{R(\Psi)}{R(\Psi) - R(\Psi')} Z\tau(\Psi - \Psi')\right)$$
$$\times \mathrm{erfc}\left[\left(\frac{R(\Psi)}{R(\Psi) - R(\Psi')} Z\tau(\Psi - \Psi')\right)^{1/2}\right]\ , \quad \Psi' < \Psi\ ,$$

$$G(\Psi, \Psi') = \exp[Z\tau(\Psi - \Psi')]\ , \qquad \Psi' \geq \Psi\ ,$$

and $\Psi' = \Psi(s')$. Equation (2.15) is not as simple to handle; however, we can obtain the approximate solution to this equation in the same manner as the analysis in Ref. [9]. Differentiating Eq. (2.14) with respect to Ψ and using the asymptotic expansion of the error function for $x \gg 1$ [15],

$$\sqrt{\pi}x\exp(x^2)\mathrm{erfc}(x) \sim 1 + \sum_{m=1}^{\infty}(-1)^m \frac{1\cdot 3\cdots(2m-1)}{(2x^2)^m}\ , \tag{2.16}$$

we obtain

$$\exp(-\Psi) = A\int_0^{\Psi} d\Psi' \frac{ds'}{d\Psi'}\frac{R(\Psi')h(\Psi')}{R(\Psi)(\Psi-\Psi')^{1/2}}\left\{1 - \frac{1}{Z\tau R(\Psi)}\left(\frac{R(\Psi)-R(\Psi')}{2(\Psi-\Psi')}\right.\right.$$

$$\left.\left. - \frac{dR(\Psi)}{d\Psi}\right) + O\left[\left(\frac{R(\Psi)-R(\Psi')}{Z\tau(\Psi-\Psi')R(\Psi)}\right)^2\right]\right\}\ , \tag{2.17}$$

where

$$A = <\sigma v> n_n L\frac{Z(Z\tau)^{1/2}}{1+Z\tau}\left(\frac{M}{2kT_i}\right)^{1/2}$$

The higher-order term in Eq. (2.17) is neglected when the ion temperature is low or when the logarithmic derivative of the mirror ratio is small. The integrand becomes infinitely large as Ψ' approaches Ψ, and then the approximation

$$1 - \frac{1}{Z\tau R(\Psi)}\left(\frac{R(\Psi)-R(\Psi')}{2(\Psi-\Psi')} - \frac{dR(\Psi)}{d\Psi}\right) \simeq 1 + \frac{dR(\Psi)/d\Psi}{2Z\tau R(\Psi)} \tag{2.18}$$

is valid when the mirror ratio varies smoothly. With the definition of the effective mirror ratio

$$R_e(\Psi) = \frac{R(\Psi)}{1 + (dR(\Psi)/d\Psi)/2Z\tau R(\Psi)}\ , \tag{2.19}$$

Eq. (2.17) can be written approximately by Abel's integral equation. The solution is [16]

$$AR(\Psi)h(\Psi)\frac{ds}{d\Psi} = \frac{1}{\pi}\frac{d}{d\Psi}\int_0^{\Psi} d\Psi' \frac{R_e(\Psi')\exp(-\Psi')}{(\Psi - \Psi')^{1/2}} \ . \tag{2.20}$$

The differentiation on the right-hand side can be carried out to give the result

$$\frac{ds}{d\Psi} = \frac{1}{\pi AR(\Psi)h(\Psi)}\left(\frac{R_{e0}}{\sqrt{\Psi}} + \int_0^{\Psi} d\Psi' \frac{dR_e(\Psi')/d\Psi' - R_e(\Psi')}{(\Psi - \Psi')^{1/2}}\exp(-\Psi')\right) \ . \tag{2.21}$$

Integration of Eq. (2.21) yields $s(\Psi)$ from which the shape of the potential is determined;

$$s(\Psi) = \int_0^{\Psi} d\Psi' \frac{ds'}{d\Psi'}\left(\int_0^{\Psi_1} d\Psi' \frac{ds'}{d\Psi'}\right)^{-1} \ , \tag{2.22}$$

where Ψ_1 is the potential at the plasma-sheath boundary.

Equation (2.21) is not yet the solution to the plasma equation, but is the solution to the approximated equation that is obtained from the plasma equation by differentiating with respect to Ψ. Hence, Eq. (2.22) can satisfy the plasma equation only if the potential Ψ_1,which corresponds to an integral constant, has the appropriate value. One can determine the value of Ψ_1 by substituting Eq. (2.21) into the plasma equation

$$\exp(-\Psi) = \pi^{1/2} A \frac{1 + Z\tau}{(Z\tau)^{1/2}} \int_0^{\Psi_1} d\Psi' \frac{ds'}{d\Psi'} G(\Psi, \Psi')h(\Psi') \ , \tag{2.23}$$

where $0 \leq \Psi \leq \Psi_1$. Equation (2.23) is satisfied approximately for $0 \leq \Psi \leq \Psi_1$ when Ψ_1 has the appropriate value because Eq. (2.21) is the solution to the approximated equation. Considering the characteristic of the integrand in Eq. (2.23) which rapidly decreases for $\Psi' > \Psi$, the choice of $\Psi = \Psi_1$ is most suitable to determine Ψ_1.

In general, the ion source in the sheath can be neglected because of a small thickness of the sheath and a remarkable decrease in the ionization rate which is dependent on the electron density. Hence, the requirement that the electron current and the ion current must be equal at the wall enables us to determine the wall potential Ψ_w by using the solution to the plasma equation. The ion current is evaluated by integrating Eq. (2.10) with respect to s and over the $\varepsilon - \mu$ space. The requirement described above is expressed by

$$\left(\frac{kT_e}{2\pi m}\right)^{1/2} n_0 \exp(\Psi_w) = \frac{1+Z\tau}{(Z\tau)^{1/2}} \left(\frac{2kT_i}{M}\right)^{1/2} A \int_0^{\Psi_1} d\Psi' \frac{ds'}{d\Psi'} \frac{R(\Psi')}{R_1} h(\Psi') \ , \tag{2.24}$$

where m is the electron mass and R_1 is the mirror ratio at the plasma-sheath boundary. From this equation, we obtain

$$\Psi_w = -\ln \left[\left(\frac{4\pi m}{ZM}\right)^{1/2} A \frac{1+Z\tau}{\tau} \int_0^{\Psi_1} d\Psi' \frac{ds'}{d\Psi'} \frac{R(\Psi')}{R_1} h(\Psi') \right] \ . \tag{2.25}$$

The factor $h(\Psi')$ in Eqs. (2.23) and (2.25) is canceled by that in the derivative $ds'/d\Psi'$. If the mirror ratio is expressed by a function of Ψ, the potentials Ψ_1 and Ψ_w are independent of the profile of $h(\Psi)$, but are dependent on the profile of $R(\Psi)$. It should be noted that,

in practice, the mirror ratio is a function of the axial coordinate s. Then, the potentials Ψ_i and Ψ_w also depend on the spatial variation of the particle source when the magnetic field is not uniform because the profile of $R(\Psi)$ is dependent on $h(\Psi)$ through the profile of $s(\Psi)$. This result differs from that of the earlier works [6,9]; the potentials Ψ_i and Ψ_w for an unmagnetized plasma are independent of the spatial variation of the particle source. Since the product of $h(\Psi')$ and $ds'/d\Psi'$ is also found in expressions for heat flux and the ion distribution function at the plasma-sheath boundary, which will be presented later for these qualities.

A description of $R(\Psi)$ is required to calculate Ψ_i and Ψ_w, and a specification of $h(\Psi)$ is also necessary to determine $s(\Psi)$. We now assume $R(\Psi)$ to be expressed in the simple form

$$R(\Psi) = \exp(\alpha\Psi) , \tag{2.26}$$

where α is a positive constant. When $\Psi(s)$ is monotonic with respect to s, $R(s)$ also becomes monotonic. The effective mirror ratio defined by Eq. (2.19) becomes

$$R_e(\Psi) = R(\Psi)/(1 + \alpha/2Z\tau) . \tag{2.27}$$

Considering the fact that the ionization rate dependents on the electron density, we adopt the expression for $h(\Psi)$ presented by Harrison and Thompson,

$$h(\Psi) = \exp(-\gamma\Psi) , \tag{2.28}$$

which allows the ion source to be proportional to the γ power of the electron density. Using the expression (2.26), integration in Eq. (2.21) can be carried out and $ds/d\Psi$ is obtained,

$$\frac{ds}{d\Psi} = \frac{\exp[(\gamma-\alpha)\Psi]}{\pi A(1+\alpha/2Z\tau)}\left(\frac{1}{\sqrt{\Psi}} + 2(\alpha-1)\exp[(\alpha-1)\Psi]E(\alpha-1,\Psi)\right) , \quad (2.29)$$

where the function $E(\beta, x)$ is defined by the Dawson function [12]

$$D(x) = \int_0^x \exp(t^2)dt$$

or by the error function as follows:

$$E(\beta,x) = \begin{cases} (1/\sqrt{\beta})D(\sqrt{-\beta x}) , & \beta < 0 , \\ (1/\sqrt{\beta})(\sqrt{\pi}/2)\mathrm{erf}(\beta x) , & \beta \geq 0 . \end{cases} \quad (2.30)$$

Integrating further after substitution of Eqs. (2.28) and (2.29) into Eqs. (2.22) and (2.25), we can obtain the expression for $s(\Psi)$ and Ψ_w by using the function $E(\beta, x)$.

Figure 2.2 shows the dependence of Ψ_1 and Ψ_w on the mirror ratio at $s = 1$ for the model field $R(\Psi)$ =exp($\alpha\Psi$). Through this chapter, this model field is used and a particle source of hydrogen plasma with $\gamma = 1$ and with τ=1, 10, or 100 is considered in calculating results. The potential Ψ_w increases very slowly, but Ψ_1 increases considerably as R_1 becomes larger. This tendency is obvious in the case of small τ: the value of Ψ_1 for τ=1 enlarges by about a factor of 3 when R_1 changes from 1 to 2. The normalized

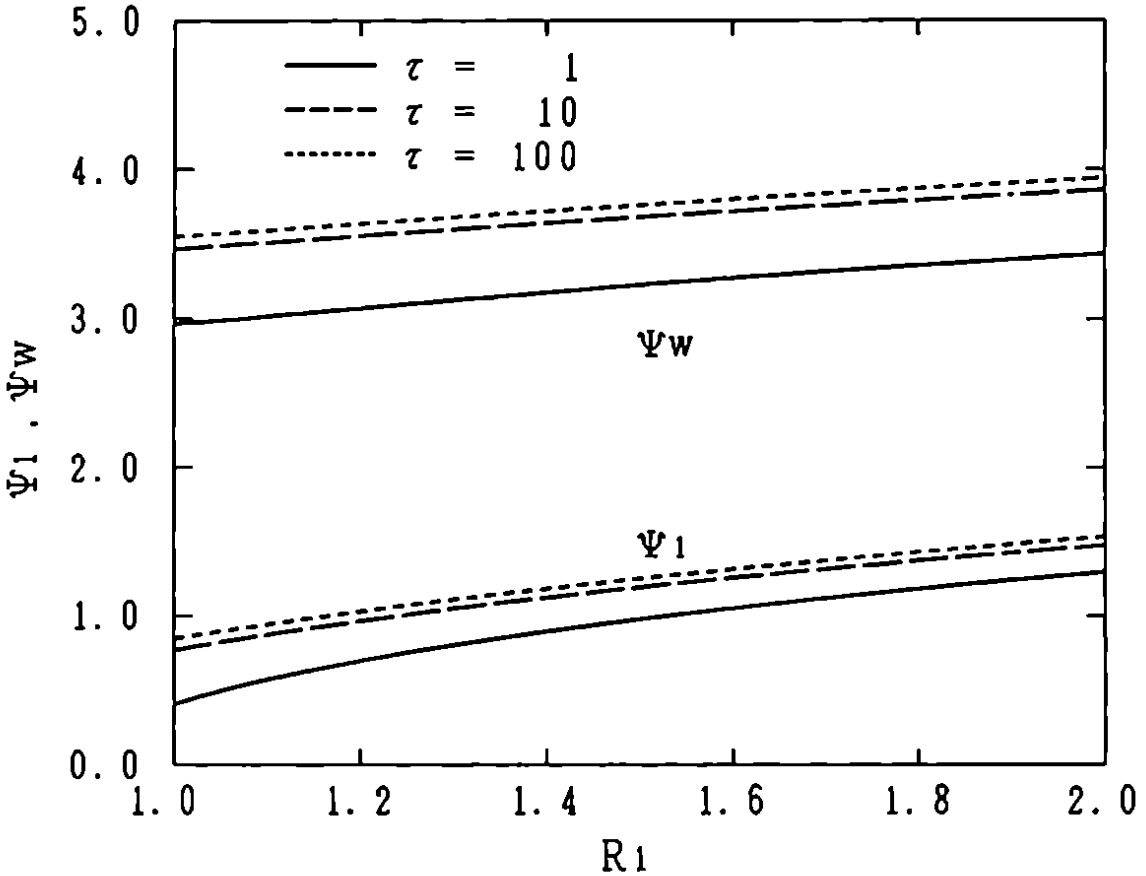

FIG. 2.2. The normalized potential at the plasma-sheath boundary Ψ_1 and the normalized wall potential Ψ_w as a function of the mirror ratio at the boundary, $R_1 \equiv B_0/B_1$, for the model field $R(\Psi)=\exp(\alpha\Psi)$. Hydrogen plasma with τ=1, 10, or 100 are considered.

potential profile and the profile of the mirror ratio for various value of α are shown in Fig. 2.3, and the plasma density profile is plotted in Fig. 2.4. It is seen that the potential gradient at $s=1$ has a finite value and the model field presents a realistic profile to the open magnetic field.

The accuracy of the analytic solution can be checked by calculating Eq. (2.15) numerically after substitution of Eq. (2.21). It is found that the analytic solution for various values of both τ and α satisfies the plasma equation with an accuracy up to about one-tenth of $[(dR/d\Psi)/Z\tau R]^2$, which indicates the validity of approximations introduced in Eq. (2.17).

Using the solution, we can calculate the ion distribution function explicitly. We now derive the distribution function at the plasma-sheath boundary with respect to the parallel velocity, $f_1(v_\parallel)$, which is obtained by integrating the kinetic equation with respect to x' and $v_\perp$,

$$f_1(v_\parallel) = 2\pi \int_0^\infty dv_\perp^2 \int_{x_1(\epsilon,\mu)}^L dx' \frac{S(x',\epsilon,\mu)}{v_\parallel(x',\epsilon,\mu)} ,$$

$$0 < v_\parallel^2 < 2q\phi_1/M , \qquad (2.31a)$$

$$f_1(v_\parallel) = 2\pi \int_0^{v_\parallel^2+2q\phi_1/M} dv_\perp^2 \int_0^L dx' \frac{S(x',\epsilon,\mu)}{v_\parallel(x',\epsilon,\mu)}$$

$$+2\pi \int_{v_\parallel^2+2q\phi_1/M}^\infty dv_\perp^2 \int_{x_1(\epsilon,\mu)}^L dx' \frac{S(x',\epsilon,\mu)}{v_\parallel(x',\epsilon,\mu)} ,$$

$$-2q\phi_1/M < v_\parallel^2 . \qquad (2.31b)$$

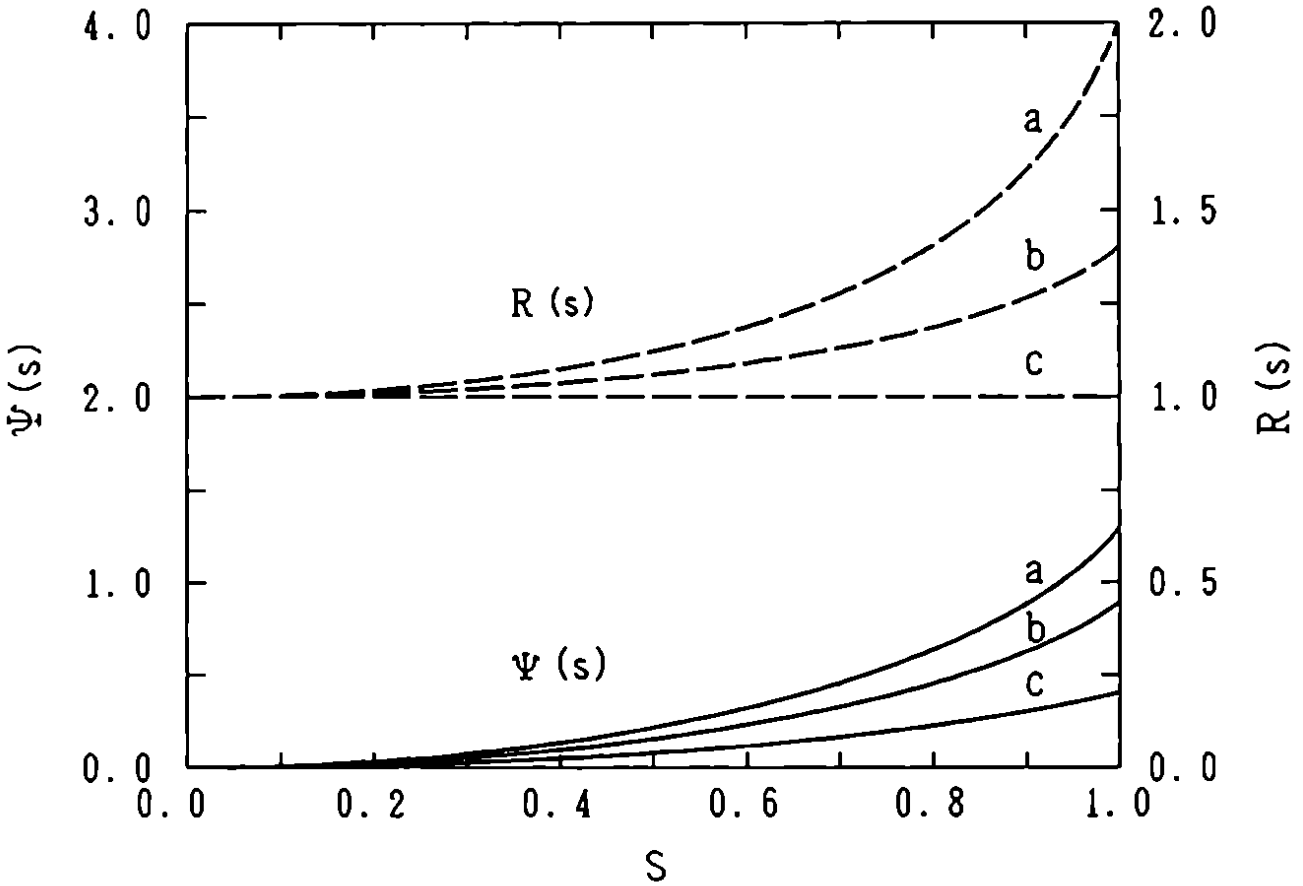

FIG. 2.3. The profile of the normalized potential $\Psi(s)$ calculated from Eq. (2.22) for the model field $R(\Psi)=\exp(\alpha\Psi)$ with (a) $\alpha=0.536$, (b) $\alpha=0.376$, and (c) $\alpha=0.0$, where the axial profile of the ion source with $\tau=1$ is chosen as $h(\Psi)=\exp(-\Psi)$.

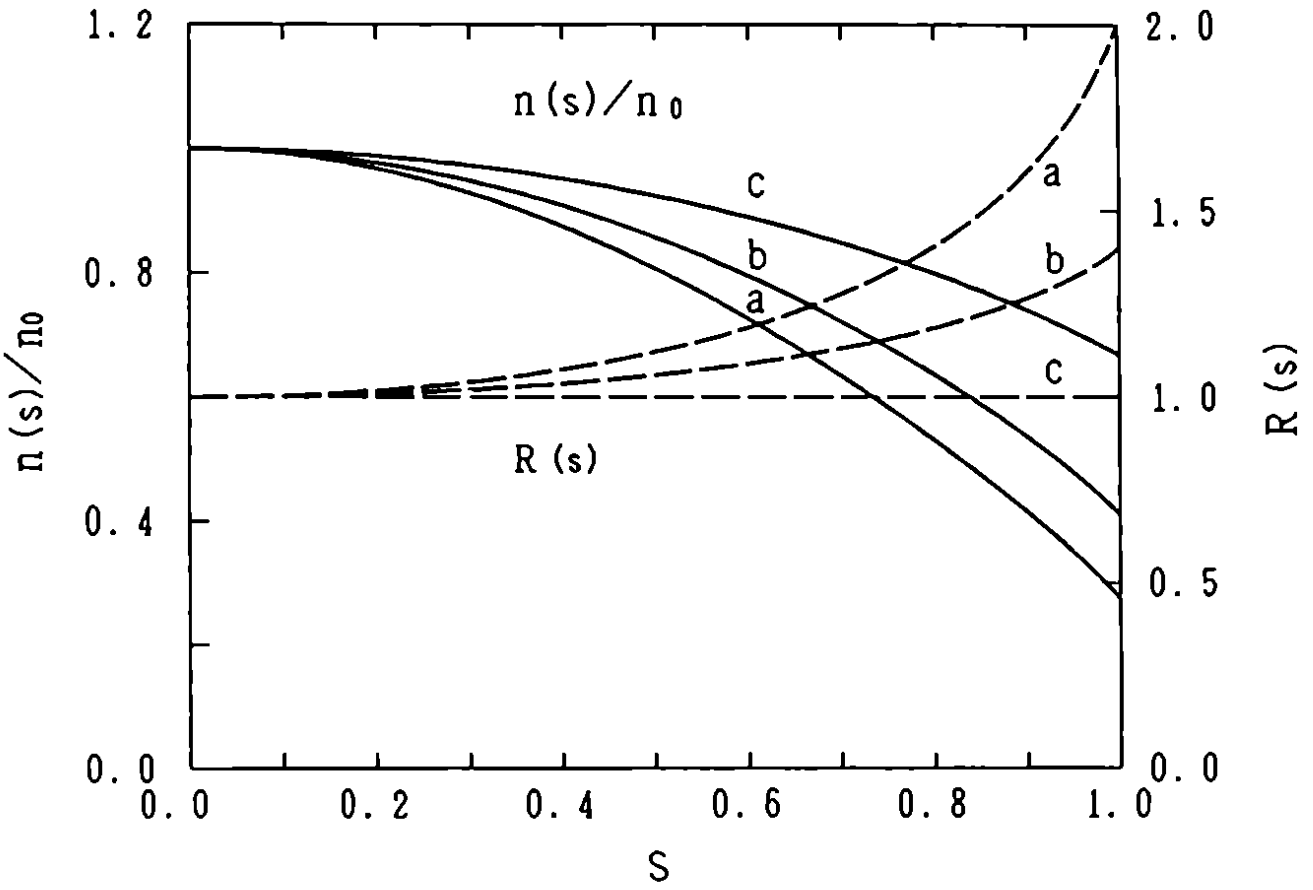

FIG. 2.4. The profile of the normalized plasma density $n(s)/n_0$ for the model field with (a) α=0.536, (b) α=0.376, and (c) α=0.0.

One can change the order of the integrations of Eqs. (2.31a) and (2.31b) with the aid of Eqs. (2.1) and (2.2) and integrate with respect to $v_\perp^2$ after substitution of Eq. (2.10). To express the distribution function, it is convenient to use the normalized quantities and the normalized parallel velocity,

$$V_\parallel^2 = M v_\parallel^2 / 2kT_e \ .$$

As a result of further calculations, we obtain the ion distribution function normalized to n_0 as

$$\frac{f_1(V_\parallel)}{n_0} = 2A \frac{1+Z\tau}{Z(Z\tau)^{1/2}} \int_{\Psi_1 - V_\parallel^2/Z}^{\Psi_1} d\Psi' \frac{ds'}{d\Psi'} h(\Psi') \exp(Z\tau\Psi_1 - \tau V_\parallel^2)$$

$$\times \left[\exp(-Z\tau\Psi') - \exp\left(-\frac{R_1}{R_1 - R(\Psi')} Z\tau\Psi' \right) \right] \ ,$$

$$0 < V_\parallel^2 < Z\Psi_1 \ , \tag{2.32a}$$

$$\frac{f_1(V_\parallel)}{n_0} = 2A \frac{1+Z\tau}{Z(Z\tau)^{1/2}} \int_0^{\Psi_1} d\Psi' \frac{ds'}{d\Psi'} h(\Psi') \left[\exp(Z\tau\Psi_1 - \tau V_\parallel^2) \exp(-Z\tau\Psi') \right.$$

$$\left. - \exp\left(\frac{R_1}{R_1 - R(\Psi')} (Z\tau\Psi_1 - \tau V_\parallel^2) \right) \exp\left(-\frac{R_1}{R_1 - R(\Psi')} Z\tau\Psi' \right) \right] \ ,$$

$$Z\Psi_1 < V_\parallel^2 \ . \tag{2.32b}$$

For the case of the model field given by Eq. (2.26), the integration in Eqs. (2.32a) and (2.32b) can also be carried out to obtain the expression by the use of the function $E(\beta, x)$ defined by Eq. (2.30). The results for various values of R_1 are shown in Fig. 2.5. The distribution function changes its shape at $V_{\parallel}^2 = Z\Psi_1$, and becomes wider with increasing R_1. Ions having a magnetic moment are accelerated in the direction of the wall not only by the electric field but also by a gradient of the magnetic field strength.

Because the distribution function at the boundary is independent of $h(\Psi)$, the mean velocity and the particle and energy fluxes of the ion at the boundary must also be independent of $h(\Psi)$, the mean velocity and the particle and energy fluxes of the ions at the boundary must also be independent of $h(\Psi)$. The mean velocity normalized to the isothermal sound speed, $C_s = [k(T_e + T_i)/M]^{1/2}$, is easily obtained by equating the ion current to the electron current as

$$U_1 = \frac{< v_{\parallel} >_1}{C_s} = \left(\frac{M}{2\pi m}\right)^{1/2} \left(\frac{\tau}{1+\tau}\right)^{1/2} \exp(\Psi_1 - \Psi_w) \ . \tag{2.33}$$

We also obtain the normalized particle flux at the boundary,

$$\Gamma_1 = \frac{R_1 n_i(1) < v_{\parallel} >_1}{n_0 C_s} = R_1 \exp(\Psi_1) U_1 \ . \tag{2.34}$$

The dependence of U_1 and Γ_1 on R_1 is shown in Fig. 2.6.

The ion energy flux entering the sheath is calculated by integrating the product $(\varepsilon - Z\Psi_1)S(x, \varepsilon, \mu)R(x)$ over the phase space (x, ε, μ) as

$$Q_i = \int dx' R' \int d^3v' \frac{1}{2} M v'^2 S(x', \epsilon, \mu) + \int dx' R' \int d^3v' Z k T_e (\Psi_1 - \Psi') S(x', \epsilon, \mu) \tag{2.35}$$

Substituting Eq. (2.10), the normalized ion energy flux is obtained in the form

$$Q_1 = \frac{Q_i}{n_0 k (T_i + T_e) C_s} \sqrt{2} A \frac{1 + Z\tau}{Z(Z\tau)^{1/2}(1+\tau)^{3/2}} \int_0^{\Psi_1} d\Psi' \frac{ds'}{d\Psi'} [2 + Z\tau(\Psi_1 - \Psi')] R(\Psi') h(\Psi') , \tag{2.36}$$

which can also be integrated analytically for the case of the model field expressed by Eq. (2.26). The first term in the integrand of Eq. (2.36) is the energy flux resulting from the kinetic energy which ions have at the point of generation. The second term is from the energy flux that ions acquire in the plasma potential. The electron energy flux into the sheath is easily calculated when a Maxwellian distribution is assumed. The normalized electron energy flux is

$$Q_{1e} = \left(\frac{2M}{\pi m}\right)^{1/2} \left(\frac{\tau}{1+\tau}\right)^{3/2} R_1 \left(1 + \frac{\Psi_w - \Psi_1}{2}\right) \exp(-\Psi_w) . \tag{2.37}$$

The normalized ion energy flux at the boundary is shown in Fig. 2.7, together with the normalized total flux, $Q_t = Q_1 + Q_{1e}$.

As shown in Figs. 2.5 and 2.6, the distribution function at the boundary broadens and the mean velocity increases as the mirror ratio becomes large. It is closely connected with the condition for the sheath formation as discussed in the next section. We can predict from

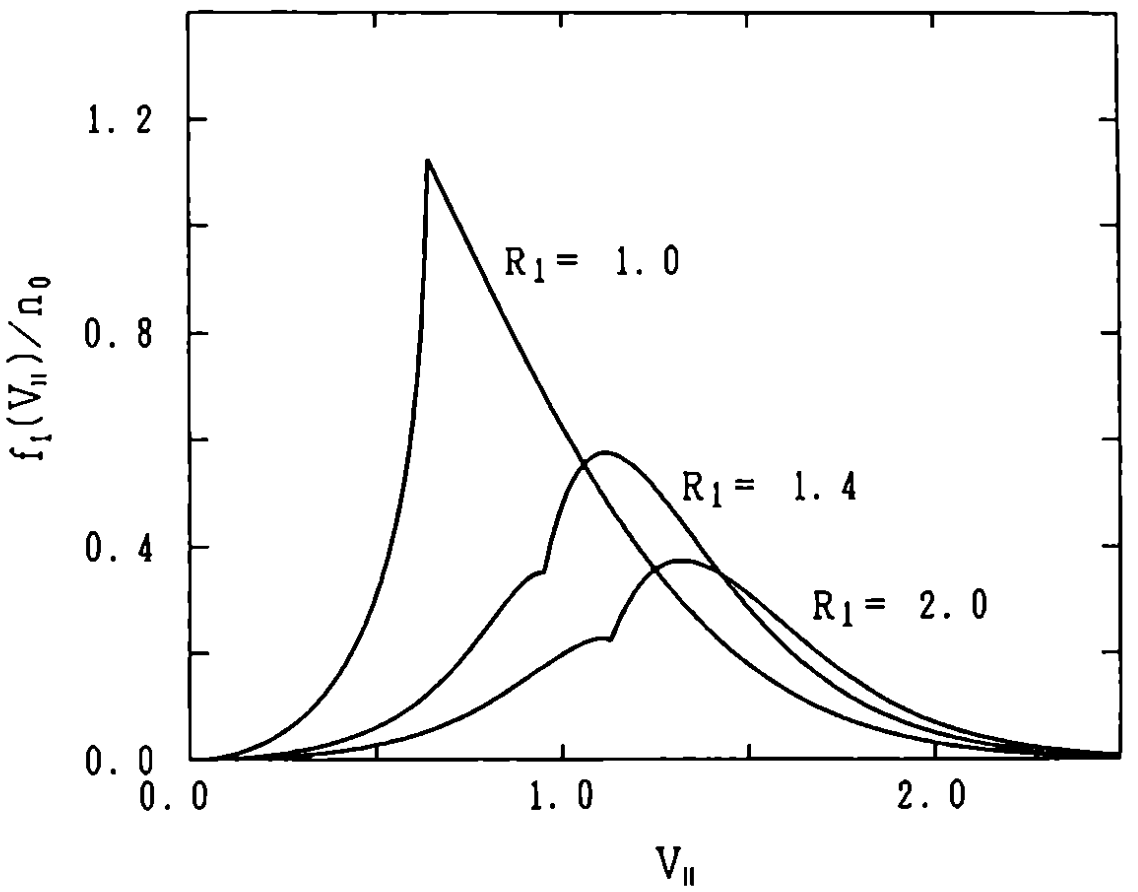

FIG. 2.5. The normalized ion distribution function with $\tau=1$ at the plasma-sheath boundary for various values of R_1.

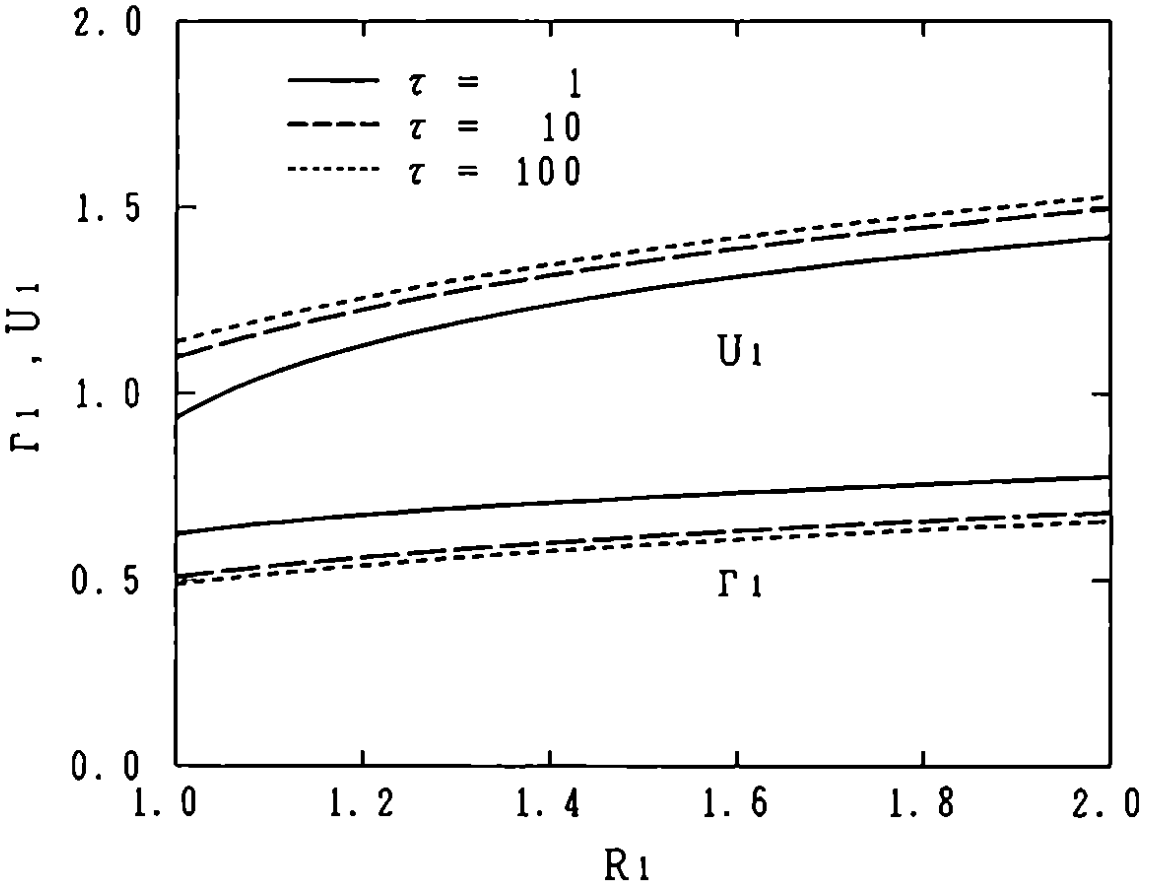

FIG. 2.6. The normalized ion mean velocity U_1 and the normalized particle flux Γ_1 at the plasma-sheath boundary as a function of the mirror ratio R_1.

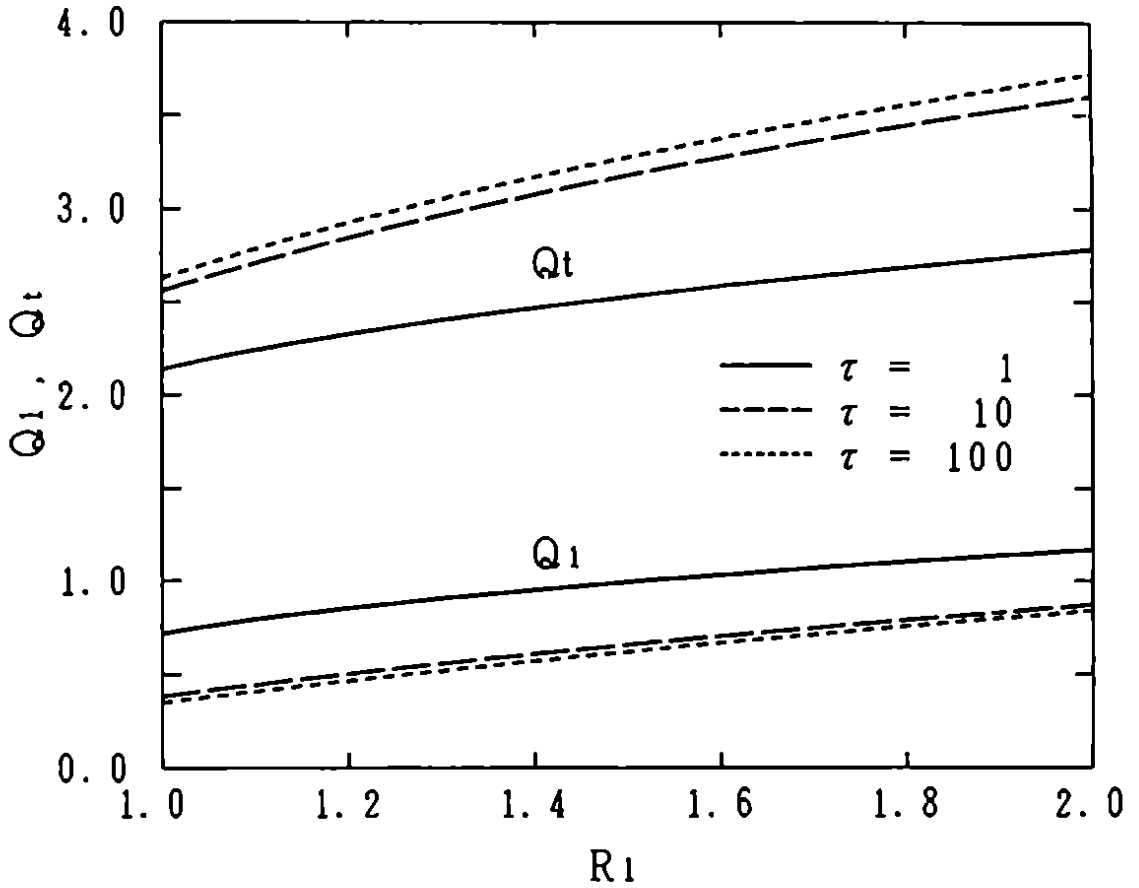

FIG. 2.7. The normalized ion energy flux Q_1 and the normalized total energy flux $Q_t = Q_1 + Q_{1e}$ at the plasma-sheath boundary as a function of the mirror ratio R_1, where Q_{1e} is the normalized electron energy flux.

the above result that the solution of the plasma equation for the monotonically increasing mirror ratio always satisfies the criterion for the sheath formation at the plasma-sheath boundary.

2.4 APPLICATION OF THE GENERALIZED BOHM CRITERION

We now show that the solution of the plasma equation satisfies the condition required for the sheath formation. The sheath is assumed to be so thin that the particle source inside the sheath can be neglected and the variation of the magnetic field in the sheath may be disregarded. On this assumption, we can apply the generalized Bohm criterion to the solution of the plasma equation: an interpretation of the generalized Bohm criterion was previously given by Bissell [14].

It is seen from Eqs. (2.6a), (2.6b), (2.7), and (2.8) that the ion density in a symmetric system is generally expressed by a function of R and Ψ. The electron density is independent of R if the electron distribution function is isotropic. Then, the solution of the plasma equation satisfies

$$Z\left(\frac{\partial n_i}{\partial \Psi}\frac{d\Psi}{ds}+\frac{\partial n_i}{\partial R}\frac{dR}{ds}\right)\Bigg|_{s=1}=\frac{dn_e}{d\Psi}\frac{d\Psi}{ds}\Bigg|_{s=1} \tag{2.38}$$

at the plasma-sheath boundary because the quasi-neutrality holds true in the plasma. The term on the left-hand side can be rewritten as

$$\left.\frac{\partial n_e}{\partial \Psi}\frac{d\Psi}{ds}\right|_{s=1} = -\left.\frac{d\Psi}{ds}\right|_{s=1}\frac{Z}{2}\int_0^\infty \frac{f_1(V_\parallel)}{V_\parallel^2}dV_\parallel \tag{2.39}$$

on the assumption of no particle source in the sheath, and the right-hand side is

$$\left.\frac{dn_e}{d\Psi}\frac{d\Psi}{ds}\right|_{s=1} = n_e\left.\frac{d\Psi}{ds}\right|_{s=1} \tag{2.40}$$

for a Maxwellian electron distribution. The expression (2.38) is obtained by differentiating the integral expression of ion density in the sheath with respect to Ψ and by setting Ψ equal to Ψ_1. Substituting Eqs. (2.39) and (2.40) into Eq. (2.38), we obtain

$$\frac{Z^2}{n_1}\int_0^\infty \frac{f_1(V_\parallel)}{V_\parallel^2}dV_\parallel = 2 + 2Z\frac{dR/ds}{d\Psi/ds}\left.\frac{\partial(n_i/n_1)}{\partial R}\right|_{s=1}. \tag{2.41}$$

We partially differentiate the right-hand side of Eq. (2.15) with respect to R and use the asymptotic expansion (2.16) of the complementary error function to get

$$\begin{aligned}&\frac{Z^2}{n_1}\int_0^\infty \frac{f_1(V_\parallel)}{V_\parallel^2}dV_\parallel \\ &\quad = 2 - 2\left.\frac{dR/ds}{d\Psi/ds}\right|_{s=1}\frac{A(1+Z\tau)}{\tau R_1}\frac{n_0}{n_1}\int_0^{\Psi_1} d\Psi'\frac{ds'}{d\Psi'}\frac{R(\Psi')}{R_1}\frac{h(\Psi')}{(\Psi_1-\Psi')^{1/2}}.\end{aligned} \tag{2.42}$$

When the mirror ratio becomes large with increasing potential, the second term on the rhs has a positive value because the integral is always positive. Hence, when $dR/ds > 0$ and $d\Psi/ds > 0$ the solution of the plasma equation always satisfies the criterion at the plasma-sheath boundary,

$$\frac{Z^2}{n_1}\int_0^\infty \frac{f_1(V_{||})}{V_{||}^2}dV_{||} \leq 2\,, \tag{2.43}$$

which is the expression of the generalized Bohm criterion with the normalized velocity. The equality in Eq. (2.43) is true when $dR/ds=0$ at the plasma-sheath boundary. This criterion can also be checked by using the distribution function expressed by Eqs. (2.32a) and (2.32b). Although Eq. (2.42) is the result for the particle source given by Eq. (2.10), it can be seen from Eq. (2.41) that the solution of the plasma equation for any source function satisfies the generalized Bohm criterion when $dR/ds > 0$ and $d\Psi/ds > 0$ because the derivative $\partial n_i/\partial R$ is always negative at the plasma-sheath boundary.

The question arising from Eq. (2.41) is does the solution satisfy the generalized Bohm criterion when $dR/ds < 0$? This problem, in general, becomes hard to analyze completely because one must treat ions trapped in the well of the effective potential $\mu B_0/R(s) + Ze\Psi(s)$ when $dR/ds < 0$. If the density of the trapped ions is negligibly small near the boundary, however, one can find that $\partial n_i/\partial R$ becomes negative. When trapped ions near the boundary can be neglected and the ion source has no particle originating with zero parallel velocity, one can generally show that the derivatives $\partial n_i/\partial\Psi$ and $\partial n_i/\partial R$ always have negative finite values near the boundary. The potential gradient at the boundary must be a positive finite value to be connected to the sheath potential. Therefore, it is seen from Eq. (2.41) that in this case the solution of the plasma equation does not satisfy the generalized Bohm criterion. When there are ions generated at $V_{||}=0$, that is, $S(V_{||} = 0) \neq 0$, careful treatment of trapped ions is necessary to estimate the second term on the rhs in Eq. (2.41).

2.5 NUMERICAL SOLUTION OF THE PLASMA-SHEATH EQUATION

For the purpose of showing the validity of the analysis and to evaluate the effect of the Debye length on the potential profile near the wall, we now solve the plasma-sheath equation. Equation (2.13), which is the nonlinear integrodifferential equation, can be solved numerically by transforming it into a set of finite difference equations. We use the technique described in Ref. [9] for solving the equation. The boundary conditions on Eq. (2.13) are $d\Psi/ds|_0 = 0$ and $\Psi_0 = 0$; the normalized wall potential Ψ_w is determined as a result of the calculation. To compare the numerical result with the analytic solution, we describe the model field $R(\Psi)$ =exp($\alpha\Psi$) using the analytic solution of the plasma equation. Then, the analytic solution and the expression of Ψ_w can also be used as initial values of Ψ for the numerical calculation. The spatial variation of the particle source is expressed by $h(\Psi)$=exp($-\Psi$) using the numerical solution of the plasma-sheath equation.

Figure 2.8 shows the numerically calculated potential together with the analytical solution for the model field with α = 0.536, where the hydrogen plasma source with τ = 1 is assumed. It is seen that agreement of the analytic solution with the numerical result is nearly perfect in the plasma region when the value of λ_{D0}/L is sufficiently small. The density profiles of both ions and electrons for λ_{D0}/L=0.03 are shown in Fig. 2.9. We see from the result that the width of the sheath, in which the quasi-neutrality does not hold true, is about ten times as large as the Debye length, λ_{D0}. There is the difference between the analytic solution and the numerical results of $\Psi(s)$ in the section

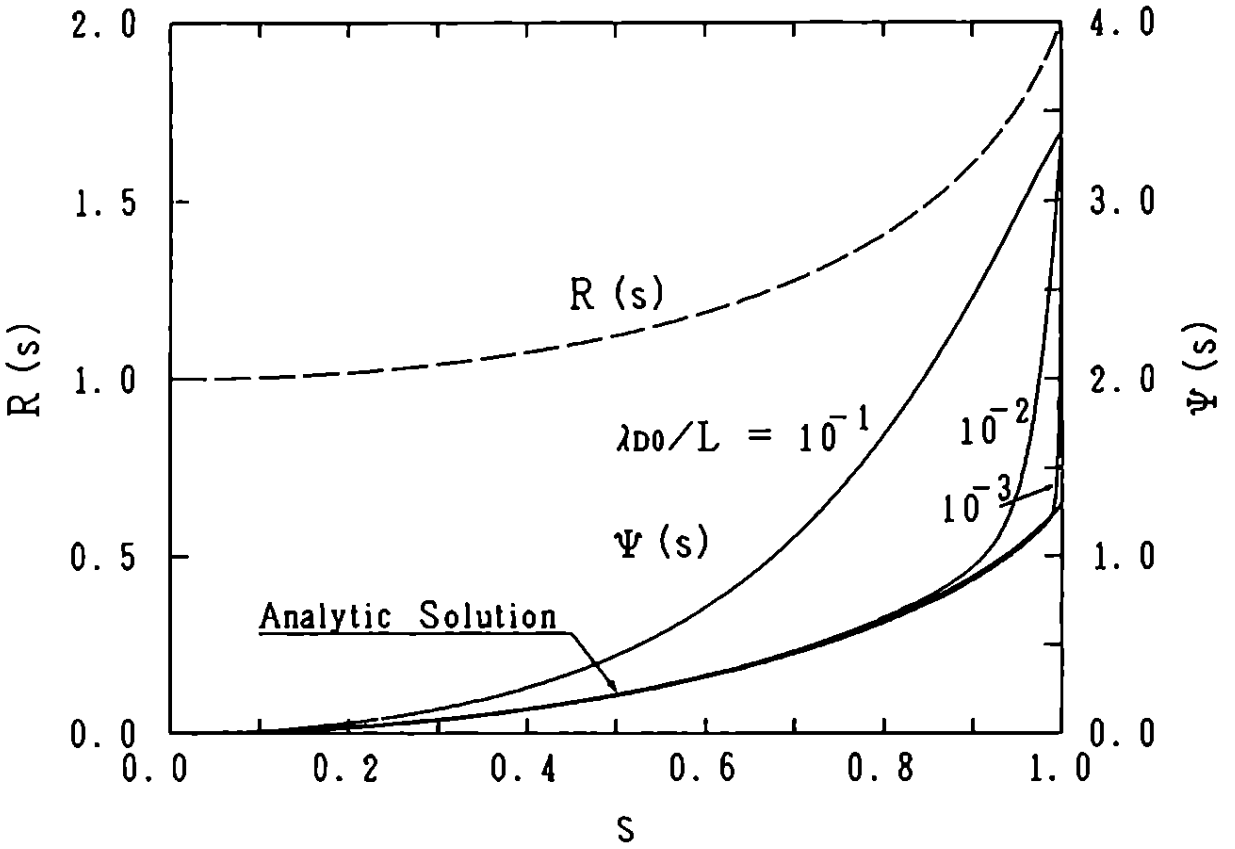

FIG. 2.8. The profile of the normalized potential $\Psi(s)$ for an ion source with $\tau=1$ for various values of λ_{D0}/L, where the model field $R(\Psi)=\exp(\alpha\Psi)$ with $\alpha=0.536$ is described by the use of the analytic solution, Ψ, (heavy line) of the plasma equation.

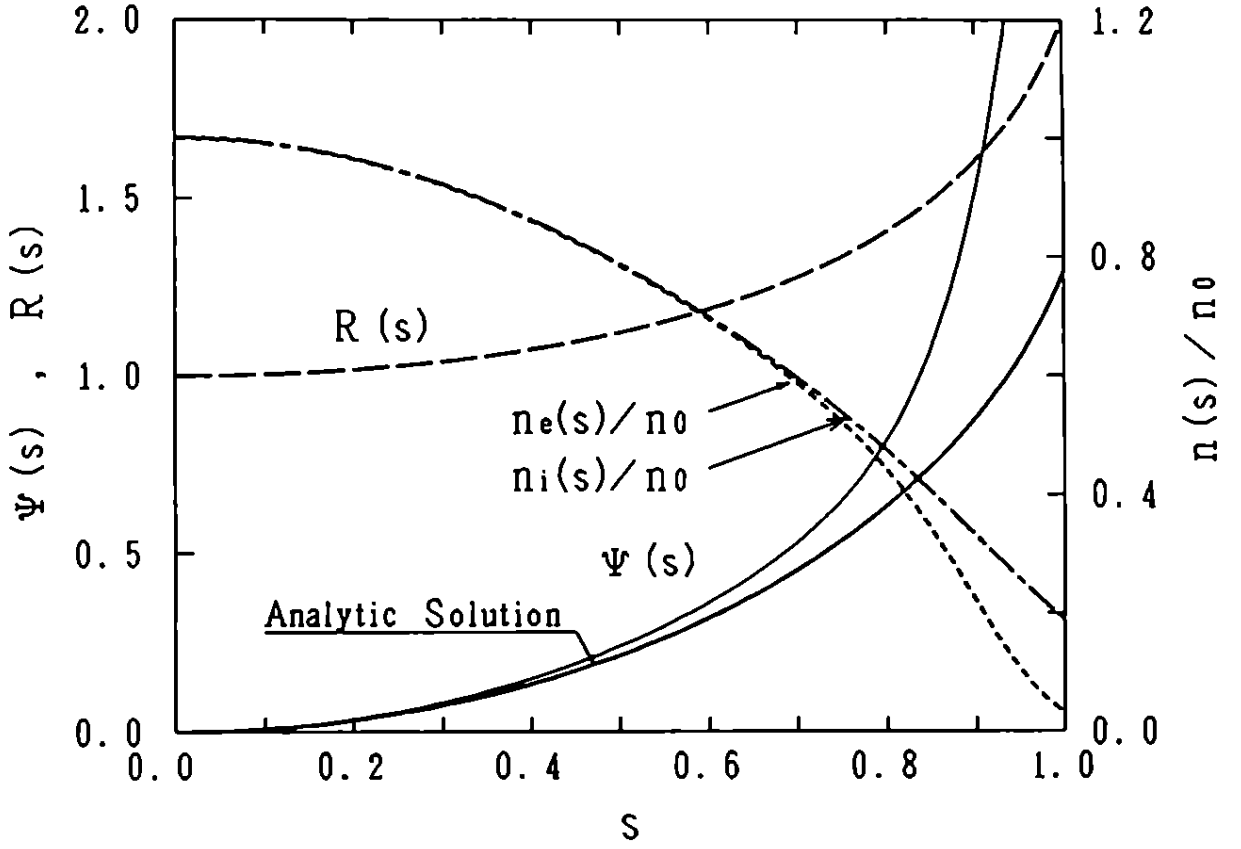

FIG. 2.9. The profile of the normalized potential $\Psi(s)$ and the normalized density of ions and electrons, $n_i(s)/n_0$, for $\lambda_{D0}/L=0.03$, where a heavy line is the analytic solution of the plasma equation.

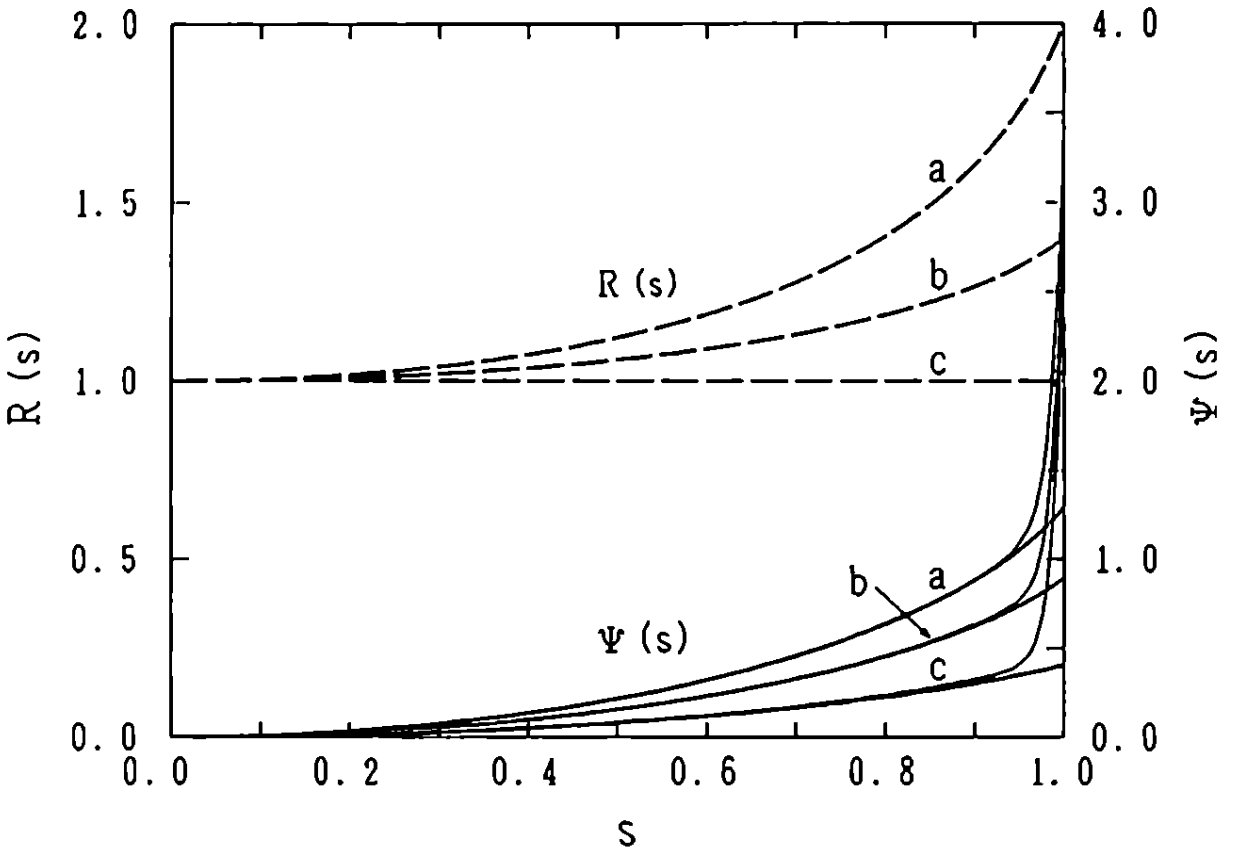

FIG. 2.10. Comparison of the numerical solution of the plasma-sheath equation (thin lines) with the analytic solution of the plasma equation (thick lines) for the model field $R(\Psi)=\exp(\alpha\Psi)$ with (a) $\alpha=0.536$, (b) $\alpha=0.376$, and (c) $\alpha=0.0$, where the value of λ_{D0}/L is 0.005.

$0 < s < 0.6$ although the quasi-neutrality holds good. This difference is considered to be caused mainly by the difference of the plasma-sheath boundary: the plasma-sheath boundary of the analytic solution is $s = 0.7$. Dependence of the potential profile on the magnetic field is shown in Fig. 2.10.

2.6 CONCLUSIONS

We have formulated the plasma-sheath equation for a collisionless plasma in an open magnetic field that has monotonically decreasing axial profiles. The ion-source distribution function with a finite temperature chosen by Emmert *et al.* has been used for the formulation. In the plasma, except for the sheath region, Abel's integral equation can be derived approximately from the plasma equation by describing the magnetic field profile as an arbitrary function of the potential, and then an open magnetic field with various kinds of axial profile. The accuracy of the analytic solution was checked numerically by substituting the solution into the plasma equation; it confirms the validity of the approximation. The analytic solution is used to express the wall potential, the ion distribution function, and the particle and energy fluxes explicitly. Results show that the magnetic profile affects the potential formed in the plasma. For the model field used in this chapter the presheath potential drop increases by about a factor of 2 when the magnetic field at the boundary weakens to half of that at the center of the plasma, and the ion distribution function becomes wider with increasing of the potential drop.

It has been shown that the solution of the plasma equation always satisfies the generalized Bohm criterion at the plasma-sheath boundary when the magnetic field monotonically decreases in the outside direction. We have also discussed this criterion when the magnetic field monotonically increases.

The plasma-sheath equation is solved numerically for various profiles of the magnetic field. The sheath is formed near the walls with a width about ten times as long as the Debye length, and the analytic solution for any profile of the magnetic field agrees well with the numerical results in the presheath when the Debye length is sufficiently small. The potential drop in the sheath is larger than that in the presheath and is almost independent of the magnetic field profile. Consequently, although the ion energy at the wall is somewhat large as compared with that for a uniform magnetic field, the increase in energy is not expected to be so large that it causes a remarkable increase in sputtering due to ions.

The presheath potential near the wall has an important roll in impurity control in a variety of reactor scenarios. If the potential drop in the plasma is large, ionized impurities will be reflected to a divertor or end plate without flowing into the main plasma. Therefore, an expanding magnetic field is effective not only to reduce the power density on targets but also to prevent an inflow of impurities. The fact that the potential profile depends on the magnetic field profile also implies the possibility of potential control in the open region by changing the magnetic field profile.

Concerning the potential formation in an open magnetic field, it is an open problem as to whether the static potential is formed or not when the magnetic field monotonically

increases. In this case one must take the existence of trapped ions into consideration to treat this problem.

REFERENCES

[1] L. S. Hall, Nucl. Fusion **17**, 681 (1977).

[2] L. C. Steinhauer, Phys. Fluids **29**, 3379 (1986).

[3] S. Sato, M. Sugihara, and N. Fujisawa, J. Nucl. Mater. **121**, 199 (1984).

[4] P. C. Stangeby, in *Physics of Plasma-Wall Interaction in Controlled Fusion*, eds. D. E. Post and R. Behrisch (Plenum Press, New York, 1986) p. 41.

[5] L. Tonks and I. Langmuir, Phys. Rev. **34**, 876 (1962).

[6] E. R. Harrison and W. B. Thompson, Proc. Phys. Soc. London **74**, 145 (1959).

[7] A. Caruso and A. Cavaliere, Nuovo Cimento **26**, 1389 (1962).

[8] S. A. Self, Phys. Fluids **6**, 1762 (1963).

[9] G. A. Emmert, R. M. Wieland, A. T. Mense, and J. N. Davidson, Phys. Fluids **23**, 803 (1980).

[10] R. C. Bissell and P. C. Johnson, Phys. Fluids **30**, 779 (1987).

[11] R. L. F. Boyd and J. B. Thompson, Proc. R. Soc. A **252**, 102 (1959).

[12] B. Bertotti and A. Cavaliere, Nuovo Cimento **35**, 1244 (1965).

[13] J. E. Allen, J. Phys. D **9**, 2331 (1976).

[14] R. C. Bissell, Phys. Fluids **30**, 2264 (1987).

[15] M. Abramowitz and I. Stegun, in *Handbook of Mathematical Functions* (Dover, New York, 1974), pp. 298, 692.

[16] C. E. Pearson, in *Handbook of Applied Mathematics* (Van Nostrand Reinhold, New York, 1983), p. 603.

CHAPTER 3

Effects of an Expanding Open Magnetic Field on the Plasma Presheath

3.1 INTRODUCTION

A plasma flowing to a wall in the presence of a nonuniform magnetic field is an important problem for research on magnetically confined plasmas as well as on the plasma source used in plasma processing. Potential developed in a plasma flowing along a nonuniform open magnetic field becomes an issue when we approach the subject of the plasma flow, energy transport, an inflow of high-Z impurity ions, and plasma-surface interactions in an open region of confinement systems. In the presence of an expanding magnetic field, ions are accelerated toward the plate and their density drops accordingly. If electrons remain close to a Maxwellian distribution then the electrostatic potential will increase following the Boltzmann relation. Accelerated ions will also facilitate formation of a shielding positive space charge at the plasma boundary. Therefore, the expanding

magnetic field is expected to be available not only for enlargement of the potential drop along a field line but also for stabilization of the sheath potential.

The problem of plasma flow to a wall and the potential formation has drawn attention since the first kinetic analysis in the context of discharge plasmas was done by Tonks and Langmuir [1]. Progress on the theoretical treatment of this problem has been made by a number of workers over many years [2-4]. In the previous analyses the plasma is either unmagnetized or magnetized by a uniform field.

Recently, Sato and Miyawaki formulated the plasma-sheath equation for a collisionless plasma with a finite-temperature particle source in an expanding magnetic field [5], in which the same ion source function used by Emmert *et al.* is adopted and Boltzmann electrons is assumed. They obtained an analytic solution by introducing some simplifying approximations and presented the potential profile, the potential at the sheath edge, and the wall potential as well as the particle and energy fluxes to the sheath for different magnetic mirror profiles. Hussein and Emmert numerically simulated the same plasma and investigated the dependence of the presheath potential on both the spatial distribution of the particle source and the magnetic field strength profiles [6]. They compare the simulation results with the analytical solution obtained by Sato and Miyawaki, showing that the simulation results agree well with Sato and Miyawaki for low mirror ratios but deviate as the mirror ratio increases. Although they concluded that the differences between them is attributed to the approximation made in the analysis, the differences mainly originate in a particle source used in the analysis and in the simulation. The particle source in the analysis has a spatial profile in proportion to the plasma particle

density but that in the simulation has a uniform spatial profile .

In this chapter, we numerically analyze effects of a nonuniform open magnetic field on potential formation in the plasma in contact with a wall by solving the plasma equation formulated previously. We compare the numerical results with the analytical ones and also with the simulation ones to show justice of approximations in the analysis carried by Sato Miyawaki and to check accuracy of the simulation code developed by Hussein and Emmert. Moreover, we investigated the dependence of the potential profile on the spatial distribution of the particle source and show upper and lower limits of the potential drop in the presheath to indicate controlability of the presheath potential by applying an expanding magnetic field. We also discuss an effect of the nonuniform magnetic field on sheath formation using a calculated ion distribution function.

In Sec. 3.2, we describe the model and write the plasma equation. An effect of a nonuniform magnetic field on sheath formation is briefly discussed in Sec. 3.3. The numerical results are presented and discussed in Sec. 3.4, and the conclusions are given in Sec. 3.5.

3.2 MODEL AND PLASMA EQUATION

The model and coordinate system used throughout this chapter is illustrated in Fig. 3.1. The collisionless plasma contained between two perfectly absorbing walls located at $x = \pm L$ is symmetric about $x = 0$. The Debye length is assumed to be small compared

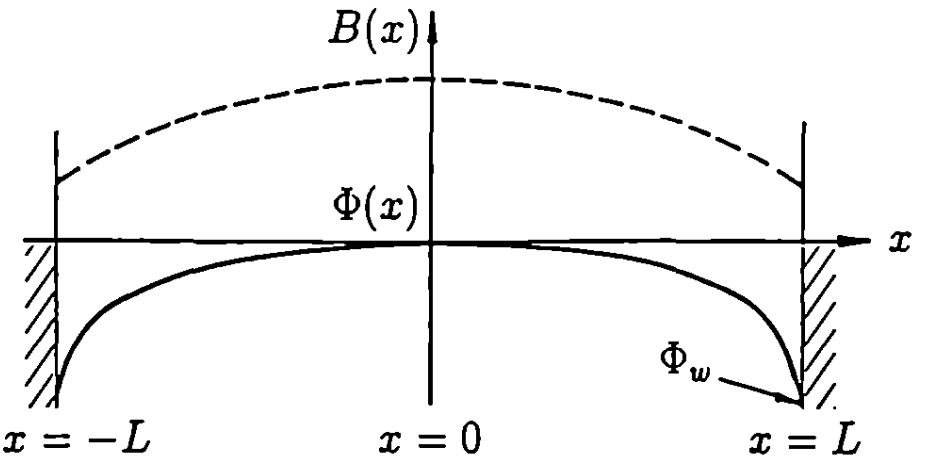

FIG. 3.1. The geometry and coordinate system, and axial profiles of the potential and the magnetic field strength.

with macroscopic scale length, and then quasineutrality along field lines holds true over the whole region except the sheath region.

Using the energy ϵ and the magnetic moment μ, we can describe the kinetic equation for ions by

$$\sigma v_{\parallel}(x,\epsilon,\mu)\frac{\partial f(x,\epsilon,\mu,\sigma)}{\partial x} = S(x,\epsilon,\mu)\ , \tag{3.1}$$

where

$$v_{\parallel}(x,\epsilon,\mu) = \left[2\left(\epsilon - \mu B(x) - q\phi(x)\right)/M\right]^{1/2} \tag{3.2}$$

is the speed of ion along the field line, $\sigma(=\pm 1)$ denotes the direction of the ion motion, $f(x,\epsilon,\mu,\sigma)$ is the ion distribution function, $S(x,\epsilon,\mu)$ is the source term for the ions, M is mass, q is the ion charge, $\phi(x)$ is the electrostatic potential, and $B(x)$ is the magnetic field strength. The ion source used by Emmert *et al.* is expressed in the form

$$S(x,\epsilon,\mu) = S_0 h(x)\frac{M^2}{4\pi(kT_i)^2}v_{\parallel}(x,\epsilon,\mu)\exp\left(\frac{-[\epsilon - q\phi(x)]}{kT_i}\right)\ , \tag{3.3}$$

where S_0 is the source strength, k is Boltzmann's constant, T_i is the source temperature, and $h(x)$ expresses the spatial distribution of the source. The boundary conditions of the distribution function are $f(-L,\epsilon,\mu,+1) = 0$ and $f(L,\epsilon,\mu,-1) = 0$. The distribution function $f(x,\epsilon,\mu,\sigma)$ is obtained by integrating Eq. (3.1) along the trajectory of ions and then ion density $n_i(x)$ is calculated by integrating the distribution function over the $\epsilon - \mu$ space.

Since the electrons are in a retarding electrostatic potential, the electrons can be assumed to have a Boltzmann distribution with temperature T_e. Results of particle simulation shows that the bulk of electrons approaches to the Boltzmann distribution ever if the mean free path is much larger than the scale length of a plasma [7]. We can equate ion and electron charge densities in the presheath region to obtain the the plasma equation. Introducing the nondimensional variables

$$\Psi(s) = -e\phi(s)/kT_e, \quad R(s) = B_0/B(s), \quad s = x/L, \quad Z = q/e,$$

and

$$\tau = T_e/T_i \ ,$$

we describe the plasma equation derived by Sato and Miyawaki in the form

$$n_0 \exp(-\Psi(s)) = ZS_0L\left(\frac{\pi M}{2kT_i}\right)^{1/2} \int_0^1 ds' G(s,s')h(s') \ , \tag{3.4}$$

where

$$G(s,s') = \exp[Z\tau(\Psi(s) - \Psi(s'))]\mathrm{erfc}[Z\tau(\Psi(s) - \Psi(s'))^{1/2}]$$

$$- \left(\frac{R(s) - R(s')}{R(s)}\right)^{1/2} \exp\left(\frac{R(s)}{R(s) - R(s')} Z\tau(\Psi(s) - \Psi(s'))\right)$$

$$\times \mathrm{erfc}\left[\left(\frac{R(s)}{R(s) - R(s')} Z\tau(\Psi(s) - \Psi(s'))\right)^{1/2}\right] \ , \ s' < s \ ,$$

$$G(s,s') = \exp[Z\tau(\Psi(s) - \Psi(s'))] \ , \qquad s' \geq s \ ,$$

The electrostatic potential in the presheath is obtained by solving Eq. (3.4) and the wall potential Ψ_w also determined from the requirement of equal ion and electron fluxes to the wall.

3.3 EFFECT ON SHEATH FORMATION

The sheath is assumed to be so thin that the particle source and variation of the magnetic field strength can be neglected inside the sheath. The solution of the plasma equation satisfies quasineutrality in the presheath and the particle flux is conserved in the sheath. Using quasineutrality at the sheath edge and conservation of the particle flux in the sheath, we can derive the relation

$$< V_{\parallel}^{-2} > \; = \; \frac{2}{Z^2} + \frac{2}{Z} \frac{dR/ds}{d\Psi/ds} \frac{\partial (n_i/n_1)}{\partial R}\bigg|_{s=1}, \tag{3.5}$$

where $V_{\parallel} = (M v_{\parallel}^2/2kT_e)^{1/2}$ is the normalized parallel velocity and the brackets $< >$ denote averaging with the ion distribution function [5]. The second term of rhs of Eq. (3.5) describes an effect of the nonuniform magnetic field. When the magnetic field is expanding, that is $dR/ds > 0$, the plasma equation for any source function satisfies the generalized Bohm criterion,

$$< V_{\parallel}^{-2} > \; \leq \; \frac{2}{Z^2}, \tag{3.6}$$

because the derivative $\partial n_i/\partial R$ in Eq. (3.5) is always negative at the sheath edge. The equality in Eq. (3.6) is true when the magnetic field is uniform or the field singularity appears at the sheath edge [8,9]. Appearance of the field singularity depends on both the spatial distribution and the velocity distribution of the particle source. If there is no particle source in the vicinity of the sheath edge or the particle source has no ions with zero parallel speed like Emmert's source, the field singularity does not appears and the derivative $d\Psi/ds$ has a finite value. In this case the generalized Bohm criterion is fulfilled with the inequality sign. Oversatisfaction of the Bohm criterion is favorable for formation of a shielding positive space charge at the plasma boundary and then one can expect that an expanding magnetic field has a stabilizing effect on the sheath potential.

3.4 NUMERICAL RESULTS AND DISCUSSION

For the purpose to demonstrate effects of the expanding magnetic field on the presheath potential, we now solve the plasma equation expressed by the nonlinear integral equation. This equation can be solved numerically by transforming it into a set of finite difference equations. We can obtain the numerical solution with a high accuracy better than 10^{-5} by iterating on the potential until it converges. We express the model field $R(s)$ as a function of the coordinate s and assume the temperature of ion T_i to equal the electron temperature T_e.

At first, to show justice of simplifying approximations introduced in the analysis by

Sato and Miyawaki and to check accuracy of the simulation code developed by Hussein and Emmert, we compare the calculation results with the analytical ones and the simulation ones. Figure 3.2 shows the potential profile in the presheath of a collisionless hydrogen plasma flowing along a magnetic field with a magnetic mirror profile used by Sato and Miyawaki. Different two spatial profiles of the particle source generate different potential profiles. The dotted lines are the values computed by Sato and Miyawaki for the particle source with the spatial distribution $h(s) = n(s)/n_0$ and broken lines are the simulation result by Hussein and Emmert for the particle source with $h(s) = 1$. The analytical solutions closely agree with the numerical results and an error due to the approximations made in the analysis is smaller than two percent. The simulation results also agrees well with the numerical ones but deviate near the sheath edge. This difference seems to be attributed to construction of a numerical grid in their simulation, which make their code less accurate near the sheath edge. Fig. 3.3 shows the dependence of the potential at the sheath edge Ψ_1 and that at the wall Ψ_w on the mirror ratio R_1. Excellent agreement between the numerical results and the analytical solution is obtained over the wide range of the mirror ratio; the difference is within two percent over the range of R_1 from 1 to 10. Some difference is observed between numerical results and simulation ones, which is considered mainly an error due to construction of a computational grid in the simulation. Hussein and Emmert. have concluded that the differences between Sato and Miyawaki's results and theirs are attributed to the approximations made in the analysis in Ref. [5], comparing their simulation results with the analytical solution. We, however, can see from Figs. 3.2 and 3.3 that these differences are mainly due to the

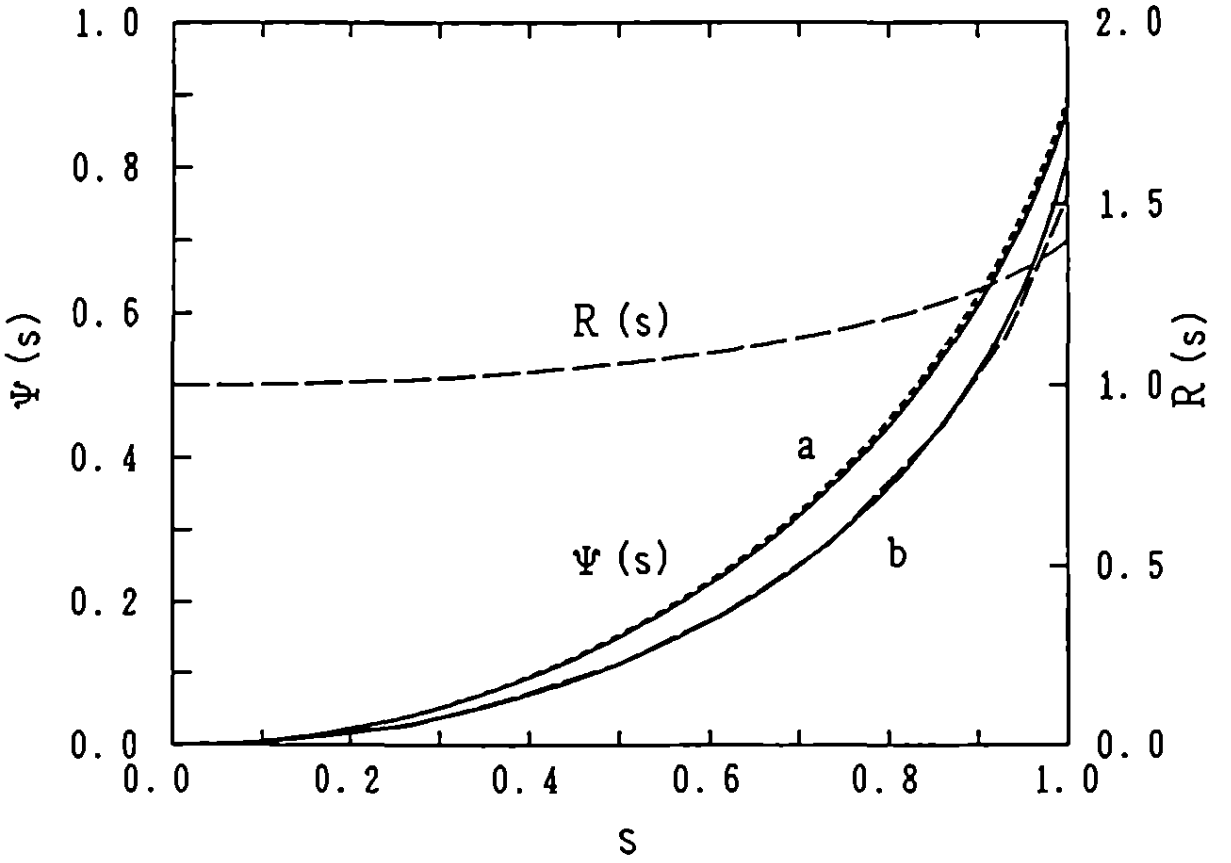

FIG. 3.2. The normalized potential profile in the presheath for the particle source with the spatial distribution (a) $h(s) = n(s)/n_0$ and (b) $h(s) = 1$. The model field b in Ref. [5] is used for the magnetic mirror profile. A dotted line is the analytical solution by Sato and Miyawaki for $h(s) = n(s)/n_0$, and a broken line is the simulation result by Hussein and Emmert for $h(s) = 1$.

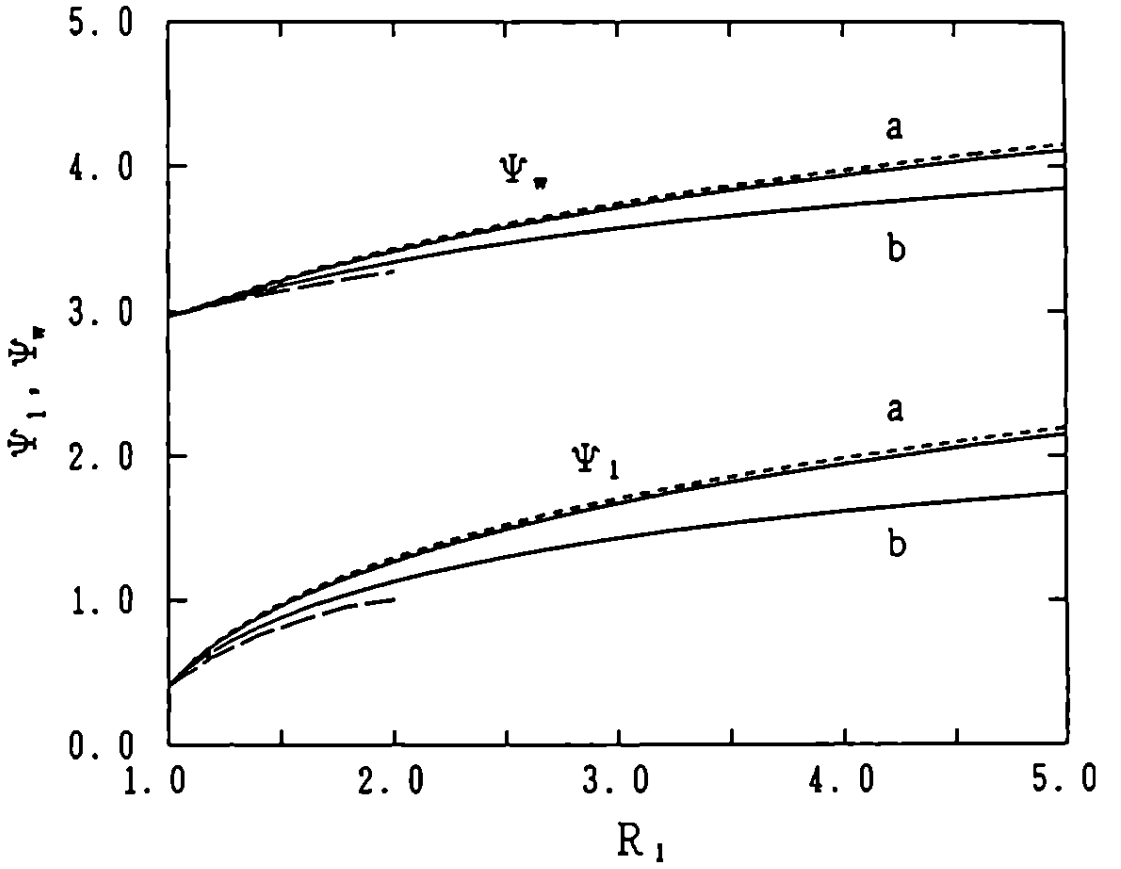

FIG. 3.3. The normalized potential at the wall Ψ_w and that at the sheath edge Ψ_1 as a function of the edge mirror ratio R_1 for the particle source with (a) $h(s) = n(s)/n_0$ and (b) $h(s) = 1$. The model field in Ref. [5] is used. Dotted lines are the analytical solutions for the particle source with $h(s) = n(s)/n_0$ by Sato and Miyawaki, and broken lines are the simulation results for the particle source with $h(s) = 1$ by Hussein and Emmert.

different spatial profile of the particle source.

The dependence of the electrostatic potential and the particle density on the magnetic mirror ratio is illustrated in Figs. 3.4 and 3.5, where the spatial profile of the particle source is given by the Gaussian of the form $h(s) = \exp(-25s^2)$. The parabolic profile of the magnetic mirror ratio given by $R(s) = 1 + (R_1 - 1)s^2$ is used heretofore. In the case of a constant magnetic field, the potential changes only over the source region and is constant elsewhere. Upon applying the expanding magnetic field, the potential continues to vary in the sourceless region. The potential drop increases with increasing of the edge magnetic mirror ratio R_1. We can compute the ion distribution function using the expression (3.31) in Ref. [5]. Figure 3.6 shows the ion distribution function at the sheath edge for various magnetic mirror ratios. The expanding magnetic field accelerates the plasma toward the wall and then the plasma is predicted to satisfy a condition for sheath formation at the sheath edge. The value of $< V_{\|}^{-2} >$ calculated from the ion distribution function is equal to 2.0 in the uniform magnetic field and it becomes smaller than 2.0 in the presence of the nonuniform magnetic field. Then the generalized Bohm criterion is marginally satisfied in the uniform magnetic field and is oversatisfied in the expanding magnetic field. The value of $< V_{\|}^{-2} >$ also is checked to agree with the value calculated from Eq. (3.5). From these results we can expect that the expanding magnetic field have a stabilizing effect on sheath formation.

In the presence of the nonuniform magnetic field, the potential drop in the presheath considerably depends on the spatial distribution of the particle source. Figures 3.7 and 3.8 illustrate the dependence of the potential and the particle density on the spatial

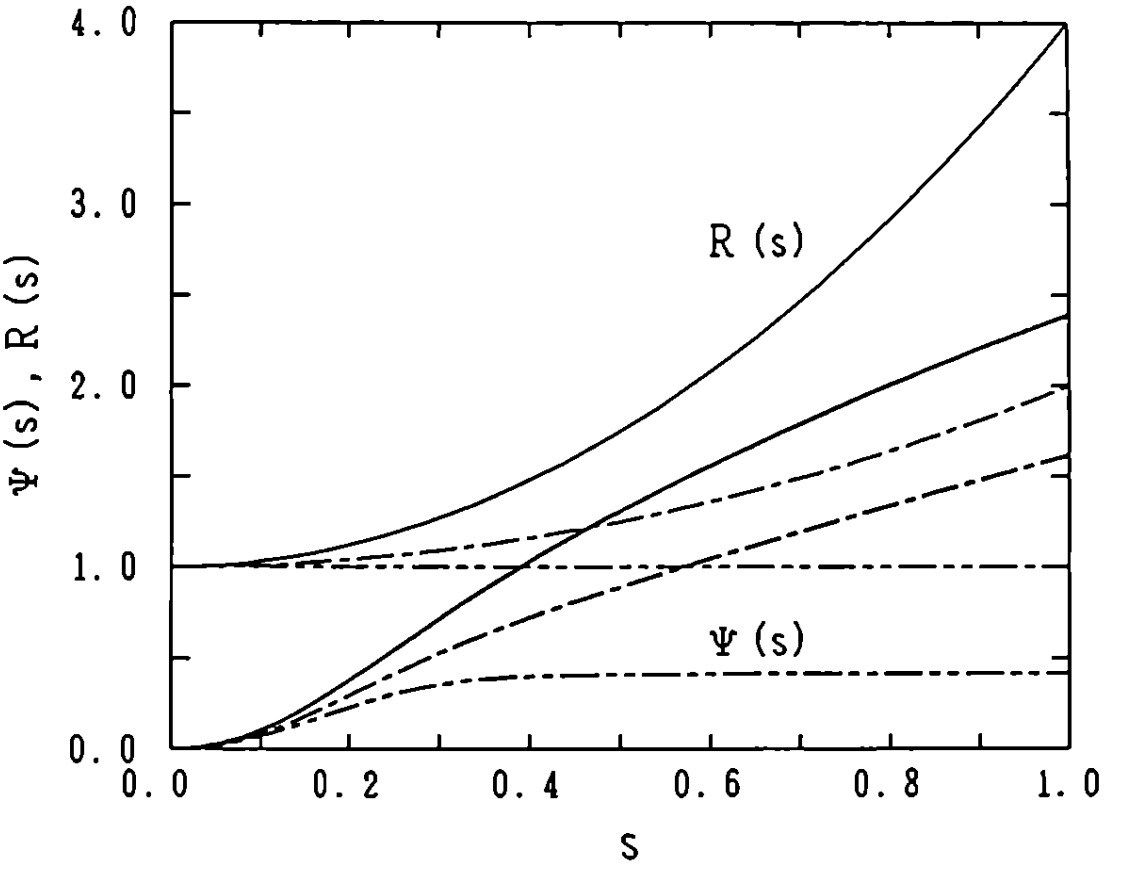

FIG. 3.4. The normalized potential profiles for the magnetic mirror ratio profile $R(s) = 1 + (R_1 - 1)s^2$ with $R_1 = 1.0$, 2.0, and 4.0, where the spatial distribution of the particle source is chosen as $h(s) = \exp(-25s^2)$.

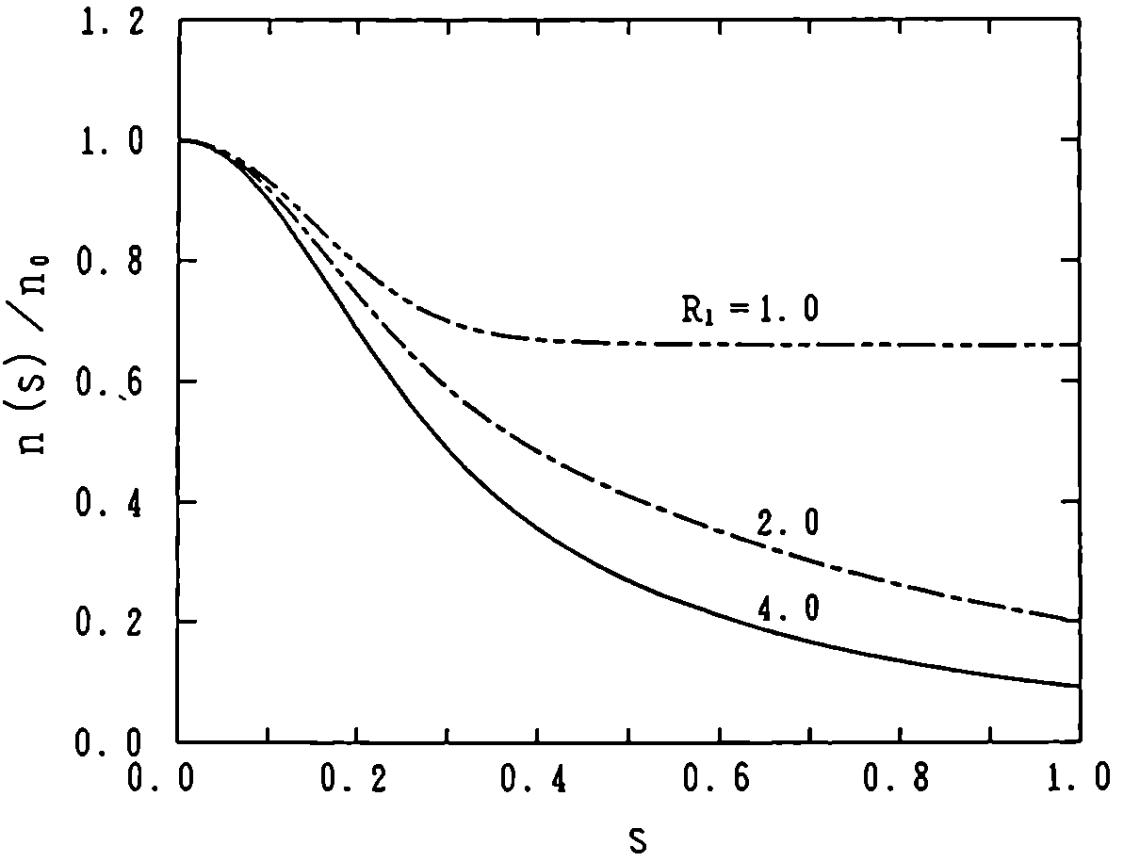

FIG. 3.5. The profile of the normalized plasma density $n(s)/n_0$ for the magnetic mirror ratio R_1 = 1.0, 2.0, and 4.0.

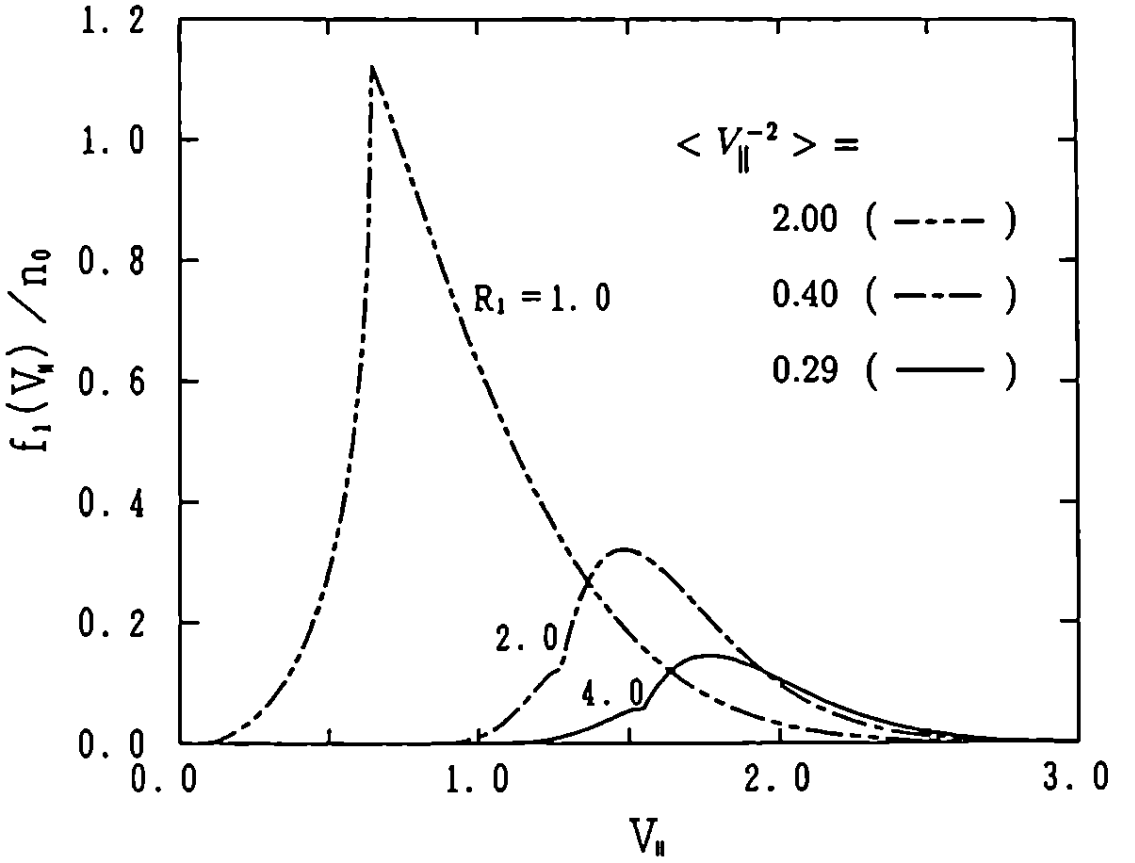

FIG. 3.6. The normalized ion distribution function at the sheath edge for various values of R_1. The value $< V_{\parallel}^{-2} >$ is eqnal to 2.0 in the case of the uniform magnetic field and smaller than 2.0 in the case of the expanding magnetic field.

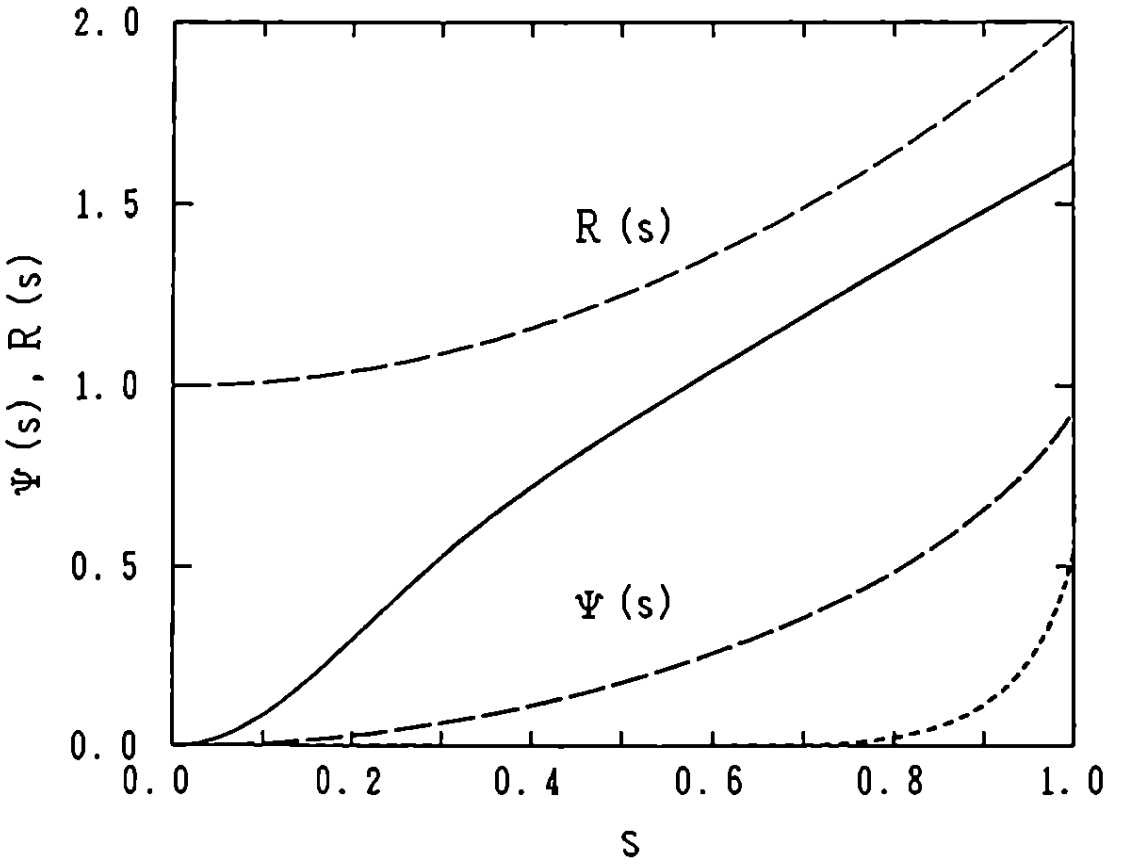

FIG. 3.7. The normalized potential profile for the partial source with the spatial distributions $h(s) = \exp(-25s^2)$(———), $h(s) = 1$ (– – – –), and $h(s) = \exp(-25(1-s)^2)$ (· · · · · · · ·). The magnetic mirror ratio profile is chosen as $R(s) = 1 + s^2$.

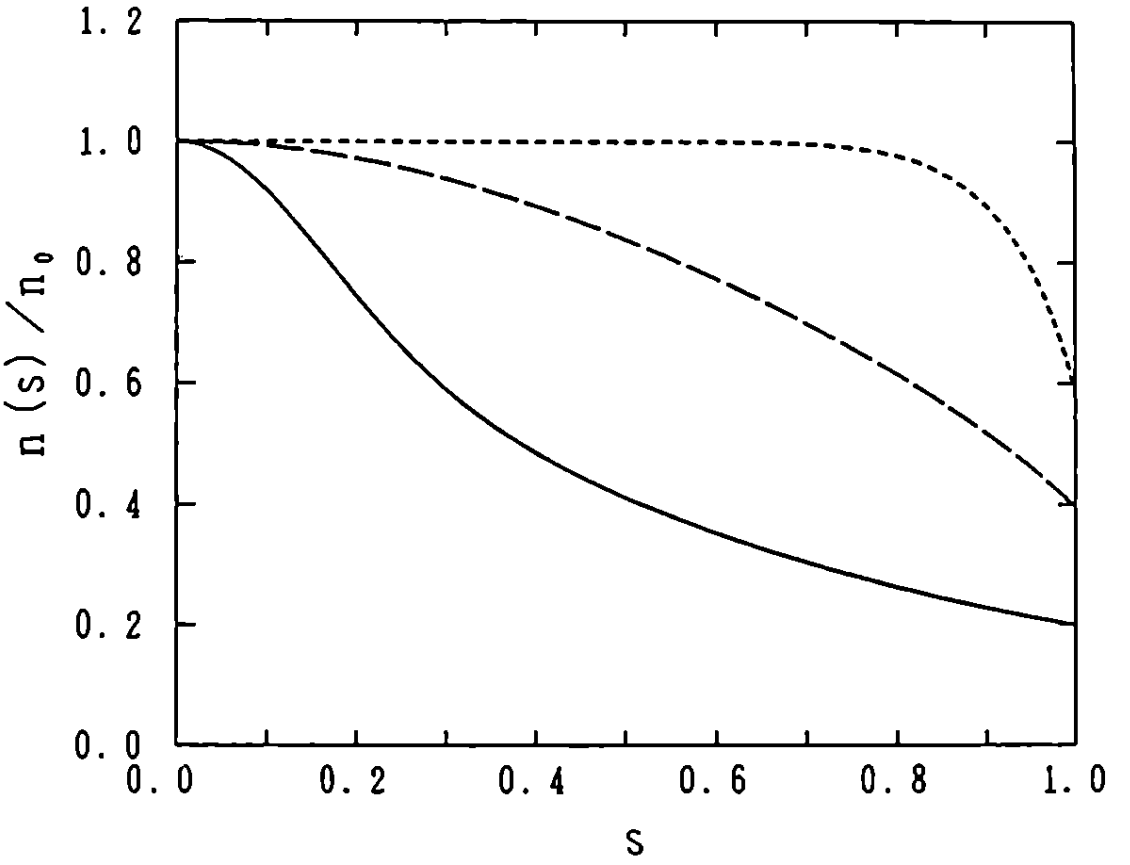

FIG. 3.8. The profile of the normalized plasma density $n(s)/n_0$ for the particle source with $h(s) = \exp(-25s^2)$ (———), $h(s) = 1$ (– – – –), and $h(s) = \exp(-25(1-s)^2)$ (· · · · · · · ·).

distribution of the particle source. The calculation is carried for three typical spatial distributions. In the case of the particle source near the plate, the potential is only developed over the region where the particle source exists. The only magnetic field in the source region affects the potential formation, but the magnetic field inside the particle source has no effect. This can be seen from Eq. (3.4) in which the integrand G is independent of the magnetic mirror ratio if $s' \geq s$. On the contrary, in the case of the particle source near the center, the potential is developed not only over the source region but also over the sourceless region. The potential development in the region outside the particle source is the result of the expansion of the magnetic flux tube. Figure 3.9 shows the ion distribution at the sheath edge for various spatial profiles of the particle source. The plasma flow velocity at the sheath edge exceeds the ion sound velocity and the generalized Bohm criterion is fulfilled with the inequality sign.

From results shown in Fig. 3.7, we can predict that the potential Ψ_1 has the maximum value when the particle source is concentrated at the center and has the minimum value when the particle source is localized near the wall. The maximum value is independent of the mirror ratio profile but dependent on the mirror ratio at the sheath edge R_1. Figure 3.10 shows the dependence of the upper and lower limits of potentials Ψ_1 and Ψ_w on the mirror ratio R_1. The region bounded by these limits show the region in which we can control the presheath potential by changing the mirror ratio and the profile of the magnetic field. Broken lines are results for the particle source with $h(s) = 1$. The wall potential increases gradually but the potential drop in the sheath decreases slightly with the mirror ratio. Results in Figs. 3.7 and 3.10 show that we can effectively control the

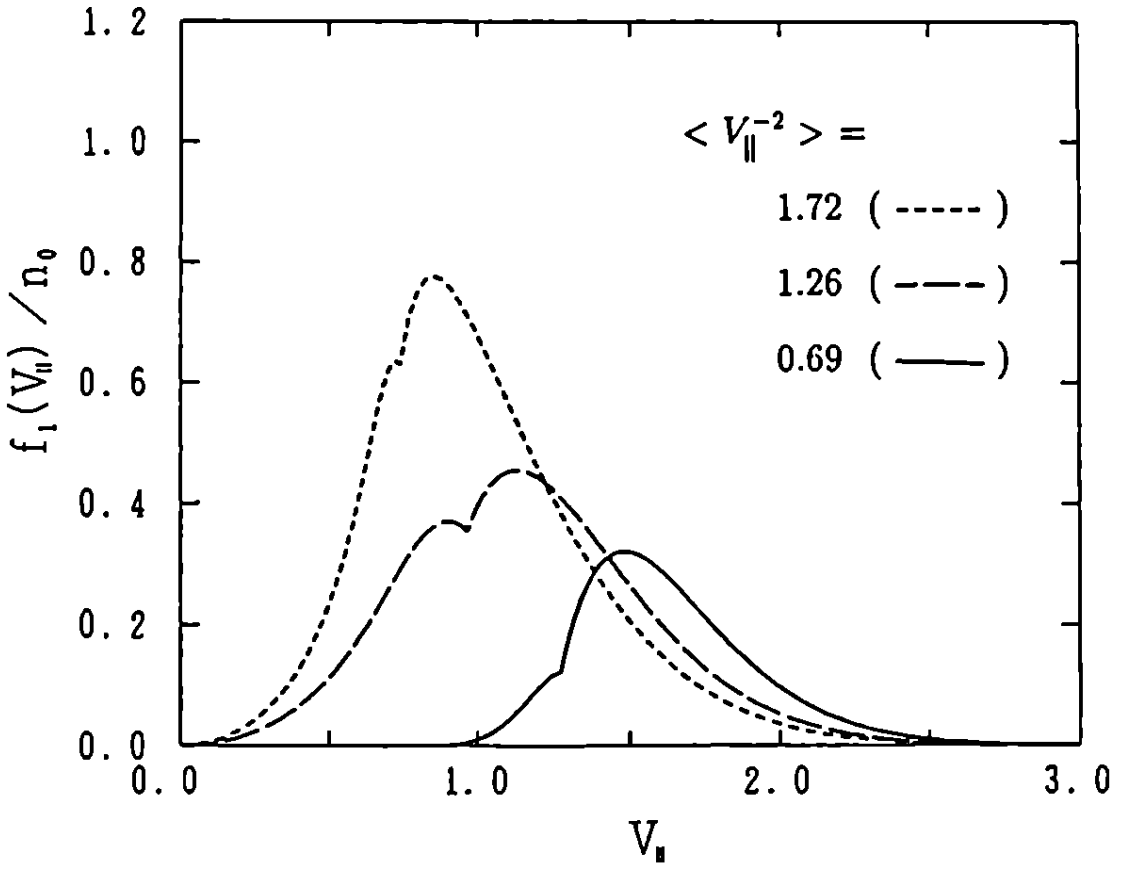

FIG. 3.9. The normalized ion distribution function at the sheath edge for the particle source with $h(s) = \exp(-25s^2)$ (———), $h(s) = 1$ (– – – –), and $h(s) = \exp(-25(1-s)^2)$ (--------). The value $< V_{||}^{-2} >$ is always smaller than 2.0.

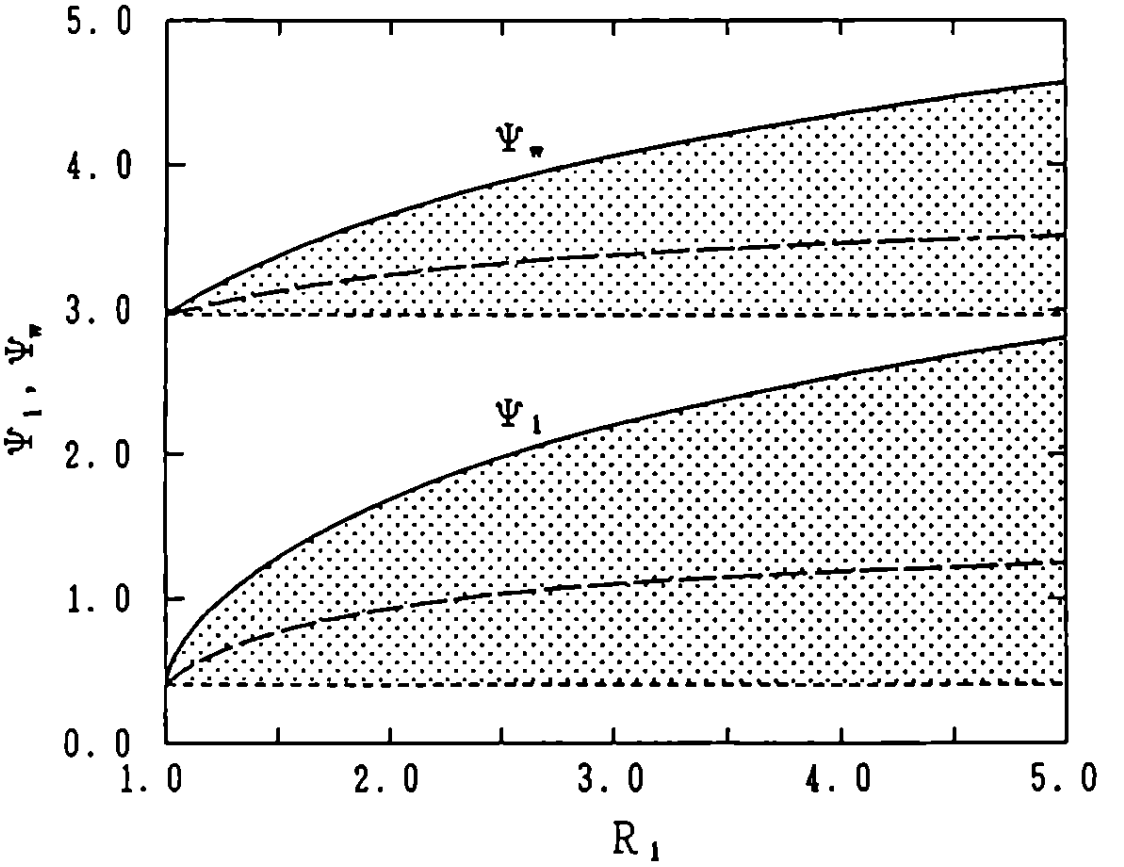

FIG. 3.10. The upper and lower limits (——— and -------) of the normalized potential at the sheath edge, Ψ_1, and those of the potential at the wall, Ψ_w, as a function of the edge mirror ratio R_1. Bracken lines are results for the particle source with $h(s) = 1$.

presheath potential in the source region or in the region outside the source by applying the expanding magnetic field with an adequate mirror ratio profile.

3.5 CONCLUSIONS

We have investigated formation of the presheath potential in the presence of an expanding magnetic field by numerically solving the plasma equation for the collisionless plasma. We have checked validity of the analysis and accuracy of the simulation code by comparing the present calculation results with previously published analytical solutions and recently published simulation results. Results show that analytical solutions obtained by Sato and Miyawaki are available over a wide range of the mirror ratio, and the present result of the potential profile also agrees with the simulation result obtained by Hussein and Emmert in the inner region, but slightly deviates in the region near a wall.

We have analyzed the dependence of the presheath potential profile on the spatial profile of the particle source and that of the magnetic field strength. Results show that a particle source profile has a considerable effect on the potential drop in the presence of a nonuniform magnetic field. If a plasma source exists in the interior of the plasma, we can effectively enlarge the potential drop in the presheath by increasing the magnetic mirror ratio. We have shown the upper and lower limits of the presheath potential as a function of the magnetic mirror ratio. The potential drops can be controlled within

these limits by applying an expanding magnetic field with a proper field strength profile.

We have also discussed an effect of a nonuniform magnetic field on sheath formation by calculating the ion distribution function. The plasma is accelerated by the gradient of the magnetic field strength and the plasma flow velocity at the sheath edge exceeds the sound velocity. The plasma flow in the presence of the expanding magnetic field satisfies the generalized Bohm criterion with the inequality sign if the sheath edge does not exhibit the the singularity.

REFERENCES

[1] L. Tonks and I. Langmuir, Phys. Rev. **34**, 876 (1929).

[2] E. R. Harrison and W. B. Thompson, Proc. Phys. Soc. London **74**, 145 (1959).

[3] G. A. Emmert, R. Wieland, A. Mense, and J. Davidson, Phys. Fluids **23**, 803 (1980).

[4] R. C. Bissel and P. C. Johnson, Phys. Fluids **30**, 779 (1987).

[5] K. Sato, F. Miyawaki, and W. Fukui, Phys. Fluids B **1**, 725 (1989).

[6] M. A. Hussein and G. A. Emmert, Phys. Fluids B **2**, 218 (1990).

[7] T. Takizuka, K. Tani, M. Azumi, and K. Shimizu, J. Nucl. Mater. **128 & 129**, 104 (1984).

[8] K.-U. Riemann, Phys. Fluids B **1**, 961 (1989).

[9] K.-U. Riemann, J. Phys. D : Appl. Phys. **24**, 493 (1991).

CHAPTER 4

Potential Formation in a Collisionless Plasma Flowing out through the Magnetic Throat

4.1 INTRODUCTION

The problem of calculating the electrostatic potential in plasma flow along spatially varying magnetic field lines to a wall arises in various fusion devices as well as in plasma processing techniques. Knowledge of the electrostatic potential profile in a collisionless plasma is necessary to understand the behavior of plasmas in the end region of mirror machines [1,2], in the edge layer of field-reversed configurations [3], or in the divertor of toroidal herical systems [4]. Moreover, knowledge of the potential variation is the key to knowing parameters of a plasma for design of a direct energy convertor and for evaluation of its efficiency [5-7]. This problem is also interest in connection with high temperature divertor plasma operation of a toroidal magnetic fusion system aiming at confinement improvement and reduction of the heat load on a plate [8].

The problem of the potential formation in plasma flow to a wall has drawn attention since the first kinetic analysis in the context of discharge plasmas was done by Tonks and Langmuir in 1929 [9]. Progress of the theoretical treatment of this problem has been made by a number of workers over many years [10-12]. An important aspect of a plasma flowing to a wall that remained ignored in these previous works, however, is spatial variation of the magnetic field strength along field lines, which provide the presheath mechanism through divergence of particle flux and conversion of kinetic energy perpendicular to field lines into parallel kinetic energy.

The characteristics of plasma axial flow through a magnetic mirror was investigated using a fluid computer code by Rognlien and Brengle [13]. Calculations were made for several explicit examples to study the behavior of plasma flow. It requires a kinetic treatment to verify characteristics of the potential formed in a plasma escaping through a nonuniform magnetic field in detail. There have been several kinetic models which consider the potential profile along spatially varying magnetic field lines in mirror systems in order to evaluate the thermal barrier depth [14,15] and the height of the plug potential [16], but, these models are not applicable to a plasma escaping through the mirror throat to a wall. Recently, a plasma originating from ionization of warm neutrals in a divergent magnetic field was treated with kinetic analyses [17-19]. Their analyses provide an important basis for the study of potential formation in a plasma mainly produced by recycling of the neutral gas, such as a plasma in the divertor chamber of a toroidal system.

In this chapter, we investigate the characteristics of the potential in collisionless

plasma flow along spatially varying magnetic field lines to a wall using a kinetic treatment. Ionization of neutrals is assumed to be neglected. We derive necessary conditions to be satisfied for the formation of a monotonically falling potential due to nonuniformity of the magnetic field in a plasma flowing out through the magnetic throat. Moreover, we numerically solve Poisson's equation for model distribution functions to examine the potential formation along magnetic field lines. We also consider the effect of trapped electrons on the presheath potential and briefly discuss the controllability of the potential by the combination of a spatially varying magnetic field and the electron cyclotron heating.

The outline of the chapter is as follows. Formation of the presheath potential due to nonuniformity of the magnetic field is described by using the quasi-neutrality approximation of the plasma in Sec. 4.2. Model distribution functions of ions and electrons are picked out to obtain the expression of the plasma-sheath equation in Sec. 4.3. Results of numerical calculations are presented and discussed in Sec. 4.4. The conclusions are summarized in Sec. 4.5

4.2 FORMATION OF A MONOTONICALLY FALLING POTENTIAL

A spatially varying magnetic field provides formation mechanism of the presheath potential through divergence of the particle flux and acceleration of plasma particles by the parallel component of the Lorentz force. We consider a simple profile of magnetic

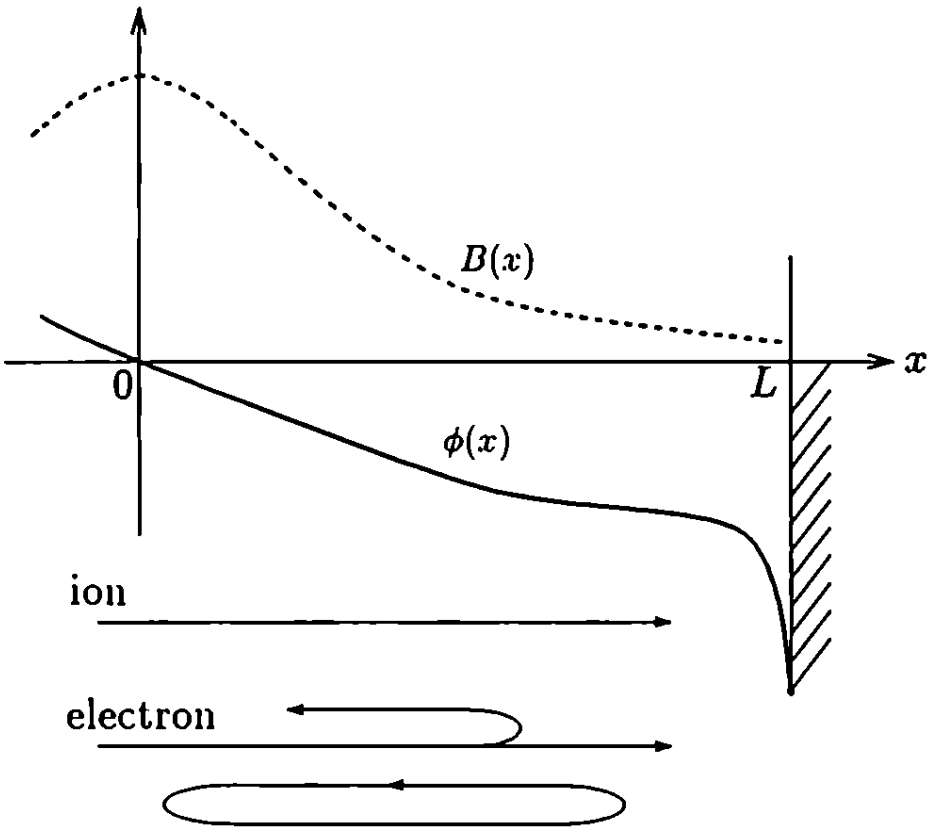

FIG. 4.1. Schematic diagram of the magnetic field profile (dotted line) and the electrostatic potential profile (solid line) in the open region. Typical paths of particles are schematically shown in the region between the mirror throat and the floating wall.

field strength as sketched in Fig. 4.1. Plasma particles coming out through the magnetic throat at $x = 0$ receive the force from the expanding magnetic field which accelerate them towards the wall located at $x = L$, and their density drops accordingly. Ions escaping from the throat are accelerated both by the magnetic field and by the electrostatic potential. Most of electrons in the open region, which consist of electrons passing through the magnetic throat and electrons trapped between the throat and the wall, are reflected by the potential $\phi(x)$. A plasma is neutralized at the wall, which is perfectly absorbing and electrically floating. The ion motion is assumed to be collisionless on the scale length of the magnetic field variation. We also neglect a particle source outside the throat, assuming the particle density of a plasma originating in the outer region much smaller than the one of the plasma flowing through the throat.

The distribution functions of ions and electrons satisfy the Vlasov equation. Thus we can generally express the steady-state distribution function as a function of constants of motion on the assumption of no particle source. The energy of a particle,

$$\varepsilon = \frac{1}{2} m_j (v_\perp^2 + v_\parallel^2) + q_j \phi(x) \quad , \tag{4.1}$$

is a constant of motion, where m_j is the mass, q_j is the charge, and $v_\perp$ and $v_\parallel$ are the perpendicular and parallel components of velocity. The electrostatic potential formed in the plasma, $\phi(x)$, is defined as zero at $x = 0$. The magnetic moment,

$$\mu = \frac{1}{2} m_j v_\perp^2 R(x)/B_0 \quad , \tag{4.2}$$

is taken as a constant of motion, like ϵ, where the mirror ratio $R(x)$ is the ratio of the magnetic field strength B_0 at $x = 0$ to the local value $B(x)$ at axial coordinate x. The subscript 0 denotes the value at $x = 0$ throughout this chapter.

Particle density of species j is obtained as a function of $\phi(x)$ and $R(x)$ by integrating the distribution function $f_j(\epsilon, \mu)$ over the velocity space,

$$n_j(\phi(x), R(x)) = \int f_j(\epsilon, \mu) d^3v.$$

The particle density of a plasma with no particle source is expressed by a function not explicitly dependent on x, but implicitly dependent on x through $\phi(x)$ and $R(x)$. The particle density $n_i(\phi(x), R(x))$ always has a form different from $n_e(\phi(x), R(x))$ even if the distribution function $f_i(\epsilon, \mu)$ is the same as $f_e(\epsilon, \mu)$, because the sign of the ion charge, $q_i = Ze$, is opposite to that of the electron charge, $q_e = -e$. Here Z is the charge number of ions. The electrostatic potential is determined, in general, from Poisson's equation

$$\nabla^2\phi = e\Big[n_e\big(\phi(x), R(x)\big) - Zn_i\big(\phi(x), R(x)\big)\Big]/\epsilon_0 \tag{4.3}$$

if the profile of $R(x)$ is imposed externally. One can see that, as long as the characteristic scale length, L_c, for potential variation is large compared to the Debye length λ_D, the solution for $\phi(x)$ obtained from Eq. (4.3) is well approximated by the one obtained from the quasi-neutral approximation $Zn_i - n_e = 0$. The two solutions differ by $O(\lambda_D^2/L_c^2)$ and the solution to Eq. (4.3) satisfy charge-neutrality to the same order. Differentiating $Zn_i - n_e = 0$ with respect to x, we obtain

$$\frac{\partial(Zn_i - n_e)}{\partial\phi}\frac{d\phi(x)}{dx} + \frac{\partial(Zn_i - n_e)}{\partial R}\frac{dR(x)}{dx} = 0 \quad . \tag{4.4}$$

Then, if there is no singular point, we can determine the potential $\phi(x)$ over the entire region except for the sheath region from the differential equation

$$\frac{d\phi(x)}{dx} = -\frac{\partial(Zn_i - n_e)/\partial R}{\partial(Zn_i - n_e)/\partial\phi}\frac{dR(x)}{dx} \quad , \tag{4.5}$$

once we give the magnetic field profile by a function of x.

We first consider the potential formation in the open region between the magnetic throat and the wall using Eq. (4.5). Some electrons in the open region are trapped by a well of the effective potential $\mu B_0/R(x) - e\phi(x)$ as illustrated in Fig. 4.1. Since the value of $\partial(Zn_i - n_e)/\partial R$ in Eq. (4.5)depends on a ratio of trapped- to reflected-electron density, trapped electrons will have considerable effects upon the potential formation in the plasma. The trapped-electron density, in general, becomes large with increasing the mirror ratio $R(x)$ in the same manner as the confined-ion density in a mirror system, while the particle density of escaping ions and that of passing electrons drop in inverse proportion to $R(x)$. One can easily see that $\partial(Zn_i - n_e)/\partial R$ is always negative for an isotropic electron distribution function such as a Maxwellian, which fully fills the trapped region of velocity space, because the electron density is independent of R for an isotropic distribution function. The derivative $\partial(Zn_i - n_e)/\partial R$ is negative in the whole range of R for all but very small trapped-electron densities. In this case, we obtain a monotonically falling solution $\phi(x)$ to Eq. (4.5)continuing from $x = 0$ to $x = L$, if the

derivative $\partial(Zn_i - n_e)/\partial\phi$ is negative throughout the open region. This solution satisfies a necessary condition for the formation of the stable sheath potential just in front of the wall, which is expressed by $\partial(Zn_i - n_e)/\partial\phi \leq 0$. The derivative $\partial(Zn_i - n_e)/\partial R$ can have a positive value for very small trapped-electron densities, and then a monotonically falling solution is obtained if the derivative $\partial(Zn_i - n_e)/\partial\phi$ is positive for $x > 0$. We, however, can exclude such a solution because it does not satisfy the necessary condition for the sheath formation at the plasma-sheath boundary.

The inequality $\partial(Zn_i - n_e)/\partial\phi \leq 0$ for the formation of a monotonically falling potential gives the restriction to the ion distribution function. Since ions streaming towards the wall are accelerated by the effective potential $\mu B_0/R(x) + Ze\phi(x)$, all ions move in one direction if particles originating in the open region can be neglected. In this case, the inequality is rewritten in the form [20]

$$\frac{Ze}{M}\int_0^\infty dv_\parallel \frac{f_i(v_\parallel)}{v_\parallel^2} \leq \frac{\partial n_e}{\partial\phi} \tag{4.6}$$

by using the ion distribution function, where M is the ion mass. The expression (4.6) agrees with the generalized Bohm criterion for the stable sheath formation presented by Harrison and Thompson [10] when the electron distribution function is a Maxwellian with temperature T_e. It is well known that the generalized Bohm criterion is satisfied only if the ion drift velocity is supersonic. Thus, the ion drift velocity in the outer region of the throat is larger than the ion acoustic velocitity when a monotonically falling potential builds up. Since the derivative $\partial n_e/\partial\phi$ is always finite for a continuous

electron distribution function, the ion distribution function f_i must be zero at $v_{\parallel} = 0$ to have a finite value of the integral in expression (4.6). On the other hand, the ion distribution function in the interior of the throat is expected to be continuous at the separatrix which divides the trapped from the passing region of velocity space, provided trapped ions exist inside the throat. These facts mean that the passing ions must be accelerated in the inside region close to the throat before their arrival at the throat so as to satisfy criterion (4.6).

Next, we consider the potential formation at the inner region close to the throat where the trapped-ion density is smaller than the passing-ion density. The electron distribution function in the inner region is expected to approach a Maxwellian due to scattering inside the throat. Since the derivative $\partial(Zn_i - n_e)/\partial R$ in Eq. (4.5)has a finite negative value in such a region, the sign of $\partial(Zn_i - n_e)/\partial\phi$ to be opposite to that of $dR(x)/dx$ for the formation of a monotonically varying potential must change from positive to negative at $x = 0$ as x increases. Consequently, it is found that a monotonically decreasing potential, which is necessary to accelerate ions, can build up in the vicinity of the throat only if criterion (4.6) is fulfilled with equality at $x = 0$.

We briefly discuss the potential formed in the inner region of the magnetic throat such as the plug cell of a tandem mirror system. In the inner region at a distance from the throat, where the trapped-ion density is much larger than the passing-ion density, in general, the derivative $\partial(Zn_i - n_e)/\partial\phi$ is negative and the derivative $\partial(Zn_i - n_e)/\partial R$ is positive. On the contrary, $\partial(Zn_i - n_e)/\partial\phi$ is positive and $\partial(Zn_i - n_e)/\partial R$ is negative just in front of the throat, as mentioned above. It is seen from this fact that there must

be a saddle point in the intermediate region where the trapped-ion density becomes comparable with the passing-ion density if a monotonically varying potential builds up over the entire region. Equations $Zn_i - n_e = 0$, $\partial(Zn_i - n_e)/\partial\phi = 0$ and $\partial(Zn_i - n_e)/\partial R = 0$ hold true at the saddle point simultaneously. Existence of such a saddle point will severely restricts distribution functions of the plasma. It is an open problem as to whether the steady-state continuous potential with a monotonically falling profile can build up or not throughout the system. It is difficult to calculate the spatial profile of $\phi(x)$ over the entire region using a kinetic treatment, because one must solve the Vlasov-Poisson equation self-consistently, determining the separatrix in velocity space under the consideration of ion motion in a nonuniform magnetic field.

4.3 MODEL DISTRIBUTION FUNCTIONS

We need to express the distribution function of electrons and ions in order to calculate the axial potential profile between the magnetic throat and the wall and the one in the vicinity of the throat. We unfortunately don't know any kinetic analyses which calculate the distribution function of ions escaping through the magnetic throat, while many calculations for confined ions have been carried out by using Fokker-Planck code. There are difficulties in determining the distribution function of the escaping plasma and the potential profile near the magnetic throat self-consistently. The particle density of ions varies along magnetic field lines through divergence of the particle flux and

acceleration by the effective potential $\mu B_0/R(x)+Ze\phi(x)$. Ion flow dynamics will roughly be described by using a drift, a spread and anisotropy of f_i. Then we choose a model distribution function for escaping ions given by

$$f_i(\varepsilon,\mu) = \frac{2n_0/Z}{\mathrm{erfc}\left[(\varepsilon_c/kT_{i\parallel})^{1/2}\right]}\left(\frac{M}{2\pi kT_{i\parallel}}\right)^{1/2}\left(\frac{M}{2\pi kT_{i\perp}}\right)$$
$$\times \exp\left(-\frac{\varepsilon-\mu B_0}{kT_{i\parallel}}\right)\exp\left(-\frac{\mu B_0}{kT_{i\perp}}\right)h(\varepsilon-\mu B_0-\varepsilon_c) \quad . \tag{4.7}$$

Here $\mathrm{erfc}(y)$ is the complementary error function and $h(y)$ is the Heaviside unit function defined by

$$h(y) = \begin{cases} 1 & , \ y \geq 0 \\ 0 & , \ y < 0 \end{cases}$$

The cutoff energy $\varepsilon_c > 0$ is introduced so as to maintain the finiteness of the integral in criterion (4.6), and the parallel temperature $T_{i\parallel}$ and the perpendicular temperature $T_{i\perp}$ are brought in to express a spread and anisotropy of the distribution function at the magnetic throat. Level surfaces of this model distribution function in $v_\parallel - v_\perp$ space at $R = 2$ and $-e\phi/kT_e = 1.7$ are shown in Fig. 4.2(a).

Electrons were assumed to be Maxwellian in almost all the previous analyses on the sheath formation[9-12,17-19]. The distribution function of electrons trapped in the expanding open magnetic field with large mirror ratio will, however, has a form different from that of electrons passing through the magnetic throat provided the interaction between them is weak. Since trapped electrons are expected to have considerable effects

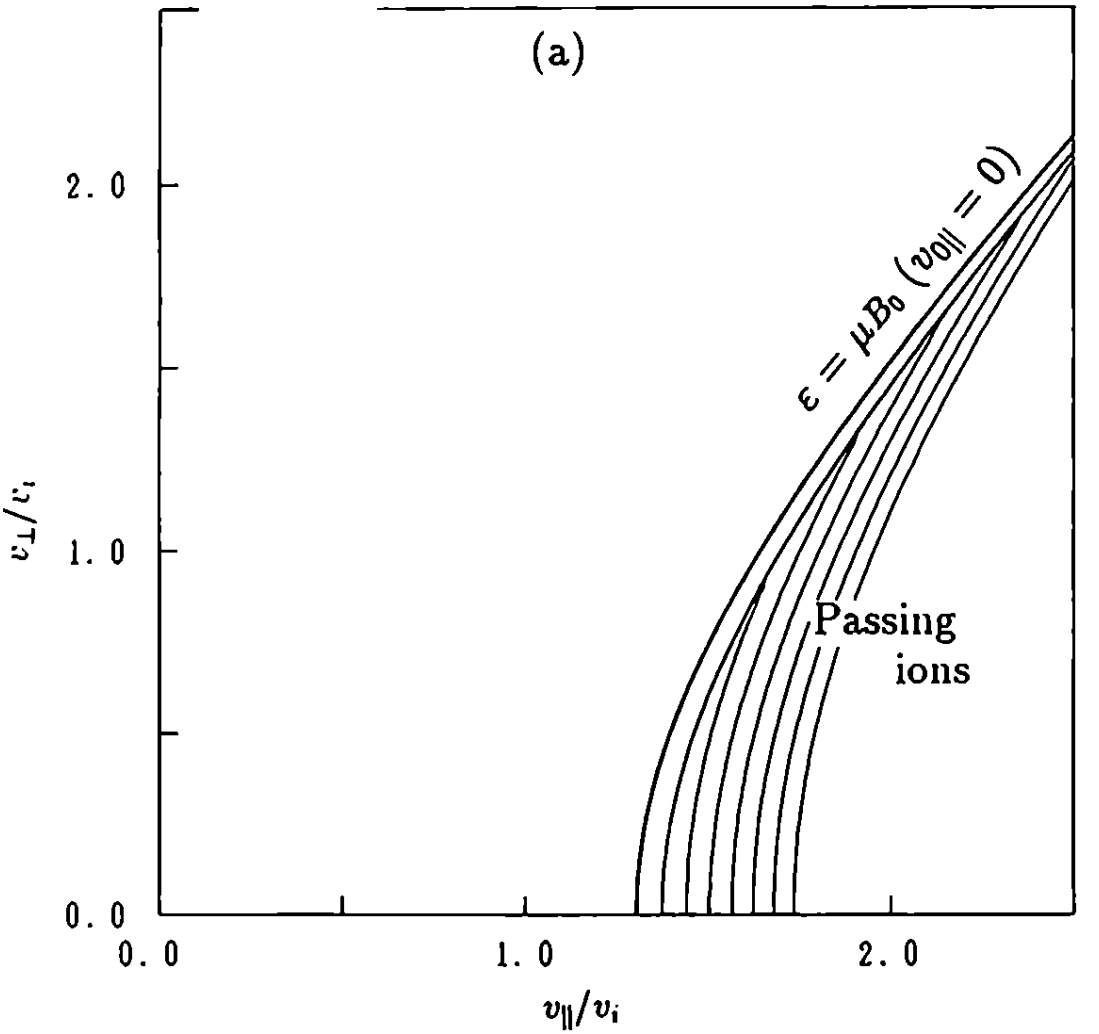

FIG. 4.2(a). Level surfaces at $R = 2$ and $e\phi/kT_e = -1.7$ for the model ion distribution function f_i given by Eq. (4.7) with $\varepsilon_c/kT_e = 0.187$, $T_{i\parallel} = T_e$ and $T_{i\perp} = 10T_e$. Here v_i is the parallel ion thermal velocity. Ratio of f_i on adjacent contours is 0.79.

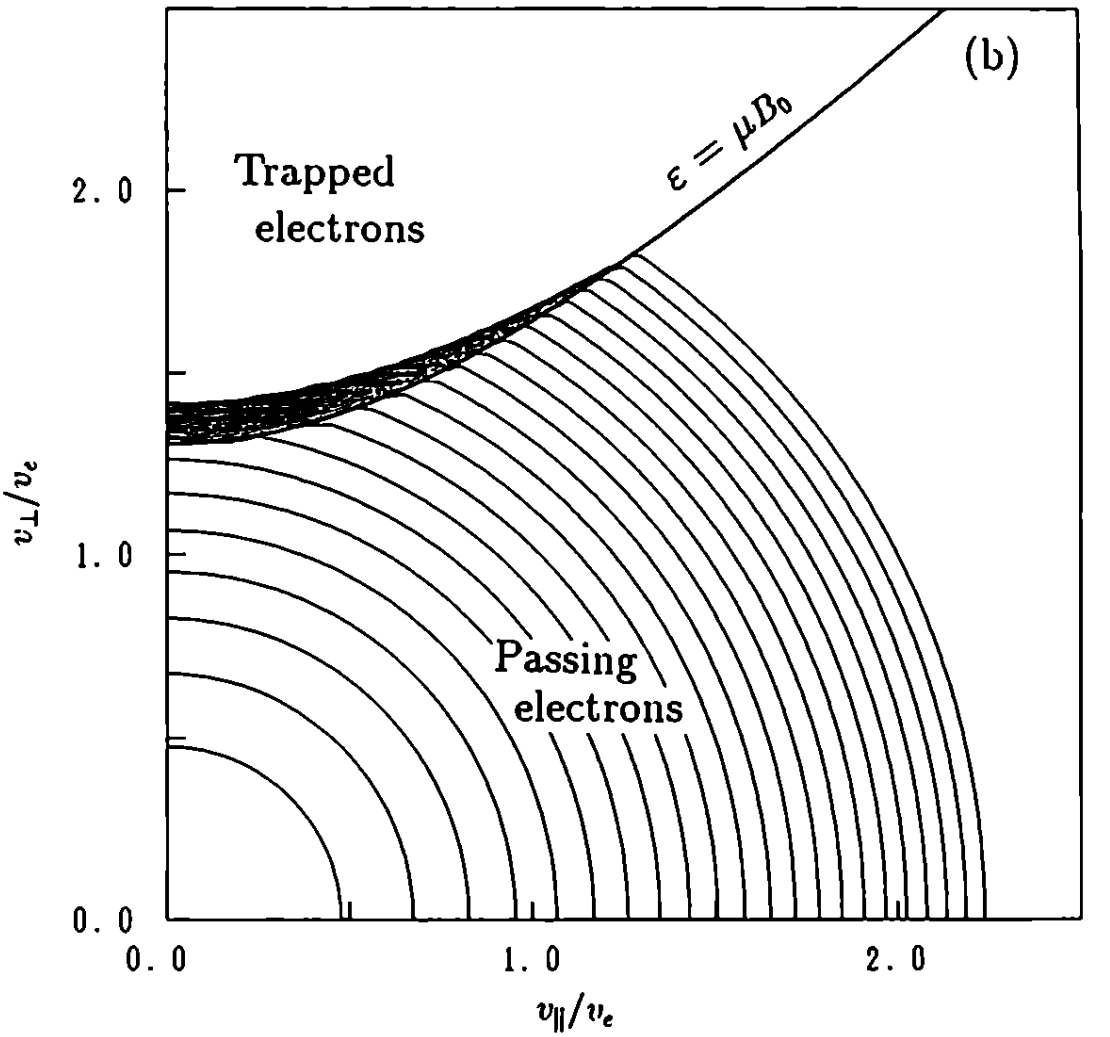

FIG. 4.2(b). Level surfaces at $R = 2$ and $e\phi/kT_e = -1.7$ for the model electron distribution function f_e given by Eq. (4.8) with $\alpha = 10$. Here v_e is the electron thermal velocity. Ratio of f_e on adjacent contours is 0.79.

on the potential formation as mentioned in the previous section, we distinguish the distribution function in the trapped region from that in the passing region of velocity space. The passing electrons are subject to relaxation inside the magnetic throat, thus we assume the distribution function in the passing region to be Maxwellian. Since the trapped electrons are supplied through scattering of the passing electrons, the distribution function must be continuous at the separatrix which divides the trapped from the passing region of velocity space. We pick a model distribution function for the electrons in the form

$$f_e(\varepsilon,\mu) = n_0 \left(\frac{m}{2\pi k T_e}\right)^{3/2} \exp\left(-\frac{\varepsilon}{kT_e}\right) g\left(\frac{\varepsilon - \mu B_0}{kT_e}\right), \tag{4.8}$$

which is continuous over the velocity space. Here m is the electron mass and the function $g(y)$ is defined by

$$g(y) = \begin{cases} 1 & , \ y \geq 0 \\ \exp(\alpha y) & , \ y < 0 \end{cases}$$

The reciprocal of the parameter α describes the degree to which the trapped-electron phase space, $\varepsilon - \mu B_0 < 0$, is filled in : $\alpha = 0$ corresponds to Maxwellian trapped electrons ; and increasing α from 0 to ∞ describes successively smaller numbers of trapped electrons. Level surfaces of the model electron distribution function with $\alpha = 10$ at $R = 2$ and $-e\phi/kT_e = 1.7$ are shown in Fig. 4.2(b).

The particle density of species j is obtained as functions of ϕ and R by integrating f_j over the velocity space. The resulting expression of the ion density is written in a relatively simple form

$$n_i(\phi, R) = \frac{n_0/Z}{\exp\left(\frac{\varepsilon_c}{kT_{i\parallel}}\right)\operatorname{erfc}\left[\left(\frac{\varepsilon_c}{kT_{i\parallel}}\right)^{1/2}\right]} \frac{T_{i\parallel}/T_{i\perp}}{1+\left(T_{i\parallel}/T_{i\perp}-1\right)R}$$

$$\times\left\{\exp\left(\frac{\varepsilon_c - Ze\phi}{kT_{i\parallel}}\right)\operatorname{erfc}\left[\left(\frac{\varepsilon_c - Ze\phi}{kT_{i\parallel}}\right)^{1/2}\right]\right.$$

$$\left.-\left(\frac{R-1}{R}\frac{T_{i\parallel}}{T_{i\perp}}\right)^{1/2}\exp\left(\frac{R}{R-1}\frac{\varepsilon_c - Ze\phi}{kT_{i\perp}}\right)\operatorname{erfc}\left[\left(\frac{R}{R-1}\frac{\varepsilon_c - Ze\phi}{kT_{i\perp}}\right)^{1/2}\right]\right\}, \tag{4.9}$$

and the electron density is

$$n_e(\phi, R) = n_0\left[\exp\left(\frac{e\phi}{kT_e}\right) - \frac{\alpha(R-1)}{1+\alpha(R-1)}\left(\frac{R-1}{R}\right)^{1/2}\exp\left(\frac{R}{R-1}\frac{e\phi}{kT_e}\right)\right]. \tag{4.10}$$

The mean drift velocity of ions is also obtained as a function of ϕ and R in the form

$$V_i(\phi, R) = \left(\frac{2kT_{i\parallel}}{\pi M}\right)^{1/2}\left[1-\frac{R-1}{R}\frac{T_{i\perp}}{T_{i\parallel}}\right]\left\{\exp\left(\frac{\varepsilon_c - Ze\phi}{kT_{i\parallel}}\right)\operatorname{erfc}\left[\left(\frac{\varepsilon_c - Ze\phi}{kT_{i\parallel}}\right)^{1/2}\right]\right.$$

$$\left.-\left(\frac{R-1}{R}\frac{T_{i\perp}}{T_{i\parallel}}\right)\exp\left(\frac{R}{R-1}\frac{\varepsilon_c - Ze\phi}{kT_{i\perp}}\right)\operatorname{erfc}\left[\left(\frac{R}{R-1}\frac{\varepsilon_c - Ze\phi}{kT_{i\perp}}\right)^{1/2}\right]\right\}^{-1}. \tag{4.11}$$

These expressions are continuous and differentiable with respect to R and ϕ, and then we can determine the presheath potential owing to nonuniformity of the magnetic field from Eq. (4.5) if the profile of the magnetic field strength is given by a function of x externally.

The ion flux per magnetic flux tube with unit cross section at the throat is given by

$$\Gamma_i = \frac{n_0}{Z}\left(\frac{2kT_{i\parallel}}{\pi M}\right)^{1/2}\left\{\exp\left(\frac{\varepsilon_c}{kT_{i\parallel}}\right)\mathrm{erfc}\left[\left(\frac{\varepsilon_c}{kT_{i\parallel}}\right)^{1/2}\right]\right\}^{-1}, \tag{4.12}$$

and the electron flux is

$$\Gamma_e = \frac{n_0}{2}\left(\frac{2kT_e}{\pi m}\right)^{1/2}\left[R_L\exp\left(\frac{e\phi_w}{kT_e}\right) - \frac{\alpha(R_L-1)^2}{1+\alpha(R_L-1)}\exp\left(\frac{R_L}{R_L-1}\frac{e\phi_w}{kT_e}\right)\right], \tag{4.13}$$

where R_L is the mirror ratio at $x = L$. The wall potential ϕ_w in Eq. (4.12), which is one of two boundary conditions to solve Poisson's equation, is uniquely determined by imposing the umbipolarity of the fluxes, $Z\Gamma_i = \Gamma_e$.

4.4 NUMERICAL RESULTS AND DISCUSSION

To examine the potential formation, we consider two type of plasmas in the present paper. One is a cold-ion plasma originating from ionization of cold neutrals inside the magnetic throat. We take temperatures as $T_{i\parallel} = 0$ and $T_{i\perp} = 0$ to model such a plasma. Another is a hot-ion plasma escaping from a device like a mirror machine, which is supplied by pitch-angle scattering of a confined plasma. We model the hot-ion plasma, taking $T_{i\parallel} = T_e$ and $T_{i\perp} = 10T_e$. The potential $\phi(x)$ over the entire region except for the sheath region is determined by solving $Zn_i - n_e = 0$ or Eq. (4.5) if the magnetic field profile is imposed externally. A continuous solution of $Zn_i - n_e = 0$ with a monotonically

falling profile exists only if the solution satisfies the inequalities $\partial(Zn_i - n_e)/\partial R \leq 0$ and $\partial(Zn_i - n_e)/\partial\phi \leq 0$ throughout the exterior of the magnetic throat, $x \geq 0$, as described in Sec. II. These inequalities restrict a range of parameters of the model distribution functions given by Eqs. (4.7) and (4.8). Figure 4.3 shows domains in $\alpha - \epsilon_c$ parameter space at any point in which we can obtain a solution of Eq. (4.5) continuous from $x = 0$ to $x = L$. A lower limit of the cutoff energy ϵ_c of the model distribution function for ions, which becomes in dependent of $T_{i\perp}$ and R_L, is evaluated by solving $Zn_i - n_e = 0$ and $\partial(Zn_i - n_e)/\partial\phi = 0$ at R=1 simultaneously. A model plasma with the lower limit of ϵ_c, the plasma marginally satisfies the generalized Bohm criterion expressed by Eq. (4.6) at the throat. An upper limit of the cutoff energy is determined from simultaneous equations $Zn_i - n_e = 0$ and $\partial(Zn_i - n_e)/\partial R = 0$ at $R = R_L$. The upper limit of ϵ_c decreases as α becomes large, that is, as the trapped-electron density decreases. This value also drops with $T_{i\perp}$, taking its minimum value at $T_{i\perp} = 0$.

In order to satisfy the generalized Bohm criterion at $x = 0$, ions coming out through the magnetic throat must have a supersonic drift speed and their distribution function must be zero at $v_{\parallel} = 0$. This fact implies the existence of the monotonically falling potential to accelerate ions in the inner region near the throat. Figures 4.4(a) and 4.4(b) show potential profiles and drift velocity profiles for the cold-ion plasma with various values of the cutoff energy ϵ_c in the vicinity of the throat, respectively. The magnetic field profile is given by $R(Z) = 1 + (R_L - 1)(x/L)^2$ with $R_L = 10$. Figures 4.5(a) and 4.5(b) show results for the hot-ion plasma. The potential $\phi(x)$ is determined by solving Eq. (4.5), which is derived by using the quasi-neutrality approximation, and

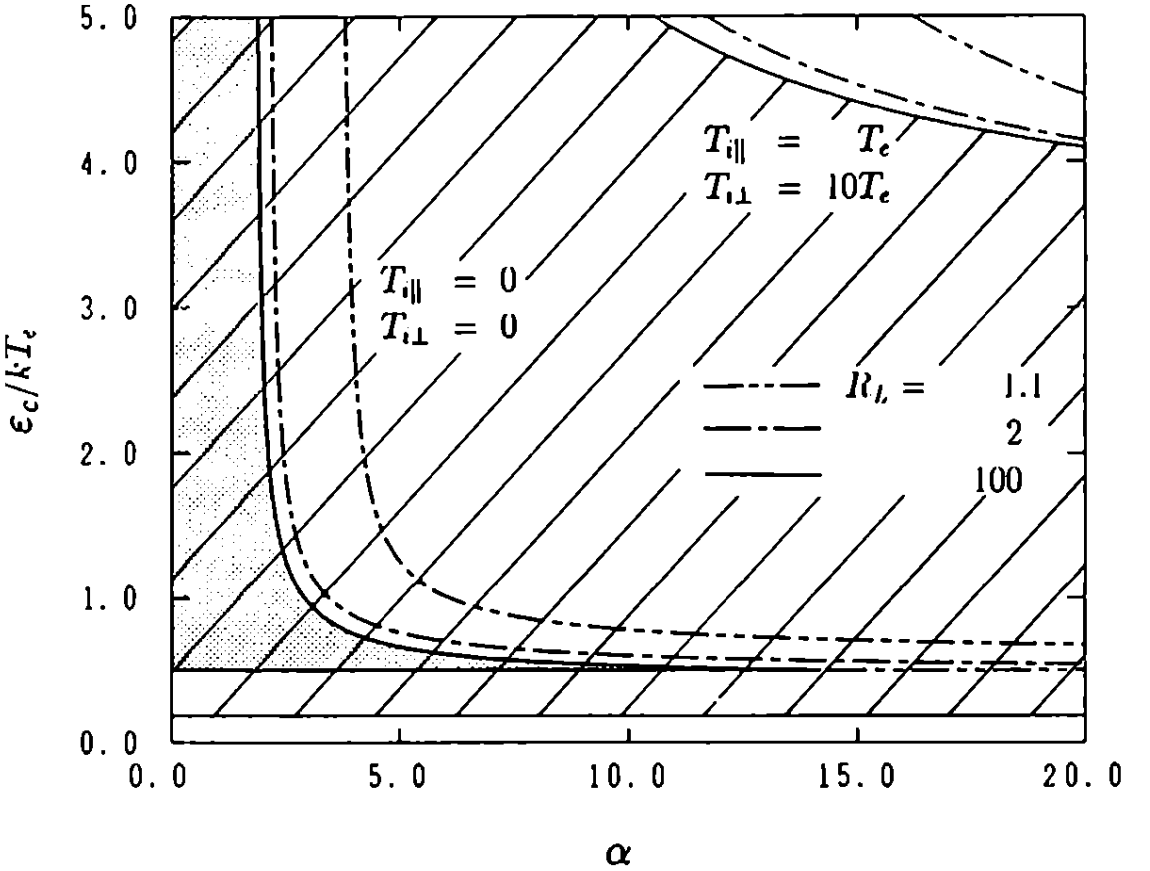

FIG. 4.3. Domain in $\alpha - \varepsilon_c$ space where monotonically varying continuous potential can be formed in the cold-ion plasma with $T_{i\parallel} = 0$ and $T_{i\perp} = 0$, and in the hot-ion plasma with $T_{i\parallel} = T_e$ and $T_{i\perp} = 10T_e$ flowing through expanding magnetic field with various mirror ratios at the wall. Here α is the reducing parameter of the model electron distribution function given by Eq. (4.8) and ε_c is the cutoff energy of the model ion distribution function given by Eq. (4.7).

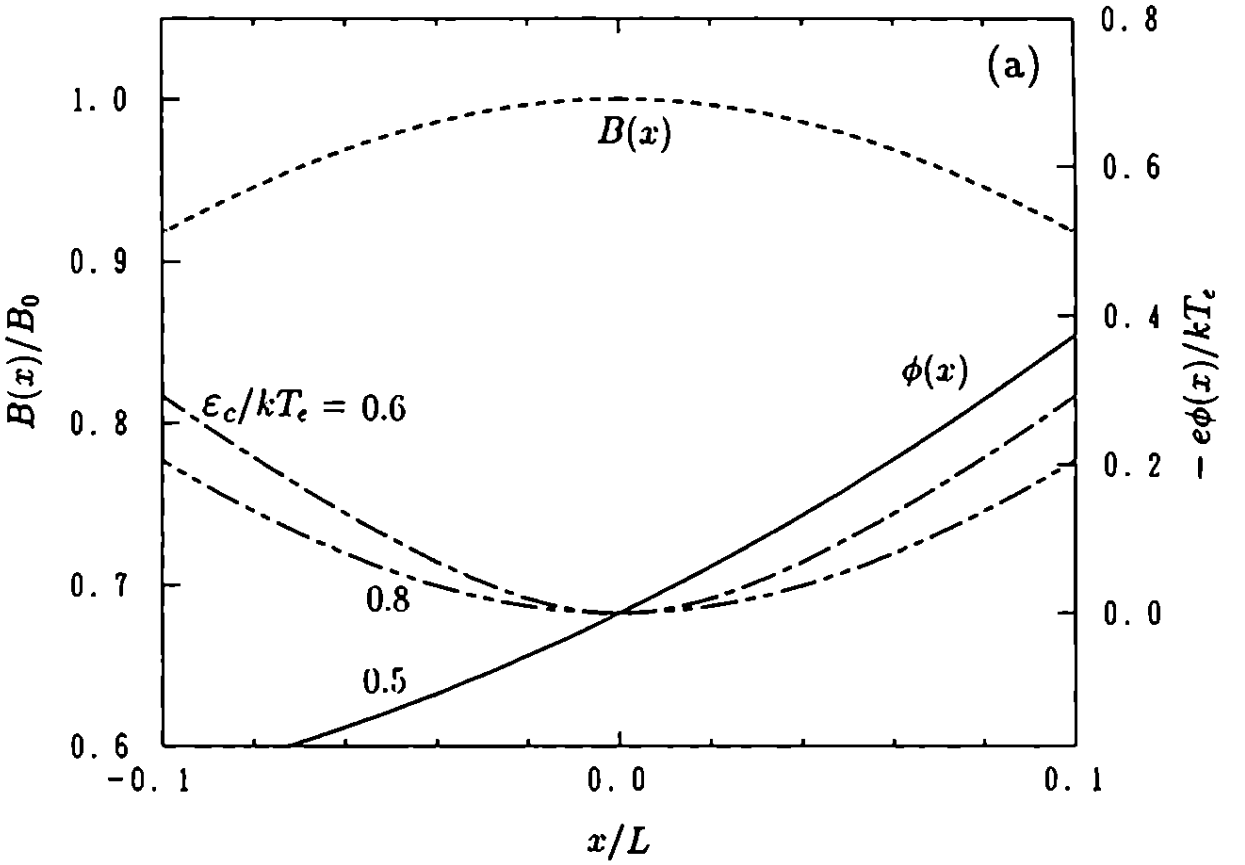

FIG. 4.4(a). Potential profiles in the cold-ion plasma with $T_{i\parallel} = 0$ and $T_{i\perp} = 0$ near the magnetic throat of the model field $B_0/B(x) = 1 + (R_L - 1)(x/L)^2$ with $R_L = 10$. The values of the cutoff energy ε_c are $\varepsilon_c/kT_e = 0.5$, 0.6, and 0.8. The generalized Bohm criterion is marginally satisfied at the throat when $\varepsilon_c/kT_e = 0.5$.

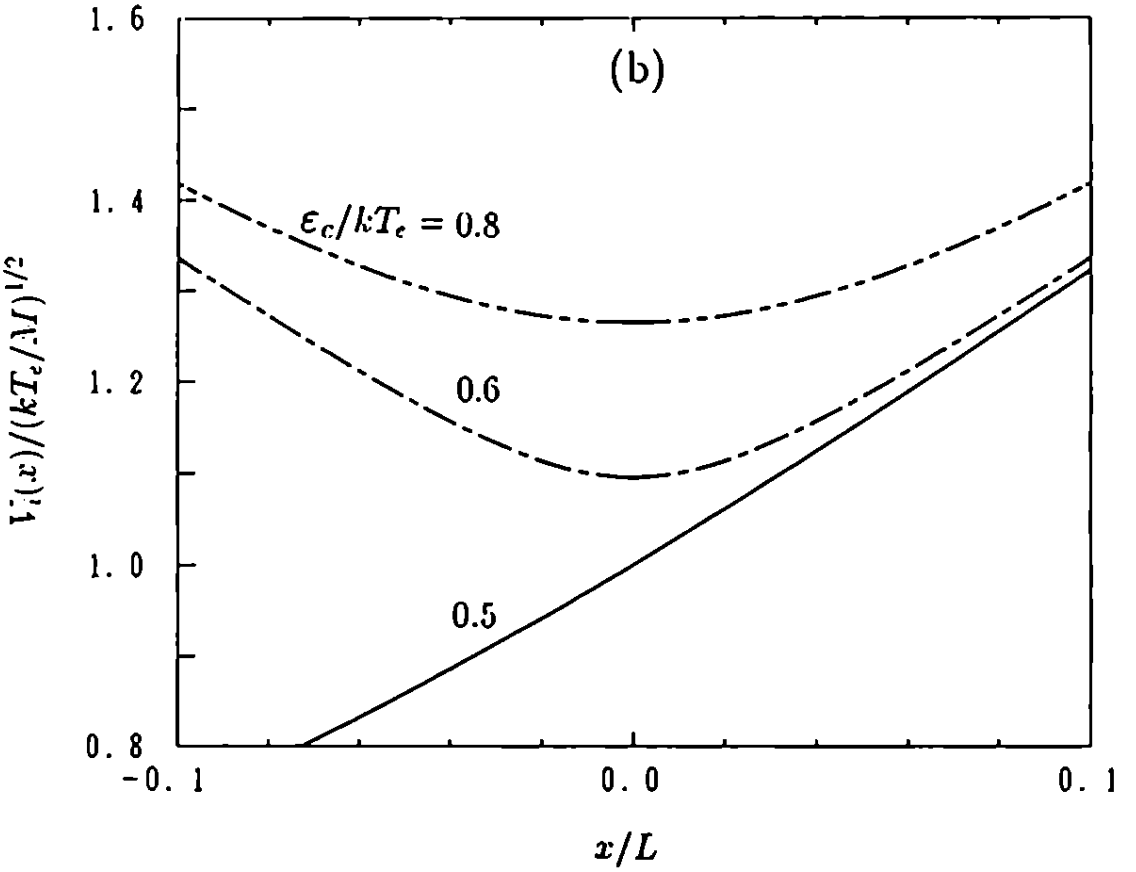

FIG. 4.4(b). Profile of the ion drift velocity of the cold-ion plasma near the magnetic throat of the model field $B_0/B(x) = 1 + (R_L - 1)(x/L)^2$ with $R_L = 10$. The values of the cutoff energy ϵ_c are $\epsilon_c/kT_e = 0.5$, 0.6, and 0.8.

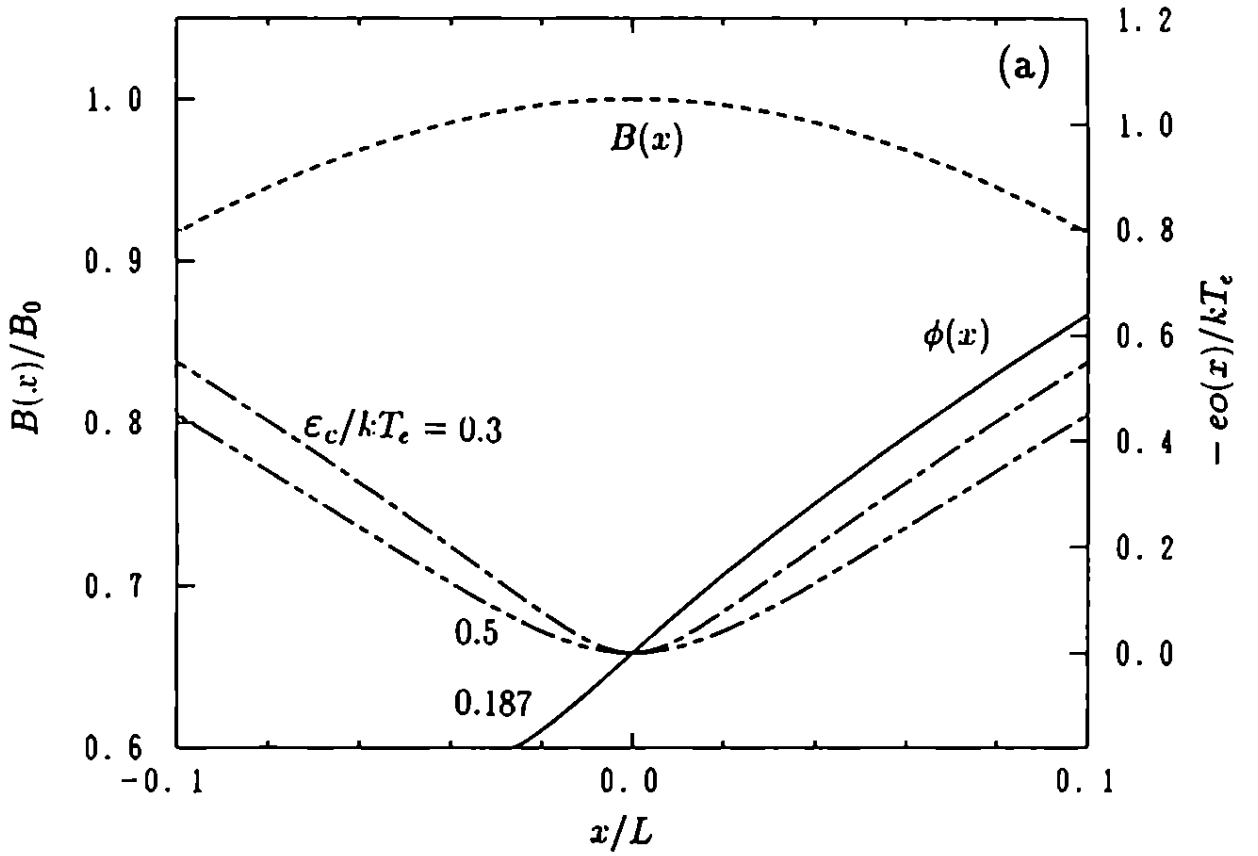

FIG. 4.5(a). Potential profile in the hot-ion plasma with $T_{i\parallel} = T_e$ and $T_{i\perp} = 10T_e$ near the magnetic throat of the model field $B_0/B(x) = 1 + (R_L - 1)(x/L)^2$ with $R_L = 10$. Values of the cutoff energy ε_c are $\varepsilon_c/kT_e = 0.187$, 0.3 and 0.5. The generalized Bohm criterion is marginally satisfied at the throat when $\varepsilon_c/kT_e = 0.187$.

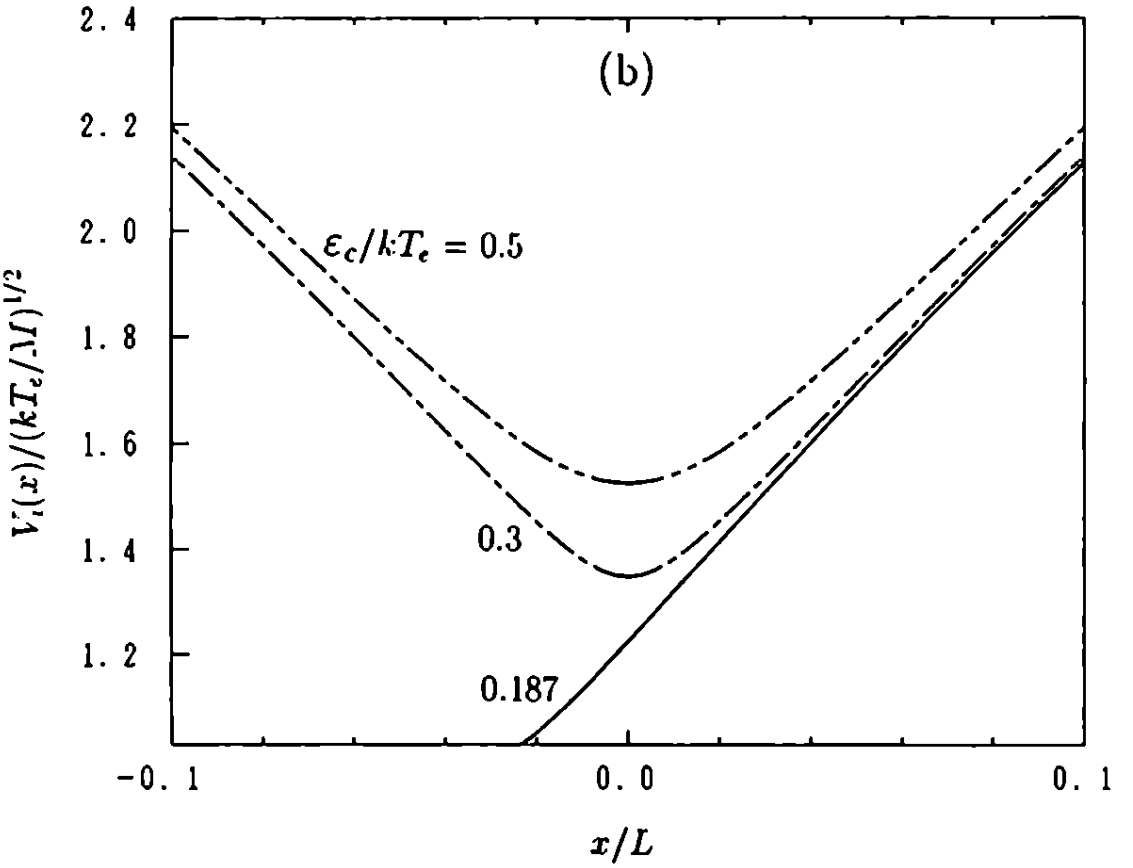

FIG. 4.5(b). Profiles of the ion drift velocity of the hot-ion plasma near the magnetic throat of the model field. The values of the cutoff energy ϵ_c are $\epsilon_c/kT_e = 0.187$, 0.3, and 0.5.

the drift velocity $V_i(x)$ is obtained from Eq. (4.11). We ignored ions trapped inside the throat in this calculation, assuming that their density, which vanishes at $x = 0$, is much smaller than the passing-ion density near the throat. Calculating results confirm the fact described in Sec. II, that is, a monotonical potential profile builds up only if the generalized Bohm criterion is fulfilled with equality at the throat. For the critical value of the cutoff energy, $\varepsilon_c/kT_e = 0.5$ for the cold-ion plasma or $\varepsilon_c/kT_e = 0.187$ for the hot-ion plasma, the gradient of the potential has a finite value at $x = 0$ nevertheless the gradient of $R(x)$ is zero at the throat. The plasma flow is accelerated from a subsonic velocity to a supersonic velocity, and the sonic transition for the cold-ion plasma occurs at the magnetic throat. The position of sonic transition moves to the inner region as temperature $T_{i\|}$ increases. For cutoff energy larger than the critical value, one can find a continuous potential profile, but it is not monotonical as indicated in Figs. 4.4(a) and 4.5(a). On the contrary, for cutoff energies smaller than the critical value, one cannot obtain a continuous solution.

Although the assumption of quasi-neutrality provides a good approximation for a smoothly varying potential in the plasma, one must numerically solve Poisson's equation to determine a potential profile over the entire region from the throat to the wall. If we approximate the problem as one-dimensional then we replace $\nabla^2\phi$ in Eq. (4.3) by $d^2\phi/dx^2$, and an appropriate set of boundary conditions consists of values of ϕ at the boundaries. The value of ϕ at the throat is defined to be zero and the one at the wall is determined from the umbipolarity of the fluxes expressed by Eqs. (4.12) and (4.13), $Z\Gamma_i = \Gamma_e$. Poisson's equation, Eq. (4.3), can be solved numerically by transforming it

into a set of finite difference equations. We use a solution of Eq. (4.5) to guess an initial set of $\phi(x)$, and ensure sufficient resolution near the wall by introducing a nonuniform grid.

Figures 4.6 and 4.7 show the numerically calculated potential for the cold-ion plasma and for the hot-ion plasma flowing along the model field $R(x) = 1 + (R_L - 1)(x/L)^2$ with $R_L = 10$, respectively. Here the hydrogen plasma with $\lambda_{D0}/L = 0.005$ is assumed. The cutoff energy of the model ion distribution function is chosen as $\epsilon_c/kT_e = 0.5$ for the cold-ion plasma and $\epsilon_c/kT_e = 0.187$ for the hot-ion plasma so as to satisfy the generalized Bohm criterion marginally at the throat. Formation mechanism of the presheath is provided by the magnetic field through particle acceleration and divergence of particle flux. Ions with a finite $T_{i\perp}$ receive the force along field lines from the magnetic field, converting their kinetic energy perpendicular to field lines into parallel kinetic energy. Acceleration of hot ions by this force induces the large potential drop near the magnetic throat. This force does not act upon cold ions with $T_{i\perp} = 0$, and then formation of the presheath potential in the cold-ion plasma is owing to divergent of the particle flux.

The solid curves A, B and C in Fig. 4.6 and D, E and F in Fig. 4.7 show solutions for successively smaller ratios of the trapped- to the total-electron numbers. The density profiles of trapped electrons, passing electrons, and passing ions of the cold-ion plasma for a Maxwellian electron distribution ($\alpha = 0$) are shown in Fig. 4.8. It is seen from Figs. 4.6, 4.7 and 4.8 that the trapped electrons remarkably affect a profile of the presheath potential. For much small trapped-electron densities, a descent of the presheath potential is localized near the magnetic throat, and then the presheath

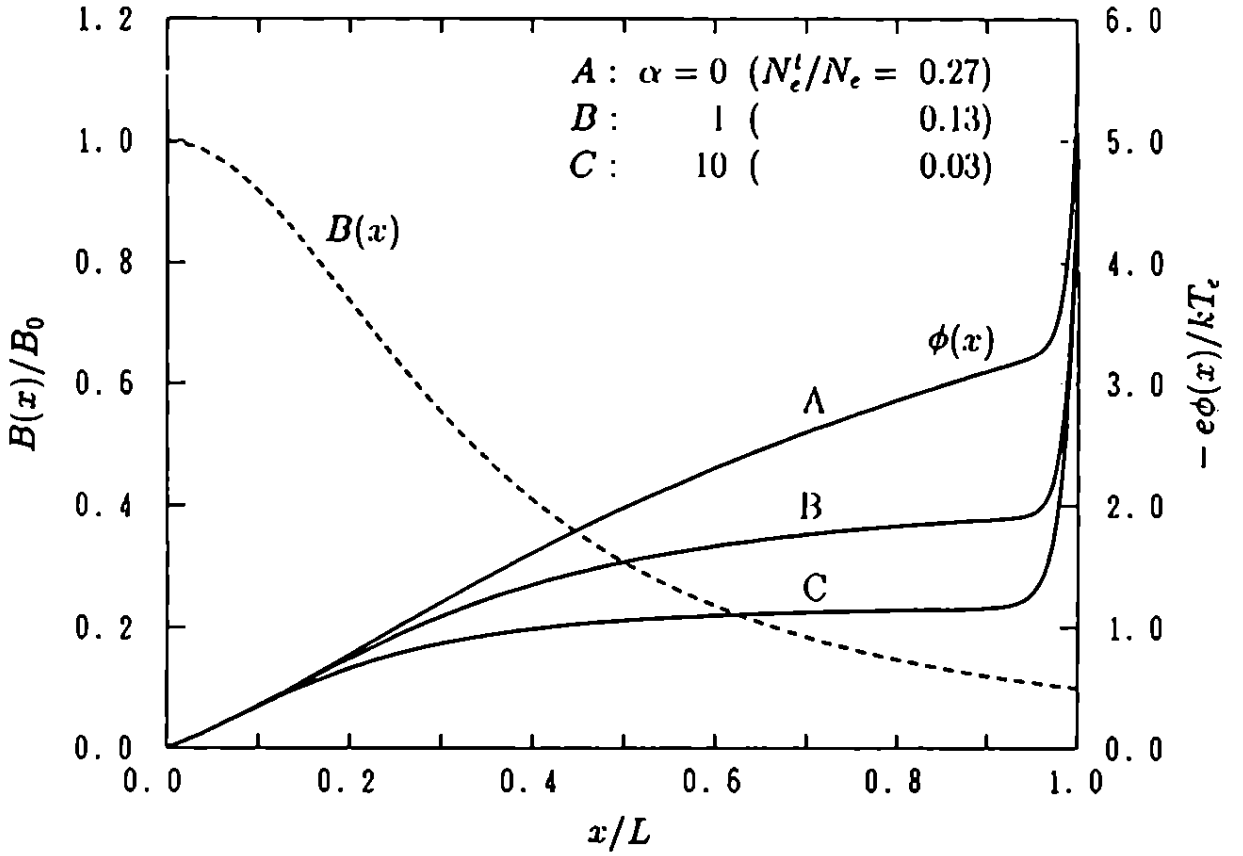

FIG. 4.6. Potential profile $\phi(x)$ in the cold-ion plasma flowing through the model field $B_0/B(x) = 1+(R_L-1)(x/L)^2$ with $R_L = 10$ for various values of the parameter α of the model electron distribution function. Parameters of the model ion distribution function are $\epsilon_c/kT_e = 0.5, T_{i\parallel} = 0$ and $T_{i\perp} = 0$. The values of α and the corresponding ratios of trapped- to total-electron numbers are : (A) $\alpha = 0$, $N_e^t/N_e = 0.27$; (B) $\alpha = 1$, $N_e^t/N_e = 0.13$; (C) $\alpha = 10$, $N_e^t/N_e = 0.03$.

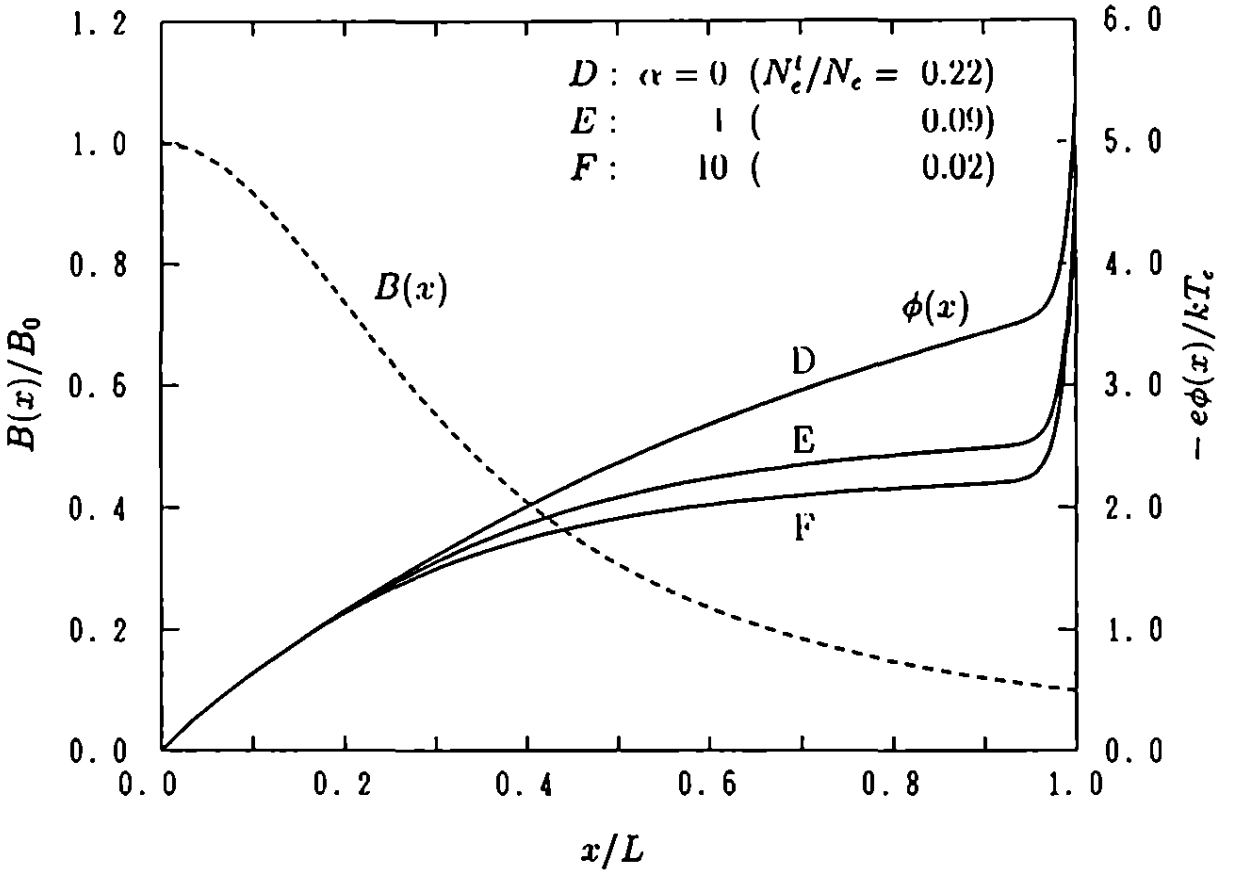

FIG. 4.7. Potential profile $\phi(x)$ in the hot-ion plasma flowing through the model field $B_0/B(x) = 1 + (R_L - 1)(x/L)^2$ with $R_L = 10$ for various values of the parameter α of the model electron distribution function. Parameters of the model ion distribution function are $\epsilon_c/kT_e = 0.187, T_{i\parallel} = T_e$ and $T_{i\perp} = 10T_e$. The values of α and the corresponding ratios of trapped- to total-electron numbers are : (D) $\alpha = 0$, $N_e^t/N_e = 0.22$; (E) $\alpha = 1$, $N_e^t/N_e = 0.09$; (F) $\alpha = 10$, $N_e^t/N_e = 0.02$.

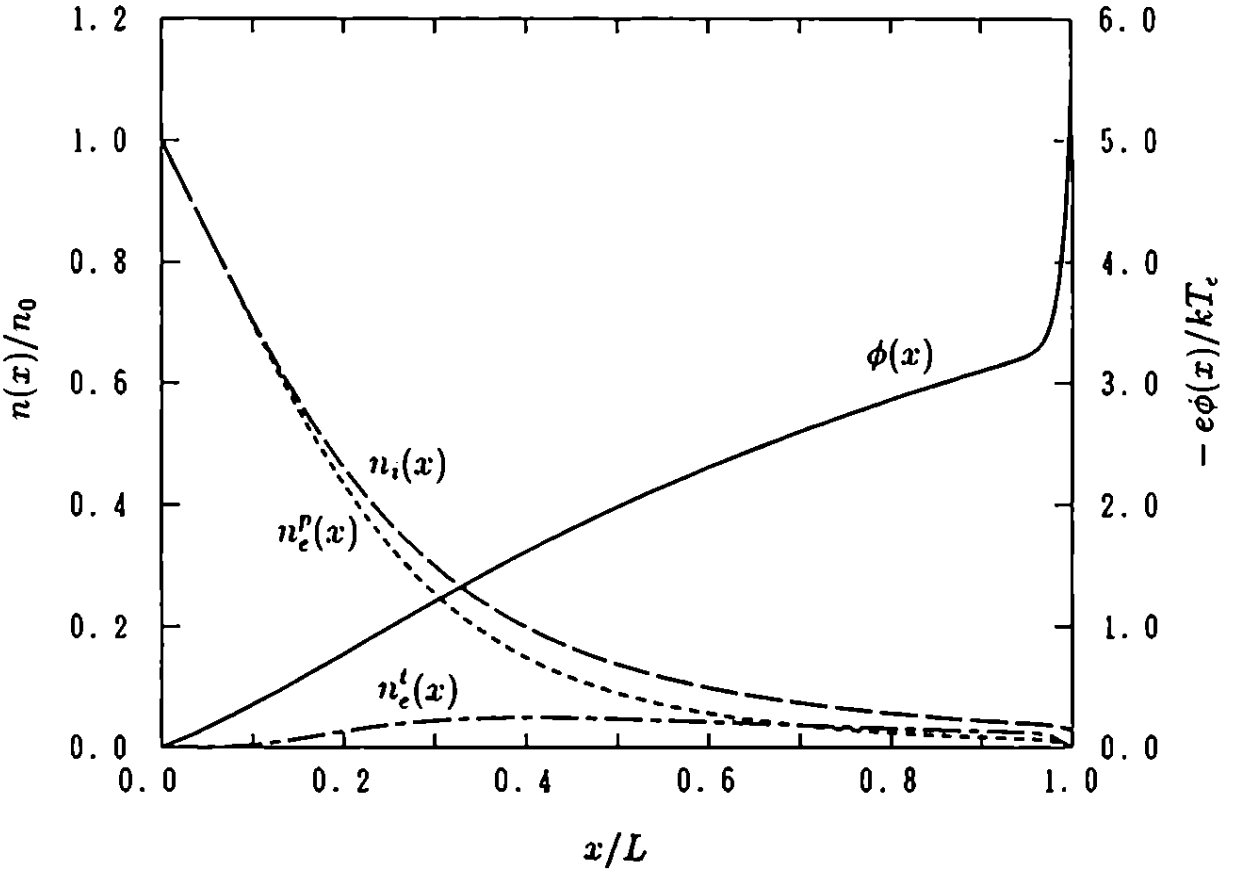

FIG. 4.8. Density profile of ions $n_i(x)$, passing electrons $n_e^p(x)$ and trapped electrons $n_e^t(x)$, and potential profile $\phi(x)$ for the model distribution functions with $\epsilon_c/kT_e = 0.5$, $T_{i\parallel} = 0$, $T_{i\perp} = 0$, and $\alpha = 0$.

potential approaches asymptotically to a constant value as the mirror ratio increases. For large trapped-electron densities, the presheath has a gradually varying potential profile and the potential drop increases with increasing of the mirror ratio. The sheath potential with width several times as large as the Debye length is formed just in front of the wall. The increase of the presheath potential drop due to the existence of trapped electrons leads to the decrease of the sheath potential.

The contribution of trapped electrons to the increase of the presheath potential drop suggests the possibility of effective potential control in the open region by increasing the trapped-electron density through ECRH (electron cyclotron resonance heating) or ionization of neutral gas in the region near the wall. Since the ECRH increases the electron energy perpendicular to magnetic field lines, electrons passing through the mirror throat can be kicked in the trapped region of velocity space by the rf field, and they are trapped until scattering out from the trapped region. In the open region with a large mirror ratio, such as the end region of a tandem mirror, almost all electrons originating from ionization near the wall are trapped in a well of the effective potential $\mu B(x)-e\phi(x)$. Hence, the ionization will contribute to the increase of the presheath potential drop provided the cooling effect of ionization is not so large. The large potential barrier at the presheath inhibits the inflow of high-Z impurity ions from the wall towards a confined plasma. Moreover, it will prevent a remarkable increase of convective electron heat loss due to secondary electron emission from the wall. It is well known that secondary electron emission has a negligibly small influence on the potential drop at the presheath under the condition of a fixed electron temperature, while it remarkably reduces the potential

drop at the sheath [21,22]. Thus, one can expect that the large potential drop at the presheath acts as a thermal insulator in place of the sheath potential when a large number of electrons are trapped in the open region of a system such as a tandem mirror, even if the sheath potential drop is reduced to a small value due to secondary electron emission. The ECRH power necessary to maintain the trapped-electron density is expected to be small compared with the convective electron heat outflow if the collision frequency is much smaller than the one inside the throat. A precise calculation considering the power balance of a plasma are necessary to make sure of the possibility of potential control.

4.5 CONCLUSIONS

We have investigated formation of the steady-state electrostatic potential in a collisionless plasma flowing out through the magnetic throat to a wall on the base of the kinetic theory. Spatially varying magnetic field provides formation mechanism of the presheath potential through acceleration of plasma particles and divergence of particle flux. A particle source in a plasma is assumed to be ignored. We have expressed Poisson's equation for a theoretical model to examine potential formation along magnetic field lines from an inside point near the magnetic throat to the wall. It is found that the plasma flow must satisfies the generalized Bohm criterion at the magnetic throat to avoid the discontinuity of the potential just beyond the throat. A monotonically falling potential can be formed only if the generalized Bohm criterion is marginally satisfied at

the throat. In this case, ions passing through the throat are accelerated from a subsonic velocity to a supersonic velocity before they arrive at the throat.

Numerical solutions to Poisson's equation show that trapped electrons in the open region affect the potential formation remarkably. For very small trapped-electron densities, the presheath potential drop is localized near the throat and the presheath potential approaches asymptotically to a constant value as the magnetic field strength decreases along magnetic field lines. For large trapped-electron densities, the presheath potential drop continuously increases with decreasing the magnetic field strength along field lines. These results suggest the possibility of effective potential control in the open region by the combination of an expanding magnetic field and the ECRH heating.

Our results obtained from the analysis and the numerical calculation present one of the bases of the total understanding of the potential formation in the open region of a mirror machine, in the edge layer of a field reversed configuration, or in the divertor of a toroidal herical system. The present results may also be applicable to a low density and high temperature plasma in a modified expanding bundle divertor of a tokamak aiming at improving the energy confinement and reducing the heat load on the wall [5].

REFERENCES

[1] L. S. Hall, Nucl. Fusion **17**, 681 (1977).

[2] G. D. Porter, Nucl. Fusion **22**, 1279 (1982).

[3] L. C. Steinhauer, Phys. Fluids **29**, 3379 (1986).

[4] T. Mizuuchi, O. Motojima, S. Besshou, A. Iiyoshi, and K. Uo, J. Nucl. Mater. **121**, 3 (1984).

[5] R. W. Moir and W. L. Barr, Nucl. Fusion **13**, 35 (1973).

[6] W. L. Barr and R. W. Moir, Nucl. Technol./ Fusion **3**, 98 (1983).

[7] H. Momota, A. Ishida, Y. Kohzaki, G. H. Miley, S. Ohi, M. Ohnishi, K. Yoshikawa, K. Sato, L. C. Steinhauer, Y. Tomita, and M. Tuszewski, Fusion Technol. **21**, 2307 (1992).

[8] N. Ohyabu, Kakuyugo Kenkyu **66**, 525 (1991).

[9] I. Langmuir, Phys. Rev. **33**, 954 (1929).

[10] E. R. Harrison and W. B. Thompson, Proc. Phys. Soc. London **74**, 145 (1959).

[11] G. A. Emmert, R. M. Wieland, A. T. Mense, and J. N. Davidson, Phys. Fluids **23**, 803 (1980).

[12] R. C. Bissell and P. C. Johnson, Phys. Fluids **30**, 779 (1987).

[13] T. D. Rognlien and T. A. Brengle, Phys. Fluids **24**, 871 (1981).

[14] R. H. Cohen, Nucl. Fusion **21**, 209 (1981).

[15] R. H. Cohen, Phys. Fluids **26**, 2774 (1983).

[16] I. Katanuma, Y. Kiwamoto, K. Ishii, and S. Miyoshi, Phys. Fluids **29**, 4138 (1986).

[17] K. Sato, F. Miyawaki, and W. Fukui, Phys. Fluids B **1**, 725 (1989).

[18] M. A. Hussein and G. A. Emmert, Phys. Fluids B **2**, 218 (1990).

[19] K. Sato and F. Miyawaki, Phys. Fluids B **3**, 1963 (1991).

[20] R. C. Bissell, Phys. Fluids **30**, 2264 (1987).

[21] G. D. Hobbs and J. A. Wesson, Plasma Phys. 9, 85 (1967).

[22] K. Sato and F. Miyawaki, J. Phys. Soc. Jpn., 61, 1453 (1992).

CHAPTER 5

Presheath and Current-Free Double Layer in a Two-Electron-Temperature Plasma

5.1 INTRODUCTION

A plasma with energetic electrons or a two-electron-population plasma is produced in various laboratory devices. In tokamak experiments using ion cyclotron frequency heating, lower-hybrid wave heating, or rf current-drive, non-thermal electrons appear in scrape-off layer due to strong rf fields [1,2]. In the tandem mirror, during strong electron cyclotron resonance heating, the electron distribution composed of two Maxwellians at different temperatures is observed in the open end region in front of end plates [3]. In the negative ion source, fast primary electrons for excitation of hydrogen molecules and slow plasma electrons for production of negative ions are required in order to improve volume production of negative hydrogen ions [4].

Two-isothermal species of electrons have also been observed in the expanding corona of a plasma heated by a laser [5]. The expansion of such a plasma and the development

of a potential double layer, called a rarefaction shock, have been investigated theoretically, and general conditions under which rarefaction shocks can exist was derived [6,7]. Recently, a laboratory experiment of the expansion of a two-electron-population plasma has been carried out by Hairapetian and Stenzel [8]. They have also observed a stationary, current-free, potential double layer which is formed due to self-consistent separation of the two electron species in the same devices [9].

The appearance of energetic electrons is expected to have a remarkable effect on potential formation in the plasma because the potential formation is closely associated with the electrons distribution. While there has been considerable theoretical activity in the problem of potential formation in a plasma bounded by the wall since the kinetic analysis in the context of discharge plasma was done by Tonks and Langmuir [10-13], we know of few attempt to verify the characteristics of the potential formed in two-electron-population plasmas.

In this chapter, we theoretically investigate the steady-state potential formation in a two-electron-temperature plasma to show possibility of steady-state potential formation, to clarify the potential structure, and to evaluate the potential drop in such a plasma. The ions are assumed to be generated by ionization of neutral atoms without thermal motion, and the electrons are assumed to have two Maxwellian distributions at different temperatures, T_h and T_c. We analytically solve the plasma equation, and check whether the analytic solution satisfies a condition for the formation of a stable sheath potential. Results calculated from the analytic solution show that the potential drop in the presheath has either a small value characterized by the cold electrons or a large one by

the hot electrons if the temperature ratio T_h/T_c is of the order of 10. There is a critical value for the hot- to total electron density ratio at which the potential drop of presheath discontinuously increase from the low level to the high one as the density ratio increases.

We also find that the steady-state monotonically decreasing potential which consists of the first presheath, a current-free double layer, the second presheath, and the sheath just in front of the wall can be set up in a lower range of the hot- to total electron density ratio around the critical value. The present double layer builds up in the plasma without plasma current, while most double layers observed in experiments [14] or theoretically investigated [15,16] require the presence of a plasma current. The double layer structure is sustained by self-consistent separation of the two electron species and generation of ions at the two presheathes. The formation mechanism is similar to that of the double layer experimentally observed by Hairapetian and Stenzel [9].

In Sec. 5.2, we present the solution of the plasma equation, and briefly discuss a condition for the formation of a stable sheath potential. The formation of the double layer and the solution of the plasma equation for the second presheath is described in Sec. 5.3. Results calculated from the analytic solutions are illustrated and discussed in Sec. 5.4, and the conclusions are summarized in Sec. 5.5.

5.2 SOLUTION OF THE PLASMA EQUATION

A collisionless plasma is assumed in a one-dimensional planar geometry with walls

at $x = \pm L$, which are perfectly absorbing and electrically floating. The electrostatic potential $\phi(x)$, which is defined to be zero at $x = 0$, is expected to be monotonically decreasing for $x > 0$ as shown Fig. 5.1. It is assumed that ions are generated by ionization of neutral atoms with kinetic energy negligibly small as compared with the electron temperature. Following the same way of Harrison and Thompson [11], the ion density $n_i(x)$ at some point x is described by a kinetic equation

$$n_i(x) = < \sigma v > n_0 n_n \int_0^x dx' \, h(x') \left(\frac{2q[\phi(x') - \phi(x)]}{M} \right)^{-1/2} , \tag{5.1}$$

where q and M are the charge and mass of the ion, $< \sigma v >$ is the ionization rate coefficient, n_0 is the electron density at $x = 0$, and n_n is the neutral atom density. The function $h(x)$ expresses the spatial variation of the ionization rate. For electrons the distribution composed of two Maxwellians at different temperatures is adopted to give the electron density

$$n_e(x) = n_{c0} \exp[e\phi(x)/kT_c] + n_{h0} \exp[e\phi(x)/kT_h] , \tag{5.2}$$

where n_{c0} and n_{h0} are the cold and hot electron particle densities at $x = 0$, and T_c and T_h are the cold and hot electron temperatures. Substituting Eqs. (5.1) and (5.2) into Poisson's equation, we obtain the integrodifferential equation

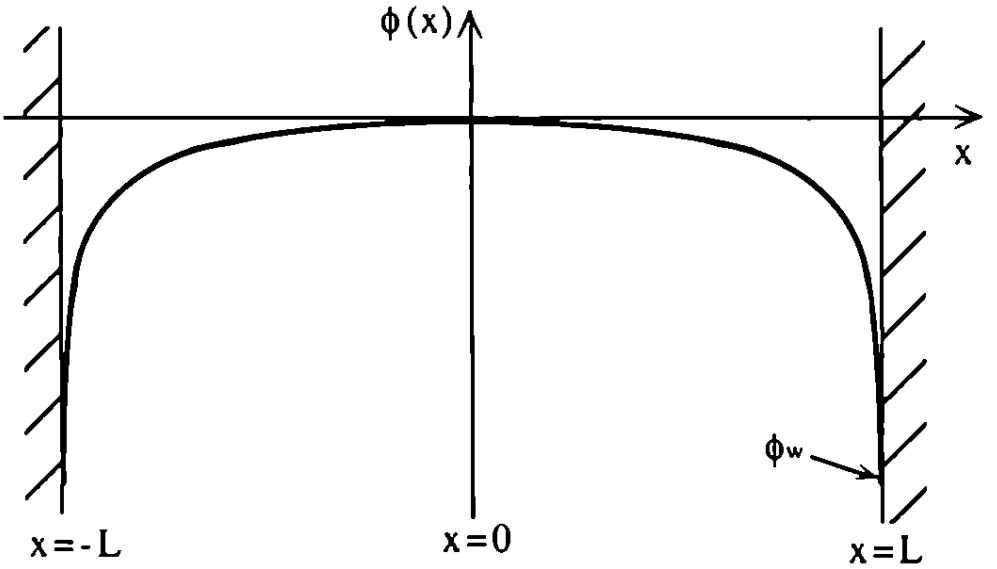

FIG. 5.1. A schematic diagram of the geometry of the problem

$$\lambda_{D0}^2 \frac{e}{kT_c}\frac{d^2\phi}{dx^2} = \frac{n_{c0}}{n_0}\exp\left(\frac{e\phi(x)}{kT_c}\right) + \frac{n_{h0}}{n_0}\exp\left(\frac{e\phi(x)}{kT_h}\right)$$

$$- < \sigma v > n_n \left(\frac{Mq}{2e}\right)^{1/2} \int_0^x dx' h(x') [\phi(x') - \phi(x)]^{-1/2} \quad , \tag{5.3}$$

where λ_{D0} is the Debye length at $x = 0$ defined by $\lambda_{D0}^2 = \epsilon_0 kT_c/n_0 e^2$.

The plasma equation, which describes the potential distribution in the plasma expect the sheath, is obtained by neglecting the second derivative term of Eq. (5.3). With the introduction of the dimensionless variables

$$s = x/L\,, \quad Z = q/e\,, \quad \alpha = n_{h0}/n_0\,, \quad \tau = T_h/T_c\,, \quad \Psi(s) = -e\phi(x)/kT_c\,,$$

the plasma equation is written in the form

$$(1-\alpha)\exp(-\Psi) + \alpha\exp(-\Psi/\tau) = A\int_0^{\Psi} d\Psi' \frac{ds'}{d\Psi'}\frac{h(\Psi')}{(\Psi - \Psi')^{1/2}} \quad , \tag{5.4}$$

where

$$A = < \sigma v > n_n \left(\frac{ZM}{2kT_c}\right)^{1/2} L$$

and $\Psi' = \Psi(s')$. Equation (5.4) is Abel's integral equation and its solution is [17]

$$Ah(\Psi)\frac{ds}{d\Psi} = \frac{1}{\pi}\frac{d}{d\Psi}\int_0^{\Psi} d\Psi' \frac{(1-\alpha)\exp(-\Psi') + \alpha\exp(-\Psi'/\tau)}{(\Psi - \Psi')^{1/2}} \quad . \tag{5.5}$$

The differentiation on the right-hand side in Eq. (5.5) can be carried out to give the reciprocal of the normalized electric field

$$\frac{ds}{d\Psi} =$$

$$\frac{1}{\pi A h(\Psi)} \left[\frac{1}{\sqrt{\Psi}} - 2(1-\alpha)\exp(-\Psi) D\left(\sqrt{\Psi}\right) - 2\frac{\alpha}{\sqrt{\tau}} \exp(-\Psi/\tau) D\left(\sqrt{\Psi/\tau}\right) \right]$$

$$, \quad 0 \leq \Psi \leq \Psi_1 \ , \tag{5.6}$$

which is inversely as $h(\Psi)$. Here $D(x)$ is the Dawson function and Ψ_1 is the potential at the plasma-sheath boundary. In the absence of a boundary condition there is always a solution to the plasma equation for any value of Ψ_1, but the solution satisfies the general Bohm criterion at the boundary only if $ds/d\Psi = 0$ at the boundary [18]. With the aid of this boundary condition, the value of Ψ_1 is determined from the equation

$$\frac{1}{2\sqrt{\Psi_1}} = (1-\alpha)\exp(-\Psi_1) D\left(\sqrt{\Psi_1}\right) + \frac{\alpha}{\sqrt{\tau}} \exp(-\Psi_1/\tau) D\left(\sqrt{\Psi_1/\tau}\right) \ . \tag{5.7}$$

Integration of Eq. (5.6) give the function $s(\Psi)$ from which the profile of the potential in the plasma up to the edge of the sheath, the so-called presheath, is determined ;

$$s(\Psi) = \int_0^{\Psi} d\Psi' \frac{ds'}{d\Psi'} \left(\int_0^{\Psi_1} d\Psi' \frac{ds'}{d\Psi'} \right)^{-1} \tag{5.8}$$

It is seen from Eqs. (5.6)-(5.8) that while the profile of the potential depends on the shape of $h(\Psi)$, the potential at the boundary is independent of it. We can calculate the profile of the presheath potential from Eq. (5.8) once the function $h(\Psi)$ is specified.

The wall potential Ψ_w is determined from the requirement that the electron flux and the ion flux must be equal at the wall. Since the particle number of ions generated in the sheath can be neglected in the limit as $\lambda_{D0}/L \to 0$, the ion flux is evaluated by integrating the particle source in the plasma as

$$Z\Gamma_i = n_0 \left(\frac{2ZkT_e}{M}\right)^{1/2} A \int_0^{\Psi_1} d\Psi' \frac{ds'}{d\Psi'} h(\Psi') \ , \tag{5.9}$$

which is independent of the shape of $h(\Psi)$ because $ds/d\Psi$ is in inverse to $h(\Psi)$. The integration in Eq. (5.9) can be carried out using Eq. (5.6). The electron flux of the two-temperature electron is expressed by

$$\Gamma_e = n_0 \left(\frac{kT_e}{2\pi m}\right)^{1/2} \left[(1-\alpha)\exp(-\Psi_w) + \alpha\sqrt{\tau}\exp\left(\frac{-\Psi_w}{\tau}\right)\right] \ , \tag{5.10}$$

and then, we obtain the equation from which the value of Ψ_w is determined as

$$(1-\alpha)\exp(-\Psi_w) + \alpha\sqrt{\tau}\exp(-\Psi_w/\tau) =$$

$$\left(\frac{16mZ}{\pi M}\right)^{1/2} \left[(1-\alpha)\exp(-\Psi_1) D\left(\sqrt{\Psi_1}\right) + \alpha\sqrt{\tau}\exp(-\Psi_1/\tau) D\left(\sqrt{\Psi_1/\tau}\right)\right] \ . \tag{5.11}$$

We now derive the sheath equation and briefly discuss a condition for the formation of the sheath potentials. Multiplying by $d\Psi/ds$ and integrating Poisson's equation, we obtain the equation which described the sheath potential as follow ;

$$\frac{1}{2}\left(\frac{\lambda_{D0}}{L}\right)^2\left(\frac{d\Psi}{ds}\right)^2 = \int_{\Psi_1}^{\Psi} d\Psi' \frac{Zn_i(\Psi') - n_e(\Psi')}{n_0} \quad . \tag{5.12}$$

Since the left band side of Eq. (5.12) is positive, the inequality

$$\int_{\Psi_1}^{\Psi} d\Psi'(Zn_i - n_e) \geq 0 \tag{5.13}$$

must hold over the range $\Psi_1 < \Psi \leq \Psi_w$, which is the condition for the formation of a stable sheath potential. For a maxwellian distribution of electron, the inequality (5.13) always holds true once the generalized Bohm criterion is satisfied at $\Psi = \Psi_1$ because of rapid decrease of the electron particle density with increase of the potential. But, for electron which has a high energy component, the inequality (5.13) doesn't always hold even if the generalized Bohm criterion is satisfied at the boundary. The ion density in the sheath is obtain from

$$n_i(\Psi) = \frac{A}{Z}\int_0^{\Psi_1} d\Psi' \frac{ds'}{d\Psi'} \frac{h(\Psi')}{(\Psi - \Psi')^{1/2}} \tag{5.14}$$

by using the solution of the plasma equation, Eq. (5.6). Carrying out some integration, we can write the inequality (5.13) as

$$\Psi - \Psi_1 - \frac{2}{\pi}\int_{\Psi_1}^{\Psi} d\Psi' \left(\frac{\Psi}{\Psi'} - 1\right)^{1/2} - \frac{4}{\pi}\int_0^{\Psi_1} d\Psi' \left[(\Psi - \Psi')^{1/2} - (\Psi_1 - \Psi')^{1/2}\right]$$

$$\times \left[(1-\alpha)\exp(-\Psi')D\left(\sqrt{\Psi'}\right) + \alpha\sqrt{\tau}\exp(-\Psi'/\tau)D\left(\sqrt{\Psi'/\tau}\right)\right]$$

$$-(1-\alpha)[\exp(-\Psi_1) - \exp(-\Psi)] - \alpha\tau[\exp(-\Psi_1/\tau) - \exp(\Psi/\tau)]$$

$$\geq 0 \ . \qquad (5.15)$$

If this condition is not satisfied over the range $\Psi_1 < \Psi \leq \Psi_w$, there is not a nonoscillatory solution which can reach to the potential Ψ_w. In this case, we can find another monotonically decreasing potential structure which consists of the first presheath, a double layer, the second presheath, and a sheath as described in the next section.

5.3 CURRENT-FREE DOUBLE LAYER AND THE SECOND PRESHEATH

When a sign of the integral in Eq. (5.12) changes from positive to negative as the potential Ψ increases, we can get a monotonically decreasing solution of Poisson's equation which can reach the wall potential by introducing formation of a double layer and the second presheath downstream from the first presheath. A double layer is a localized electrostatic potential structure created by two equal but opposite space-charge layers. The potential of the double layer placed to the first presheath is calculated from Eq. (5.12), and the edge potential Ψ_D is determined from

$$\int_{\Psi_1}^{\Psi_D} d\Psi'(Zn_i - n_e) = 0 \ . \tag{5.16}$$

This double layer is surrounded by the first and second presheathes, and is sustained by the ionization of neutral atoms in the presheath regions. Appearance of the cold ion in the second presheath enable the steady-state double layer to be set up in the plasma.

The thickness of a double layer is generally from a few ten times to several hundred times of the Debye length, then the particle source inside the double layer can be neglected in the limit as $\lambda_{D0}/L \to 0$. Neglecting the particle source in the double layer, we can describe the ion density in the second presheath by the equation

$$Zn_i(s) = An_0 \left(\int_0^{\Psi_1} d\Psi' \frac{ds'}{d\Psi'} \frac{h(\Psi')}{(\Psi - \Psi')^{1/2}} + \int_{\Psi_D}^{\Psi} d\Psi' \frac{ds'}{d\Psi'} \frac{h(\Psi')}{(\Psi - \Psi')^{1/2}} \right) \ , \tag{5.17}$$

where the first term on the right hand side is the particle density of ions produced in the first presheath and the second one is that produced in the second presheath. Equalizing the ion density to the electron density and introducing the transformation $\xi = \Psi - \Psi_D$, the plasma equation of the second presheath is written as

$$\begin{aligned} &(1-\alpha)\exp[-(\Psi_D + \xi)] + \alpha \exp[-(\Psi_D + \xi)/\tau] \\ &\quad = A \int_0^{\Psi_1} d\Psi' \frac{ds'}{d\Psi'} \frac{h(\Psi')}{(\Psi_D + \xi - \Psi')^{1/2}} + A \int_0^{\xi} d\xi' \frac{ds'}{d\xi'} \frac{h(\Psi_D + \xi')}{(\xi - \xi')^{1/2}} \ . \end{aligned} \tag{5.18}$$

Since the first integral on the right hand side is a function of ξ, Eq. (5.18) becomes Abel's integral equation and its solution is

$$Ah(\Psi_D+\xi)\frac{ds}{d\xi} = \frac{1}{\pi}\frac{d}{d\xi}\int_0^{\xi}\frac{d\xi'}{(\xi-\xi')^{1/2}}\Big[(1-\alpha)\exp[-(\Psi_D+\xi')]$$

$$+\alpha\exp\left(-\frac{(\Psi_D+\xi')}{\tau}\right) - A\int_0^{\Psi_1}d\Psi'\frac{ds'}{d\Psi'}\frac{h(\Psi')}{(\Psi_D+\xi'-\Psi')^{1/2}}\Big] \quad . \tag{5.19}$$

Putting Eq. (5.6) into Eq. (5.19) and carrying out some integration and derivation give the result

$$\frac{ds}{d\Psi} =$$

$$\frac{1}{\pi Ah(\Psi)}\left\{(1-\alpha)\left[(\Psi-\Psi_D)^{-1/2}\exp(-\Psi_D) - 2\exp(-\Psi)D\left(\sqrt{\Psi-\Psi_D}\right)\right]\right.$$

$$+\alpha\left[(\Psi-\Psi_D)^{-1/2}\exp(-\Psi_D/\tau) - \frac{2}{\sqrt{\tau}}\exp(-\Psi/\tau)D\left(\sqrt{(\Psi-\Psi_D)/\tau}\right)\right]$$

$$-\frac{1}{\pi}\int_0^{\Psi_1}\frac{d\Psi'}{\Psi-\Psi'}\left(\frac{\Psi_D-\Psi'}{\Psi-\Psi_D}\right)^{1/2}\left[\frac{1}{\sqrt{\Psi'}} - 2(1-\alpha)\exp(-\Psi')D\left(\sqrt{\Psi'}\right)\right.$$

$$\left.\left.-2\frac{\alpha}{\sqrt{\tau}}\exp(-\Psi'/\tau)D\left(\sqrt{\Psi'/\tau}\right)\right]\right\} \quad , \quad \Psi_D \le \Psi \le \Psi_2 \ . \tag{5.20}$$

The potential at the edge of the second presheath, Ψ_2, is determined from the boundary condition, $ds/d\Psi = 0$.

In the limit as $\lambda_{D0}/L \to 0$, the position of the double layer, s_D, is given by

$$s_D = \left(\int_0^{\Psi_1}d\Psi'\frac{ds'}{d\Psi'} + \int_{\Psi_D}^{\Psi_2}d\Psi'\frac{ds'}{d\Psi'}\right)^{-1}\int_0^{\Psi_1}d\Psi'\frac{ds'}{d\Psi'} \ . \tag{5.21}$$

It is seen from Eqs. (5.7), (5.15), (5.20), and (5.21) that the position s_D depends on the spatial profile of the particle source because the integrand $ds/d\Psi$ varies inversely as $h(s)$, while the potentials Ψ_1, Ψ_D, and Ψ_2 are independent of $h(s)$. The potential profiles in the first and second presheathes are, respectively, calculated from the integrals

$$s(\Psi) = s_D \int_0^{\Psi} d\Psi' \frac{ds'}{d\Psi'} \left(\int_0^{\Psi_1} d\Psi' \frac{ds'}{d\Psi'} \right)^{-1} , \quad 0 < s < s_D , \tag{5.22}$$

and

$$s(\Psi) = s_D + (1 - s_D) \int_{\Psi_D}^{\Psi} d\Psi' \frac{ds'}{d\Psi'} \left(\int_{\Psi_D}^{\Psi_2} d\Psi' \frac{ds'}{d\Psi'} \right)^{-1} , \quad s_D < s < 1 , \tag{5.23}$$

which also depend on the spatial profile of the particle source.

Since the cold electrons are reflected by the double layer potential, the electron distribution function at the second presheath is close to a Maxwellian with the temperature T_h. In this case, a nonoscillatory stable sheath potential is always formed just in front of the wall once the generalized Bohm criterion is satisfied at the edge of the second presheath. The ion flux is evaluated by integrating the particle source as

$$Z\Gamma_i = n_0 \left(\frac{2ZkT_e}{M} \right)^{1/2} A \left(\int_0^{\Psi_1} d\Psi' \frac{ds'}{d\Psi'} h(\Psi') + \int_{\Psi_D}^{\Psi_2} d\Psi' \frac{ds'}{d\Psi'} h(\Psi') \right) . \tag{5.24}$$

Carrying out the integration in Eq. (5.24) and equating the electron and ion fluxes, we obtain the equation to determine the wall potential as

$$(1-\alpha)\exp(-\Psi_w)+\alpha\sqrt{\tau}\exp(-\Psi_w/\tau)$$

$$=\left(\frac{16mZ}{\pi M}\right)^{1/2}\left\{(1-\alpha)\left[\exp(-\Psi_1)D\left(\sqrt{\Psi_1}\right)+\exp(-\Psi_2)D\left(\sqrt{\Psi_2-\Psi_D}\right)\right]\right.$$

$$+\alpha\sqrt{\tau}\left[\exp(-\Psi_1/\tau)D\left(\sqrt{\Psi_1/\tau}\right)+\exp(-\Psi_2/\tau)D\left(\sqrt{(\Psi_2-\Psi_D)/\tau}\right)\right]$$

$$-\frac{1}{\pi}\int_0^{\Psi_1}d\Psi'\tan^{-1}\left[\left(\frac{\Psi_2-\Psi_D}{\Psi_D-\Psi'}\right)^{1/2}\right]\left[\frac{1}{\sqrt{\Psi'}}-2(1-\alpha)\exp(-\Psi')D\left(\sqrt{\Psi'}\right)\right.$$

$$\left.\left.-2\frac{\alpha}{\sqrt{\tau}}\exp(-\Psi'/\tau)D\left(\sqrt{\Psi'/\tau}\right)\right]\right\}\quad . \tag{5.25}$$

The potential Ψ_w weakly depends on Zm/M, while the potentials Ψ_1, Ψ_D, and Ψ_2 are independent of it.

Using the solution, we can also calculate the ion distribution function explicitly. To express the distribution function, we use the normalized quantities and the normalized velocity, $V=(Mv^2/2kT_e)^{1/2}$. An ion generated at a point $s'\le s$ has a velocity of

$$V=\{Z[\Psi(s)-\Psi(s')]\}^{1/2}\quad . \tag{5.26}$$

If $f(V)dV$ is the number of ions at having velocities in the range V to $V+dV$, it follows that

$$f(V)dV=An_0h(s')ds'/V\quad , \tag{5.27}$$

where the right hand is the number of ions generated per second between s' and $s'+ds'$. From Eqs. (5.26) and (5.27), therefore, the distribution function at a point $s\ge s'$, normalized to n_0, is given by

$$\frac{f(V)}{n_0} = \frac{2A}{Z^{3/2}} h(s') \frac{ds'}{d\Psi'} \ , \tag{5.28}$$

which is independent of the spatial profile of the particle source. Substituting Eqs. (5.5) and (5.20), we can express the distribution function at the edge of the second presheath in the form ;

$$\begin{aligned}\frac{f_2(V)}{n_0} = \frac{2}{\pi Z^{3/2}} \Bigg\{ & (1-\alpha) \left[(\Psi' - \Psi_D)^{-1/2} \exp(-\Psi_D) - 2\exp(-\Psi') D\left(\sqrt{\Psi' - \Psi_D}\right) \right] \\ & + \alpha \left[(\Psi' - \Psi_D)^{-1/2} \exp(-\Psi_D/\tau) - \frac{2}{\sqrt{\tau}} \exp(\Psi'/\tau) D\left(\sqrt{(\Psi' - \Psi_D)/\tau}\right) \right] \\ & - \frac{1}{\pi} \int_0^{\Psi_1} \frac{d\Psi''}{\Psi' - \Psi''} \left(\frac{\Psi_D - \Psi''}{\Psi' - \Psi_D} \right)^{1/2} \left[\frac{1}{\sqrt{\Psi''}} - 2(1-\alpha) \exp(-\Psi'') D\left(\sqrt{\Psi''}\right) \right. \\ & \left. \left. - 2\frac{\alpha}{\sqrt{\tau}} \exp(-\Psi''/\tau) D\left(\sqrt{-\Psi''/\tau}\right) \right] \right\} \\ & , \ 0 < V < [Z(\Psi_2 - \Psi_D)]^{1/2} \ , \end{aligned} \tag{5.29a}$$

and

$$\begin{aligned}\frac{f_2(V)}{n_0} = \frac{2}{\pi Z^{3/2}} & \left[\frac{1}{\sqrt{\Psi'}} - 2(1-\alpha) \exp(-\Psi') D\left(\sqrt{\Psi'}\right) - 2\frac{\alpha}{\sqrt{\tau}} \exp(-\Psi'/\tau) D\left(\sqrt{\Psi'/\tau}\right) \right] \\ & , \ [Z(\Psi_2 - \Psi_1)]^{1/2} < V < (Z\Psi_2)^{1/2} \ , \end{aligned} \tag{5.29b}$$

where $\Psi' = \Psi_2 - V^2/Z$. The ion distribution is separated into two parts due to the formation of the double layer. The ions produced in the first presheath are accelerated by the double layer to form a high-energy beam expressed by Eq. (5.29b). In the same

manner, we can also get the expression of the heat flux using the solution of the plasma equation.

5.4 RESULTS AND DISCUSSION

The plasma-sheath boundary potential is obtained by finding the value of Ψ_1 that satisfied Eq. (5.7) for a particular value of the temperature ratio $\tau \equiv T_h/T_c$ and the density ratio $\alpha \equiv n_{h0}/n_0$. The results of the potential as a function of the density ratio n_{h0}/n_0 are shown in Fig. 5.2. Equation (5.7) has a triple root $\Psi_1 = 3.82$ when $\tau = 10.8$ and $\alpha = 0.33$, which is obtained by solving Eq. (5.7), $d\alpha/d\Psi_1 = 0$, and $d^2\alpha/d\Psi_1^2 = 0$ as simultaneous equations of Ψ_1, τ, and α. When $\tau < 10.8$, it has a single root over the whole range of n_{h0}/n_0 and then the potential Ψ_1 is continually changing from 0.85 to 0.85 τ as the density ratio increases. When $\tau > 10.8$, however, it has three different roots in some range of n_{h0}/n_0. In this case, we must choose the smallest one as the boundary potential in order to get physically meaningful potential profile in the presheath because the derivative $ds/d\Psi$, the reciprocal of the normalized electric field, must be a single value at any point in the real space. Following this fact we can see that the potential Ψ_1 discontinuously changes from a value of order of 1 to one of order of τ at some value of n_{h0}/n_0 when $\tau > 10.8$. It is noted that the condition $\tau > 10.8$ agrees well with a necessary condition given by $\tau > 5+\sqrt{24}$ for rarefaction shocks to exist in a laser-plasma corona [6,7].

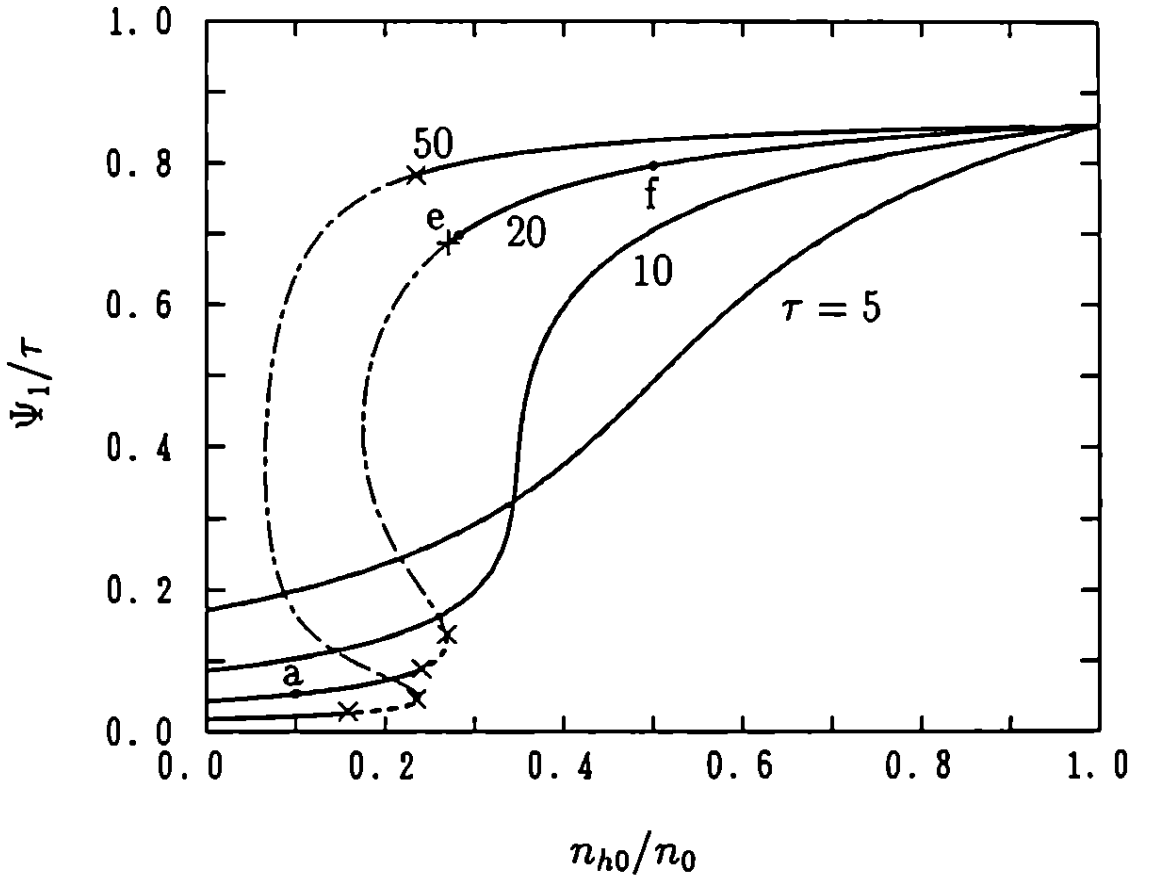

FIG. 5.2. The normalized potential (solid lines) at the plasma-sheath boundary as a function of the hot- to total density ratio n_{h0}/n_0 for various values of the temperature ratio, $\tau \equiv T_h/T_c$. The broken lines show the solution of Eq. (5.7) which doesn't satisfy a condition for the sheath formation expressed by the inequality (5.15).

It is also noted that there is the range of n_{h0}/n_0 where the condition for sheath formation described by the inequality (5.15) is not satisfied. In this range, which is indicated by using broken lines in Fig. 5.2, a monotonically decreasing potential structure composed by the first presheath, a current-free double layer, the second presheath, and the sheath builds up in the plasma in stead of the usual potential structure composed by the presheath and the sheath. The potential at the edge of the first and second presheathes, Ψ_1 and Ψ_2, are determined from the boundary condition, $ds/d\Psi = 0$, and that of the double layer, Ψ_D, is calculated from Eq. (5.16). Results for $\tau = 20$ shown in Fig. 5.3(a) and for $\tau = 50$ in Fig. 5.3(b) show that the potential drop in the first presheath is of the order of the cold electron temperature and that in the second presheath of the order of the hot electron temperature. The potential at the edge of the double layer, Ψ_D, is continuously changing from Ψ_2 to Ψ_1 as the density ratio increases.

The wall potential calculated from Eqs. (5.11) and (5.25) for a hydrogen plasma is shown in Fig. 5.4. The wall potential, which is mainly dominated by the hot electrons, is continuously changing regardless of discontinuous change of the presheath potential and the potential structure. In the range of the density ratio where the presheath potential is of the order of the hot electron temperature, most cold electrons exist in the low potential region around the plasma center because of reflection by the potential. In this range, the contribution of cold electrons to the sheath formation becomes small as seen from Eq. (5.11), and then the wall potential Ψ_w is asymptotically approaching the fixed value of 3.56τ.

The potential profile of the presheath which ends to the wall through the sheath is

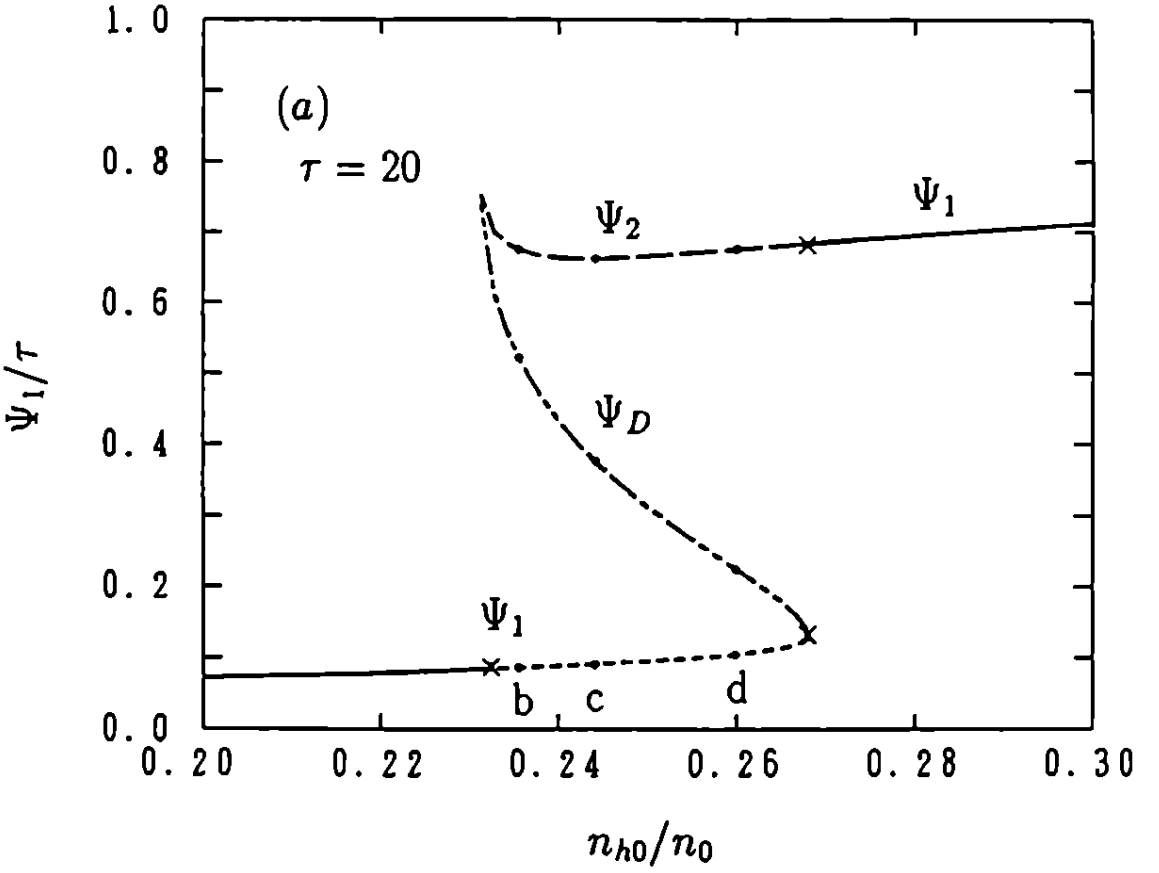

FIG. 5.3(a). The normalized potentials at the edge of the first presheath, Ψ_1, at the edge of the double layer, Ψ_D, and at the edge of the second presheath, Ψ_2, as a function of the density ratio n_{h0}/n_0 for $\tau = 20$.

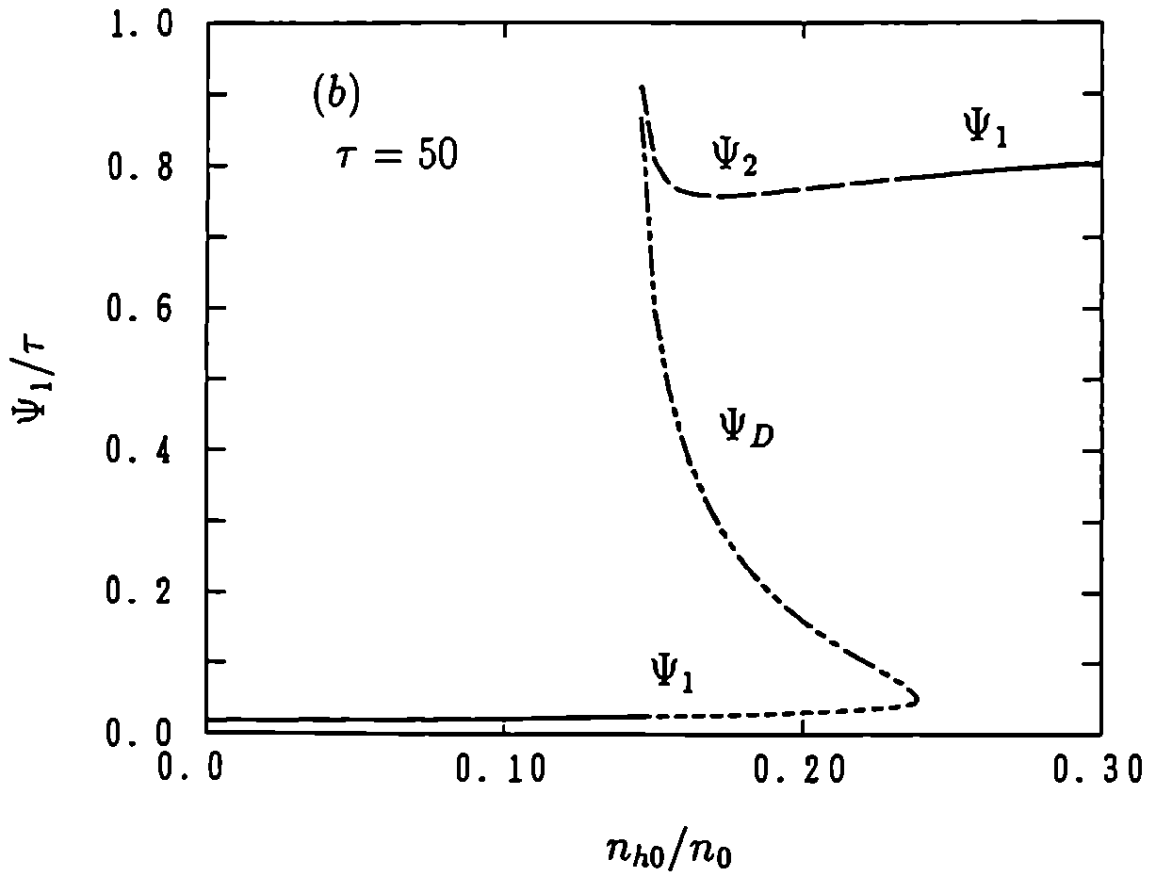

FIG. 5.3(b). The normalized potentials at the edge of the first presheath, Ψ_1, at the edge of the double layer, Ψ_D, and at the edge of the second presheath, Ψ_2, as a function of the density ratio n_{h0}/n_0 for $\tau = 50$.

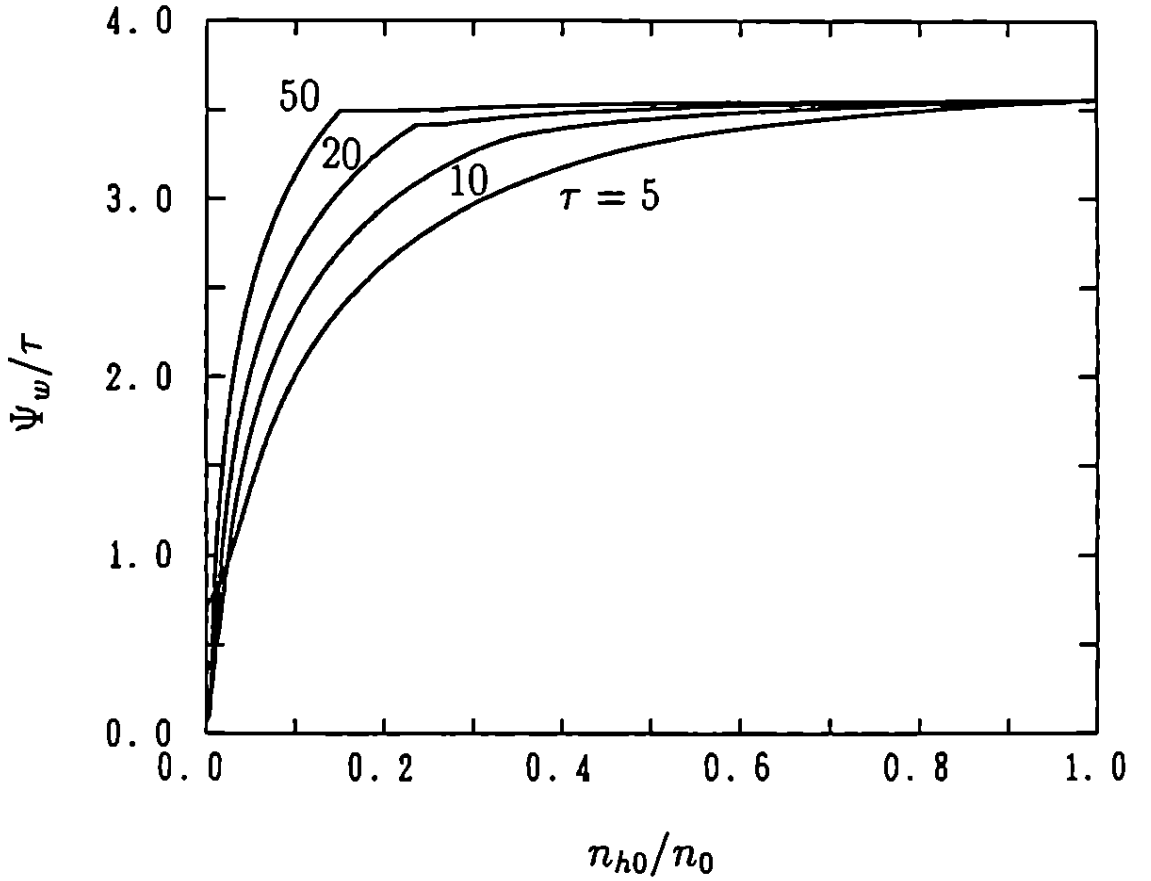

FIG. 5.4. The normalized wall potential as a function of the density ratio for a hydrogen plasma with various values of the temperature ratio.

plotted in Fig. 5.5 for various values of n_{h0}/n_0. Here we take the spatial profile of the particle source in the form $h(s) = n(s)/n_0$, assuming the constant neutral atom density and the ionization rate proportional to the electron density. Symbols a, f, and e represent the results for the points in Fig. 5.2. It is noted that between point a and b the potential drop in the presheath drastically increases as n_{h0}/n_0 increases.

The profile of the presheath potential for various value of the density ratio n_{h0}/n_0 in the range where the double layer and the second presheath build up at downstream of the first presheath is calculated from Eqs. (5.22) and (5.23). Results are shown Fig. 5.6, where b, c, and d represent the results for the points in Fig. 5.3(a). The potential drop at the current-free double layer, which marks the transition between the first and second presheathes, is illustrated by the broken line. The position of the double layer considerably depends on the spatial profile of the particle source ; if the ionization of the neutral gas is strong near the wall, the double layer get near the wall. On the contrary, it move away from the wall if the particle source is localized in the region close to the center of the plasma.

The ion distribution function at the edge of the second presheath is shown in Fig. 5.7. Due to the formation of the double layer the ion distribution function is separated into two parts. The high energy beam-like part with a small velocity spread is the distribution function of the ions produced in the first presheath and accelerated by the double layer potential, and a low energy part is one of the ions produced in the second presheath. The particle density of the cold ions is smaller than a tenth of that of the energetic ions at the second presheath.

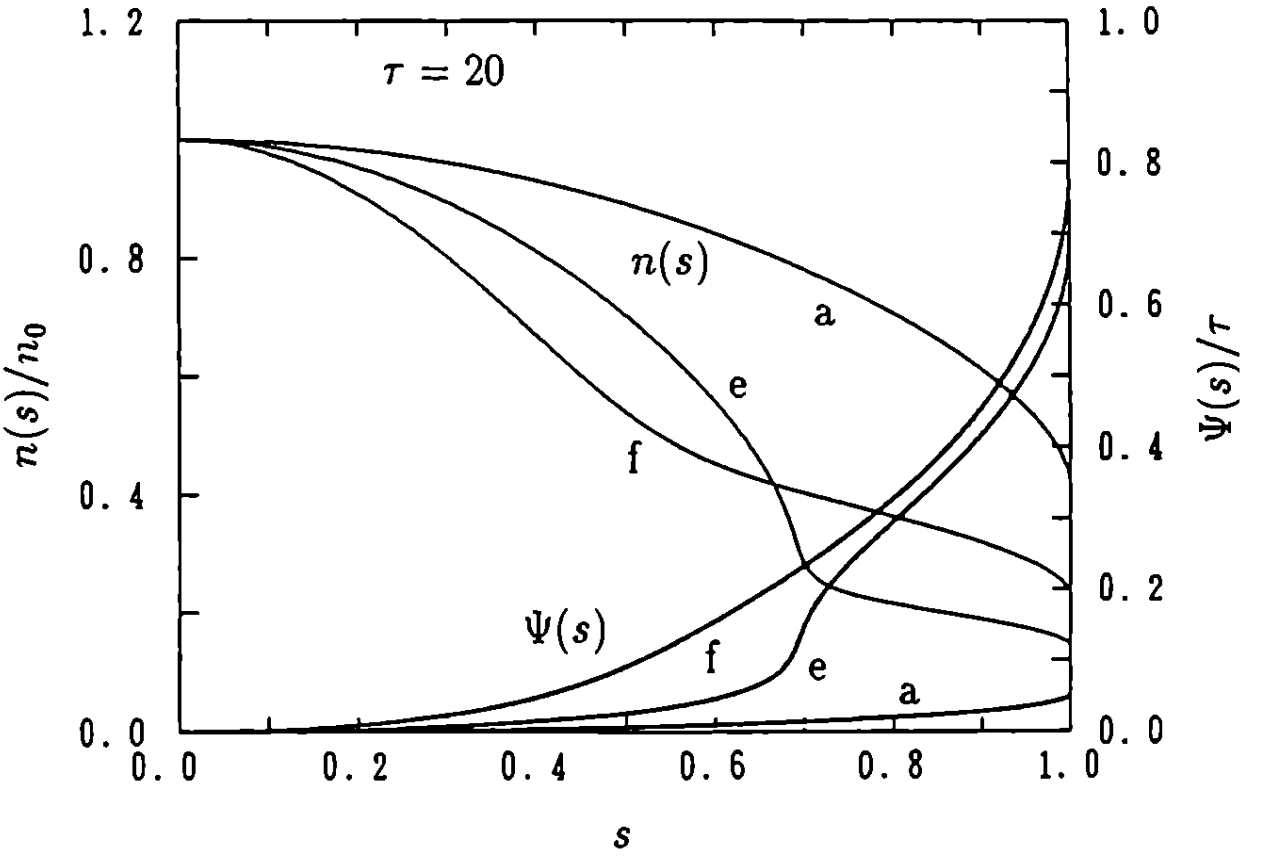

FIG. 5.5. Profiles of the normalized presheath potential (thick lines) and the particle density (thin lines) for $n_{h0}/n_0 = 0.10$, 0.28, and 0.50, where the spatial profile of the particle source is chosen as $h(s) = n(s)/n_0$. The wall is located at $s = 1$. Symbols a, e, and f represent results for the points in Fig. 5.2.

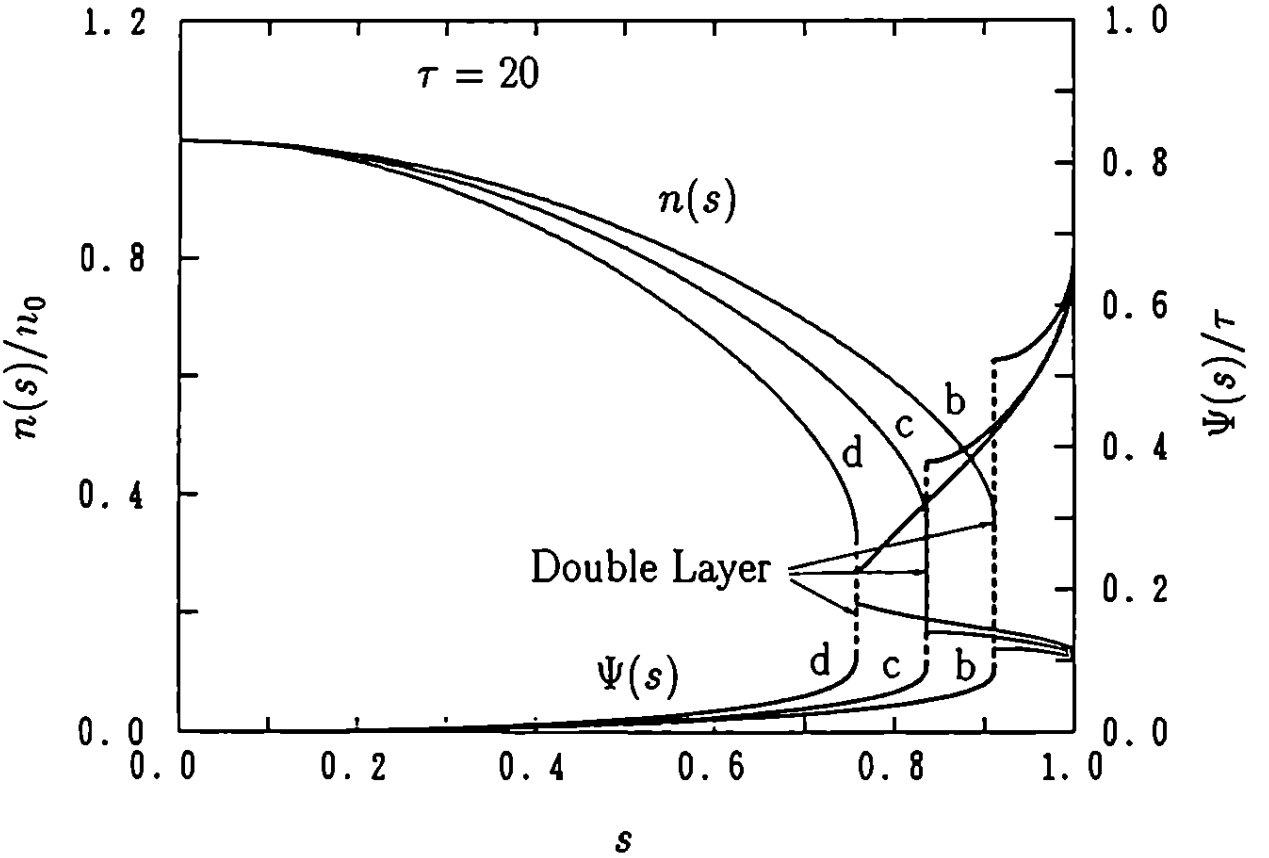

FIG. 5.6. Profiles of the normalized presheath potential (thick lines) and the particle density (thin lines) for $n_{h0}/n_0 = 0.234$, 0.244, and 0.260, where the spatial profile of the particle source is chosen as $h(s) = n(s)/n_0$. The broken lines show the potential drop at the double layer. Symbols *b*, *c*, and *d* represent results for the density ratios marked in Fig. 5.3(a).

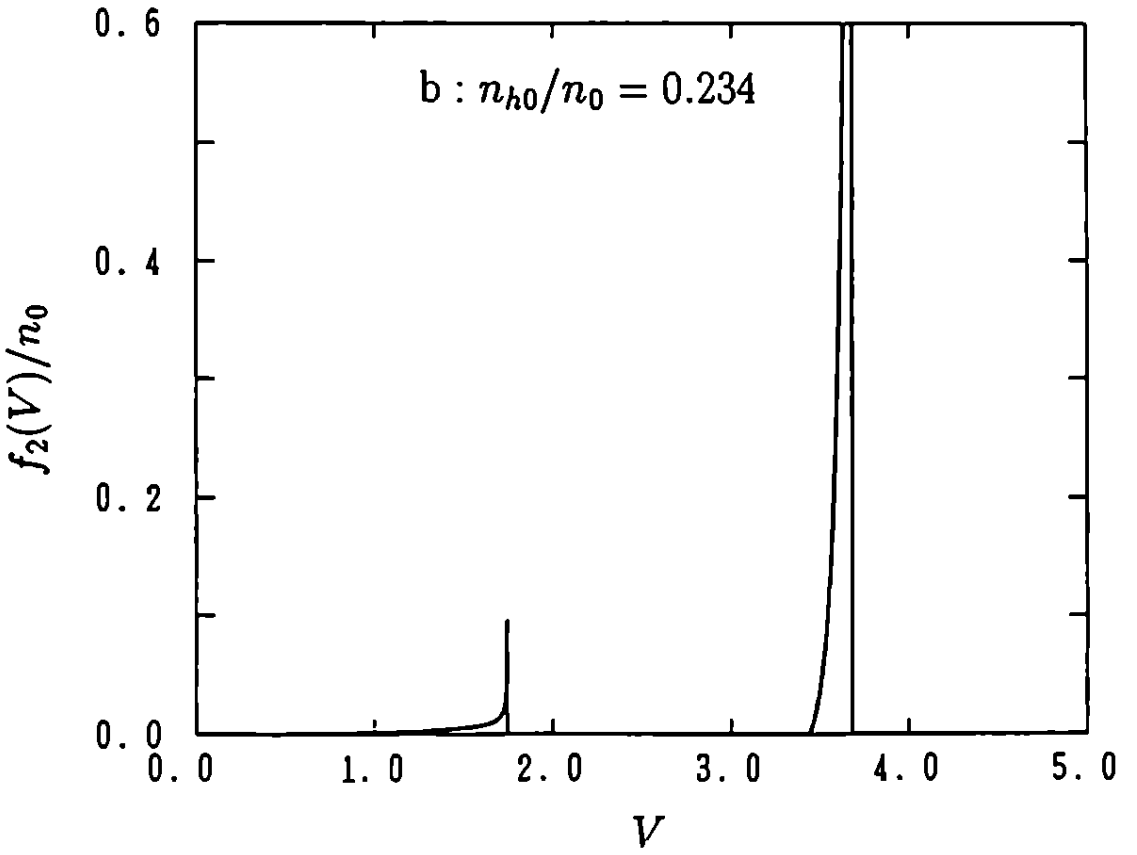

FIG. 5.7. The normalized ion distribution function at the edge of the second presheath for $Z = 1$, $\tau = 20$, and $n_{h0}/n_0 = 0.234$, where the velocity is normalized as $V = v/(2kT_c/M)^{1/2}$.

The potential profile in the double layer is numerically calculated from Eq. (5.12). We obtain the plots in Fig. 5.8, where the Debye length is defined using the cold ion temperature T_c and the particle density at $x = 0$. The potential changes gradually over the double layer, width of which is about fifty times as large as the Debye length. The corresponding profile of the particle density difference $\delta n \equiv Zn_i - n_e$ illustrated in Fig. 5.9 shows that two equal but opposite space-charge layers create the localized electrostatic potential structure. While the cold electrons are reflected by the double layer potential, many particle of the hot electrons can reach the second presheath beyond the double layer potential. The ions produced in the first presheath are accelerated toward the wall by the double layer potential. In the first stage of the double layer, the space charge becomes positive due to the reflection of the cold electrons, and it changes to negative in the second stage due to acceleration of the ions and existence of the hot electrons. A rapid change of the space charge at $x \simeq x_D + 20\lambda_{D0}$ is due to existence of a small number of the cold ions produced in the second presheath, which are reflected at the boundary and can't move in the double layer. In the present calculation we neglected ion generation at the double layer by putting the limit as $\lambda_{D0}/L \to 0$. Under the situation that the ion generation at the double layer can not be ignored, the space charge may change at the boundary continuously. It is seen from the facts mentioned above that the double layer structure is composed of four species, that is, the cold electrons, the hot electrons, the energetic ions accelerated by the double layer, and a small number of the cold ions produced in the second presheath.

A double-layer solution without current of the Vlasov-Poisson equations has previ-

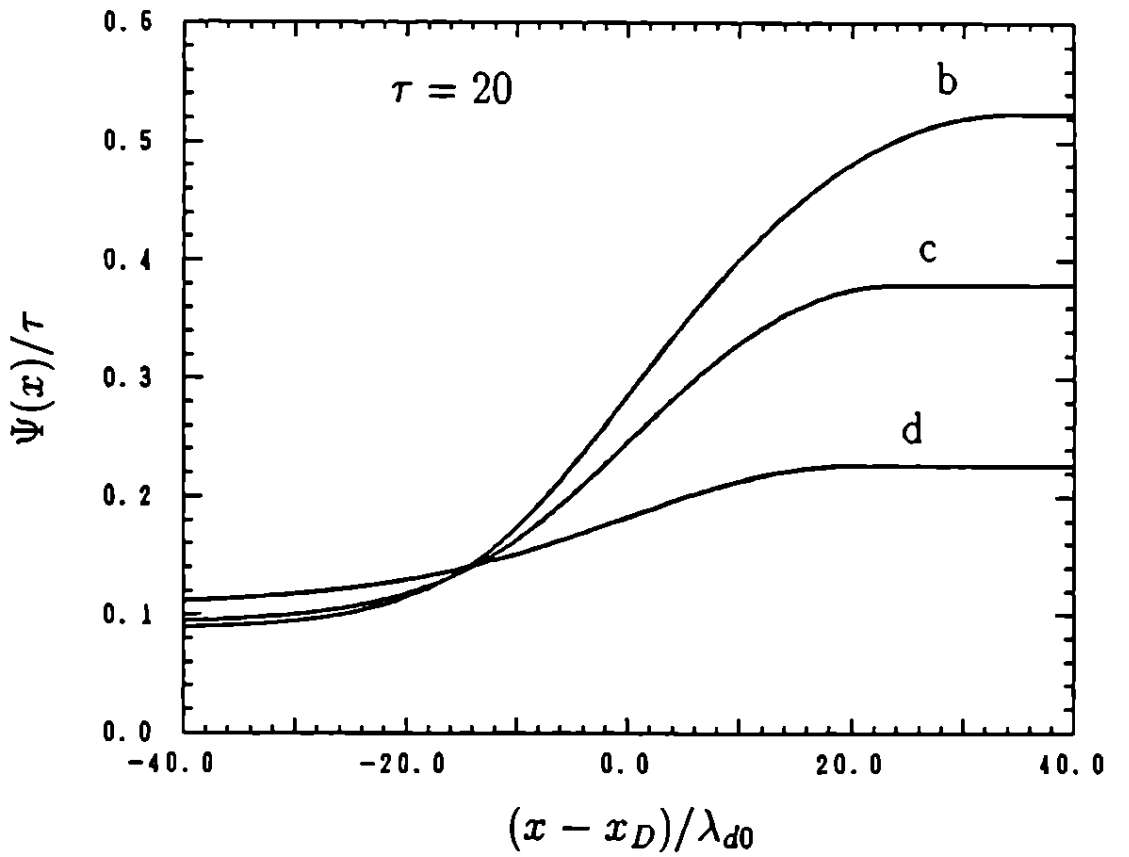

FIG. 5.8. The profile of the normalized potential at the double layer, where x_D is the position determined from $Zn_i = n_e$. The Debye length is defined using the particle density at $x = 0$ and the cold electron temperature T_c. Symbols *b*, *c*, and *d* represent results for the density ratios marked in Fig. 5.3(a).

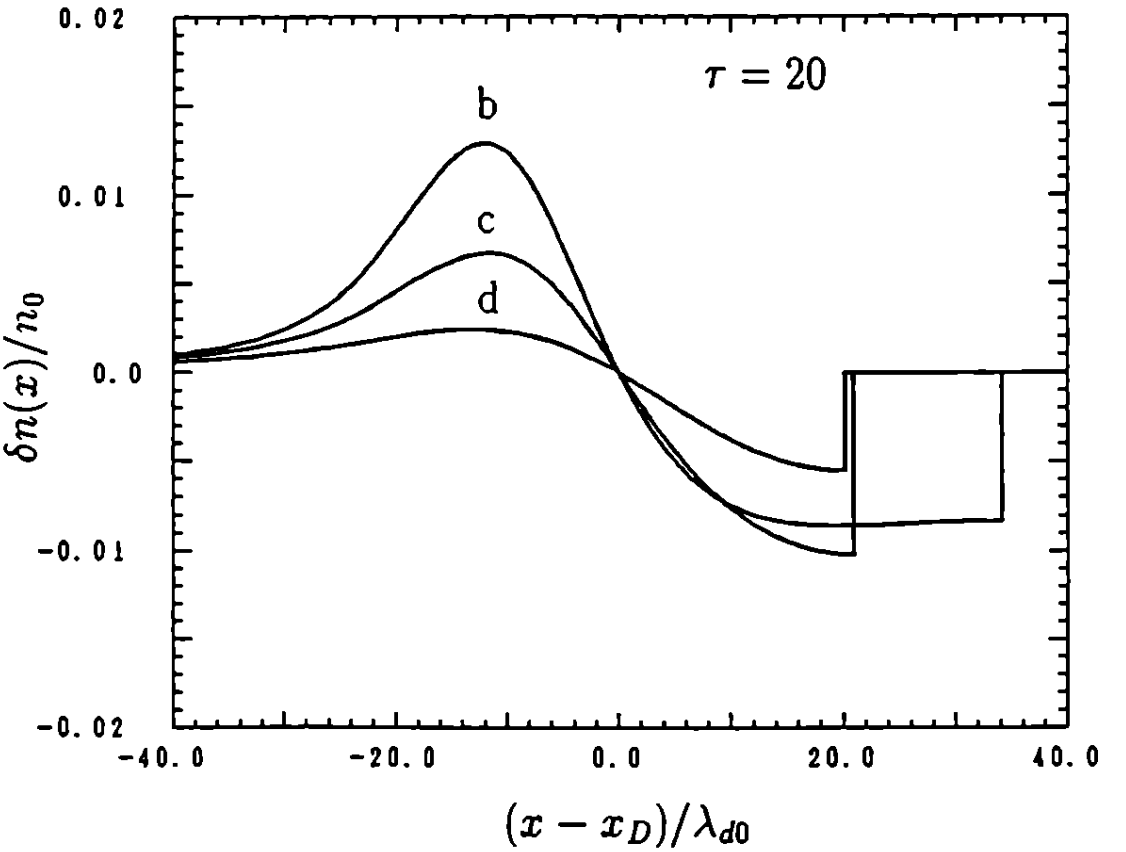

FIG. 5.9. The profile of the density difference $\delta n \equiv Zn_i - n_e$ at the double layer. A rapid change at $x \simeq x_D + 20\,\lambda_{D0}$ is due to the reflection of cold ions, which is produced in the second presheath, by the potential of the double layer.

ously been found by Perkins and Sun [19], but, the double layer described in the present chapter is different from theirs in the presence of particle flux ; a currentless solution in their analysis is found by symmetrizing the velocity distribution of the plasma, so that the solution involves no mass flow. Recently, Hairapetian and Stenzel [9] have observed a stationary, current-free, double layer in a two-electron-population plasma, which is formed due to self-consistent separation of two electron species. The double layer in their experiment is surrounded by the monotonically decreasing presheath potentials, and the potential drop at the double layer is of the order of the "effective" temperature of energetic electrons. This double layer is set up at a place far from the end plate because ionization and charge-exchange collisions are restricted to the vicinity of the gas valve located at the opposite side of the end plate. Although cold ions were not observed at downstream of the double layer, the formation mechanism and the characteristics described in their paper agree well with those presented in this chapter.

5.5 CONCLUSIONS

We theoretically have investigated the formation of an electrostatic potential due to ionization of neutral atoms in a two-electron-temperature plasma. The plasma equation is analytically solved to show the possibility of steady-state potential formation, and to evaluate the potential drop in such a plasma.

The potential drop in the plasma is continuously changing with increase of the hot- to

total electron density ratio if the hot- to cold electron temperature ratio T_h/T_c is small. It, however, is allowed to have either a small value characterized by the cold electrons or a large one by the hot electrons if $T_h/T_c > 10.8$, and discontinuously changes from the small value to the large one at a critical value for the hot- to total electron density ratio. It is found that a monotonically decreasing potential structure composed by the first presheath, a current-free double layer, the second presheath, and the sheath just in front of the wall can be steadily formed in a lower range of the density ratio around the critical value. The double layer is formed due to self-consistent separation of two electron species with different temperatures and generation of cold ions at the presheathes. The formation mechanism of the present current-free double layer seems to be the same as that of the double layer recently observed in the laboratory experiment [9]. The double layer marks the transition between the first and second presheathes with different potential levels. The position of the double layer is altered by changing the spatial profile of the particle source, and its amplitude depends on the relative density and temperature of two electron species.

REFERENCES

[1] Lipschultz, B. LaBombard, H. L. Manning, J. L. Terry, S. Knowlton, E. S. Marmar, M. Porkolab, J. Rice, Y. Takase, S. Texter, and A. Wan, Nucl. Fusion **26**, 1463 (1986).

[2] S. Takamura, A. Sato, Y. Shen, and T. Okuda, J. Nucl. Mater. **149**, 212 (1987).

[3] K. Kurihara, T. Saito, Y. Kiwamoto, and S. Miyoshi, J. Phys. Soc. Jpn. **58**, 3453 (1989).

[4] O. Fukumasa, J. Phys. D: Appl. Phys. **22**, 1668 (1989).

[5] E. K. Storm, H. G. Ahlstrom, M. J. Boyle, D. E. Campbell, L. W. Coleman, S. S. Glaros, H. N. Kornblum, R. A. Lerche, D. R. MacQuigg, D. W. Phillion, F. Rainer,D. W. Phillion, F. Rainer,R. Rienecker, V. C. Rupert, V. W. Slivinsky, D. R. Speck, C. D. Swift, and K. G. Tirsell, Phys. Rev. Lett. **40**, 1570 (1978).

[6] B. Bezzerides, D. W. Forslund, and E. L. Lindman, Phys. Fluids **21**, 2179 (1978).

[7] L. M. Wickens, J. E. Allen, and P. T. Rumsby, Phys. Rev. Lett. **41**, 243 (1978).

[8] G. Hairapetian and R. L. Stenzel, Phys. Rev. Lett. **61**, 1607 (1988).

[9] G. Hairapetian and R. L. Stenzel, Phys. Rev. Lett. **65**, 175 (1990).

[10] L. Tonks and I. Langmuir, Phys. Rev. **34**, 876 (1929).

[11] E. R. Harrison and W. B. Thompson, Proc. Phys. Soc. London **74**, 145 (1959).

[12] G. A. Emmert, R. Wieland, A. Mense, and J. Davidson, Phys. Fluids **23**, 803 (1980).

[13] K. Sato, F. Miyawaki, and W. Fukui, Phys. Fluids B **1**, 725 (1989).

[14] For a review of laboratory experiments see the following paper : N. Sato, in *Proceedings of the Symposium on Plasma Double Layers* (Roskilde, Denmark, 1982), p.116 ; N. Hershkowitz, Space Sci. Rev. **41**, 351 (1985).

[15] L. P. Block, Astrophys. Space Sci. **55**, 59 (1978).

[16] For a review see the following paper : M. A. Raadu and J. J. Rasmussen, Astrophys. Space Sci. **144**, 43 (1988) ; M. A. Raadu, Phys. Res. **178**, 25 (1989).

[17] C. E. Pearson, in *Handbook of Applied Mathematics* (Van Nostrand Reinhold, New York, 1983), p.603.

[18] K.-U. Riemann, Phys. Fluids B **1**, 961 (1989).

[19] F. W. Perkins and Y. C. Sun, Phys. Rev. Lett. **46**, 115 (1981).

CHAPTER 6

Heat Flow of a Two-Electron-Temperature Plasma through the Sheath in the Presence of Electron Emission

6.1 INTRODUCTION

Energetic electrons have been generated in a number of experimental devices during radio-frequency heating. In tokamak experiments using ion cyclotron frequency heating, lower-hybrid wave heating, or rf current drive, nonthermal energetic electrons appear in the scrape-off layer due to strong rf fields [1,2]. In the tandem mirror, during strong electron cyclotron resonance heating, the electron distribution composed of two Maxwellians at different temperatures is observed in the open-end region in front of the end plates [3].

The appearance of energetic electrons is expected to have dramatic effects on the formation of the plasma sheath. Production of energetic electrons makes the sheath voltage large [4], and hence ion sputtering is increased owing to the higher impact energy

resulting from the large potential drop at the sheath [5]. On the other hand, energetic electrons induce significant emission of secondary electrons, which can lead to marked reduction of the sheath potential and enhancement of the heat flow to walls [6,7,8]. Thus, effects of the secondary electron emission in a plasma with energetic electrons are of interest in the study of heat flow and impurity generation. It is well known that the electron emission coefficient is not able to exceed an upper limit smaller than 1.0 because an electron space charge layer formed just in front of the surface inhibits any further secondary emission [6]. The energetic electrons contribute to building up the electron space charge layer if many of them are reflected by the sheath potential. In such a case, one can expect further reduction of the limited secondary electron emission due to the existence of energetic electrons.

The purpose of this chapter is to demonstrate the effects of electrons emitted from the wall in two-electron-temperature plasma. The sheath equation and the description of heat flow in the presence of electron emission are derived in Sec. 6.2. The effects of the secondary electron emission are discussed in Sec. 6.3 by comparing solutions of the sheath equation obtained under conditions of space-charge limitation with the ones in the absence of electron emission.

6.2 SHEATH EQUATION AND HEAT FLOW

For the purpose of this chapter, it is adequate to adopt a model idealized by Hobbs

and Wesson [6]. A plasma filling the half-space $x > 0$ is in contact with an infinite plane wall located at $x = 0$ as shown in Fig. 6.1. When the plasma impacts upon the wall an electron-repelling plasma sheath must be formed in order that the loss rate of electrons and ions can be so balanced that the global loss of charge from the plasma is zero. The electrostatic sheath potential ϕ, which is defined to be zero at $x = \infty$, satisfies Poisson's equation

$$\frac{d^2\phi}{dx^2} = \frac{e}{\epsilon_0}(n_{e1} + n_{e2} - Zn_i) \ , \tag{6.1}$$

where n_{e1} is the density of primary electrons, n_i is the density of ions, and n_{e2} is the density of secondary electrons. For simplicity the ions are assumed to have a monoenergetic distribution function and to arrive at the sheath edge with an incident velocity $v(\infty)$ accelerated by a presheath potential. They are accelerated in the sheath and their density is determined by the continuity equation as

$$n_i = n_i(\infty)\left(1 - \frac{2Ze\phi}{Mv^2(\infty)}\right)^{-1/2} \tag{6.2}$$

Impact of electrons, ions, photon, metastable atom etc. cause the emissions of secondary electrons. Using the fact that the total current is zero, we have

$$Zn_i(\infty)v(\infty) = (1 - \gamma_e)n_{e1}v_{e1} - \gamma_i n_i(\infty)v(\infty) - J \ , \tag{6.3}$$

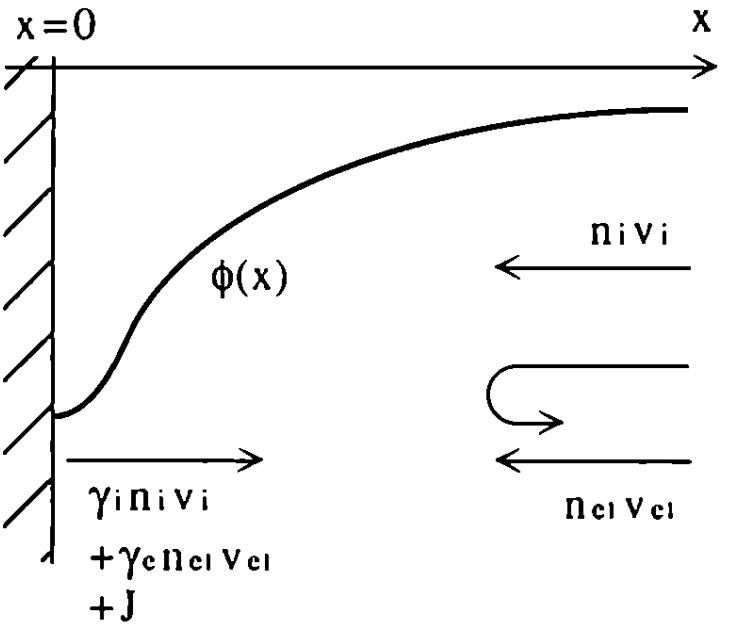

FIG. 6.1. A schematic diagram of geometry of the problem.

where γ_e and γ_i are, respectively, the emission coefficients for electrons and ions incident upon the wall, and J is the emission flux due to photons, metastable atoms, etc. It is convenient to generalize Eq. (6.3) in the form

$$Zn_i(\infty)v(\infty) = (1-\gamma)n_{e1}v_{e1} \tag{6.4}$$

by defining an effective coefficient of secondary emission

$$\gamma \equiv \frac{\gamma_e + \gamma_i/Z + J/[Zn_i(\infty)v(\infty)]}{1 + \gamma_i/Z + J/[Zn_i(\infty)v(\infty)]} \ . \tag{6.5}$$

The secondary electrons are emitted from the wall with negligible energies and then they move towards the plasma with a velocity corresponding to acceleration by a potential difference $\phi - \phi_0$, where $\phi_0 = \phi(0)$. From the continuity equation, we have

$$n_{e2}v_{e2} = \frac{\gamma}{1-\gamma} Zn_i(\infty)v(\infty) \ . \tag{6.6}$$

Thus, the particle density of secondary electron is

$$n_{e2} = Zn_i(\infty)\frac{\gamma}{1-\gamma}\left(\frac{mv^2(\infty)}{2e(\phi-\phi_0)}\right)^{1/2} \tag{6.7}$$

For primary electrons, the distribution function composed of two Maxwellians at different temperatures is adopted to give

$$n_{e1} = Zn_i(\infty)\left[1 - \frac{\gamma}{1-\gamma}\left(\frac{mv^2(\infty)}{-2e\phi_0}\right)^{1/2}\right]\left[\frac{n_{ec}(\infty)}{n_{ec}(\infty)+n_{eh}(\infty)}\exp\left(\frac{e\phi}{kT_c}\right)\right.$$

$$\left. + \frac{n_{eh}(\infty)}{n_{ec}(\infty)+n_{eh}(\infty)}\exp\left(\frac{e\phi}{kT_h}\right)\right] , \qquad (6.8)$$

where charge neutrality at $x \to \infty$, $Zn_i(\infty) = n_{e1}(\infty) + n_{e2}(\infty)$, has been assumed.

Substituting Eqs. (6.2), (6.7), and (6.8) into Eq. (6.1), we now write Poisson's equation as

$$\frac{d^2\phi}{dx^2} = \frac{Zn_i(\infty)e}{\epsilon_0}\left\{\left[1 - \frac{\gamma}{1-\gamma}\left(\frac{mv^2(\infty)}{-2e\phi_0}\right)^{1/2}\right]\left[\frac{n_{ec}(\infty)}{n_{ec}(\infty)+n_{eh}(\infty)}\exp\left(\frac{e\phi}{kT_c}\right)\right.\right.$$

$$\left. + \frac{n_{eh}(\infty)}{n_{ec}(\infty)+n_{eh}(\infty)}\exp\left(\frac{e\phi}{kT_h}\right)\right] + \frac{\gamma}{1-\gamma}\left(\frac{mv^2(\infty)}{2e(\phi-\phi_0)}\right)^{1/2}$$

$$\left. - \left(1 - \frac{2Ze\phi}{Mv^2(\infty)}\right)^{-1/2}\right\} . \qquad (6.9)$$

Multiplying by $d\phi/dx$ and integrating Poisson's equation from ∞ to x, we obtain

$$\frac{1}{2}\left(\frac{d\Psi}{d\xi}\right)^2 = \frac{2W}{Z}\left[\left(1 + \frac{Z\Psi}{W}\right)^{1/2} - 1\right] - \frac{2\gamma}{1-\gamma}\left(\frac{m}{M}\frac{W}{\Psi_0}\right)^{1/2}\Psi_0\left[1 - (1 - \frac{\Psi}{\Psi_0})^{1/2}\right]$$

$$- \left[1 - \frac{\gamma}{1-\gamma}\left(\frac{m}{M}\frac{W}{\Psi_0}\right)^{1/2}\right]\{(1-\alpha)[1-\exp(-\Psi)] + \alpha\tau[1-\exp(-\Psi/\tau)]\} ,$$

(6.10)

where

$$\xi = \frac{x}{\lambda_D}\ , \quad \alpha = \frac{n_{ch}(\infty)}{n_{cc}(\infty) + n_{ch}(\infty)}\ , \quad \tau = \frac{T_h}{T_c}\ , \quad \Psi(\xi) = -e\phi(x)/kT_c\ ,$$

$$W = Mv^2(\infty)/2kT_c\ ,$$

and the Debye length is defined by $\lambda_D^2 = \epsilon_0 kT_c/Zn_i(\infty)e^2$. There are unknown quantities, W and Ψ_0, and parameters, α and γ, in Eq. (6.10).

We shall now obtain equations which determine W and Ψ_0. From the fact that the total current is zero, we obtain the equation for determining the wall potential Ψ_0 as

$$\left[1 - \frac{\gamma}{1-\gamma}\left(\frac{m}{M}\frac{W}{\Psi_0}\right)^{1/2}\right]\left[(1-\alpha)\exp(-\Psi_0) + \alpha\sqrt{\tau}\exp(-\Psi_0/\tau)\right]$$

$$= \frac{2}{1-\gamma}\left(\frac{\pi m}{M}W\right)^{1/2} \tag{6.11}$$

The right-hand side of Eq. (6.10) must be positive for the formation of the sheath potential, $0 < \Psi < \Psi_0$, because the electric field $d\Psi/d\xi$ always has a real value. The initial incident energy of ions, W, is determined from this boundary condition at the sheath edge. It has been shown that the generalized Bohm criterion is fulfilled with the equality sign at the plasma-sheath boundary, $\Psi = 0$ [9]. This fact gives

$$W\left[(1-\alpha) + \frac{\alpha}{\tau}\right]$$

$$= \frac{1}{2} + \frac{\gamma}{1-\gamma}\left(\frac{m}{M}\right)^{1/2}\left(\frac{W}{\Psi_0}\right)^{3/2}\left\{\frac{1}{2} + \Psi_0\left[(1-\alpha) + \frac{\alpha}{\tau}\right]\right\}\ , \tag{6.12}$$

which is a modified form of the Bohm criterion [10].

Equations (6.11) and (6.12) can be used for estimating values of W and Ψ_0. Utilizing the smallness of $(m/M)^{1/2}$, we can obtain an approximate solution of Eq. (6.12) as

$$W \simeq \frac{1}{2}\left[(1-\alpha)+\frac{\alpha}{\tau}\right]^{-1} \quad , \tag{6.13}$$

which is independent of the emission coefficient. Since the incident energy W is corresponds to the potential drop in the presheath, Eq. (6.13) suggests the negligibly small influence of the secondary electron emission on the presheath potential. If $\tau \gg 1$ and $\alpha \leq (1-\gamma)^{-1}(2\pi m/\tau M)^{1/2}$, the wall potential is characterized by the cold ion temperature and the value of Ψ_0 can approximately evaluated by

$$\Psi_0 \simeq -\ln\left\{(1-\alpha)^{-1}\left[\frac{2}{1-\gamma}\left(\pi\frac{m}{M}W\right)^{1/2}-\alpha\sqrt{\tau}\right]\right\} \quad . \tag{6.14}$$

On the contrary, the wall potential is characterized by the hot electron temperature, if $\alpha > (1-\gamma)^{-1}(2\pi m/\tau\ M)^{1/2}$. In this range of the density ratio, the normalized wall potential Ψ_0 is roughly estimated by

$$\Psi_0 = -\tau\ln\left\{\frac{1}{\alpha}\frac{2}{1-\gamma}\left(\pi\frac{m}{M}\frac{W}{\tau}\right)^{1/2}\right\} \quad . \tag{6.15}$$

The emission of secondary electrons causes a remarkable reduction of the sheath potential when γ approaches 1.0, while the associated increase in the ion energy necessary to maintain stability of the sheath is negligibly small.

The electron emission is limited due to the space-charge effect in the sheath. One can see from Eq. (6.10) that the emission coefficient γ can not exceed an upper limit γ_c smaller than 1.0 because the right hand side of Eq. (6.10) must be positive all over the sheath. The equation to determine the value γ_c is obtained by equating the right hand side of Eq. (6.10) at the wall as

$$\frac{2W}{Z}\left[\left(1+\frac{Z\Psi_0}{W}\right)^{1/2}-1\right]-\frac{2\gamma}{1-\gamma}\left(\frac{m}{M}\frac{W}{\Psi_0}\right)^{1/2}\Psi_0$$
$$-\left[1-\frac{\gamma}{1-\gamma}\left(\frac{m}{M}\frac{W}{\Psi_0}\right)^{1/2}\right]\{(1-\alpha)[1-\exp(-\Psi_0)]+\alpha\tau[1-\exp(-\Psi_0/\tau)]\}$$
$$=0\ . \qquad (6.16)$$

For $\gamma > \gamma_c$ a very shallow potential well is formed just in front of the wall so as to reflect a fraction of the secondary electrons to the wall, satisfying $d\Psi/d\xi = 0$ at the bottom of the potential well. When the coefficient γ exceeds γ_c, an electron space charge layer formed in front of the wall inhibits any further secondary emission. As a result of the space-charge effect, the effective γ is maintained equal to γ_c. It should be noted that the space charge of hot electrons has the effect of suppressing the electron emission when Ψ_0 is of the order of τbecause hot electrons reflected by the sheath potential contribute to forming the negative space charge layer. The limiting values Ψ_{0c}, W_c, and γ_c are determined by solving Eqs. (6.11), (6.12), and (6.16) simultaneously.

We now evaluate the energy flux Q to the wall. Each primary electron striking the wall carries, on average, an energy of $2kT_c(1+\tau\Gamma_{eh}/\Gamma_{ec})/(1+\Gamma_{eh}/\Gamma_{ec})$, and the ratio of the particle flux of hot electrons to that of cold electrons is expressed by $\Gamma_{eh}/\Gamma_{ec} =$

$\alpha/(1-\alpha)\tau^{1/2}\exp[\Psi_0(1-1/\tau)]$. Each ion has the energy $kT_e(W+\Psi_0)$ at $x=0$. The secondary electrons make a negligible contribution to Q at $x=0$ because of their low initial energy. Thus, the energy flux Q is expressed by

$$Q = Zn_i(\infty)v(\infty)kT_e\left\{\frac{2}{1-\gamma}\frac{1-\alpha+\alpha\tau^{3/2}\exp[\Psi_0(1-1/\tau)]}{1-\alpha+\alpha\tau^{1/2}\exp[\Psi_0(1-1/\tau)]}+\frac{W}{Z}+\Psi_0\right\} . \tag{6.17}$$

The thermal insulation effect of the sheath can be evaluated by comparing the energy flux with the electron free-flow energy flux expressed by

$$Q_{ef} = Zn_i(\infty)\left(\frac{2kT_e}{\pi m}\right)^{1/2}kT_e\left[(1-\alpha)+\alpha\tau^{3/2}\right] . \tag{6.18}$$

The energy flux ratio, $F(\gamma)\equiv Q/Q_{ef}$, is given by

$$F(\gamma) = \left(\pi\frac{m}{M}W\right)^{1/2}\left[(1-\alpha)+\alpha\tau^{3/2}\right]^{-1} \times\left\{\frac{2}{1-\gamma}\frac{1-\alpha+\alpha\tau^{3/2}\exp[\Psi_0(1-1/\tau)]}{1-\alpha+\alpha\tau^{1/2}\exp[\Psi_0(1-1/\tau)]}+\frac{W}{Z}+\Psi_0\right\} . \tag{6.19}$$

The smallest value of F is obtained when $\gamma=0$, and the maximum value occurs when $\gamma=\gamma_c$.

6.3 CONSEQUENCES OF SECONDARY ELECTRON EMISSION

In order to show the effects of secondary electron emission on the sheath potential and heat flow, we now compare results obtained under the conditions of space-charge limitation with the ones in the absence of electron emission. The normalized potential drop in the sheath, Ψ_0, and the normalized incident energy of ions, W, for $\gamma = 0$ are determined by solving Eqs. (6.11) and (6.12) simultaneously. Figure 6.2 shows the sheath potential and the incident energy of ions as a function of the the fraction of hot electrons at the sheath edge, $\alpha \equiv n_{eh}(\infty)/[n_{ec}(\infty) + n_{eh}(\infty)]$, and Fig. 6.3 shows the energy flux ratio, taking the temperature ratio $\tau \equiv T_h/T_c$ as a parameter. The electron emission coefficient γ, the normalized sheath potential Ψ_{0c}, and the normalized incident energy W_c under the conditions of space-charge limitation are obtained from numerical solution of nonlinear simultaneous equations, Eqs. (6.11), (6.12), and (6.16). The limited electron emission coefficient, γ_c, is shown in Fig. 6.4, the sheath potential and the incident energy of ions are in Fig. 6.5, and the energy flux ratio is in Fig. 6.6.

Comparison of the results in Figs. 6.5 and 6.6 with those in Figs. 6.2 and 6.3. shows that the normalized sheath potential imposed by space-charge saturation is a small value of the order of 1.0 if the fraction of hot electrons is less than $(1-\gamma)^{-1}(2\pi m/\tau M)^{1/2}$. The electron emission leads to a considerable reduction of the sheath potential in this range, so that the energy flux is enhanced to a value near the electron free-flow energy flux. The energy flux ratio F_c has the maximum value at a particle density ratio around $(1-\gamma)^{-1}(2\pi m/\tau M)^{1/2}$. Comparison of the results also confirms the fact that secondary

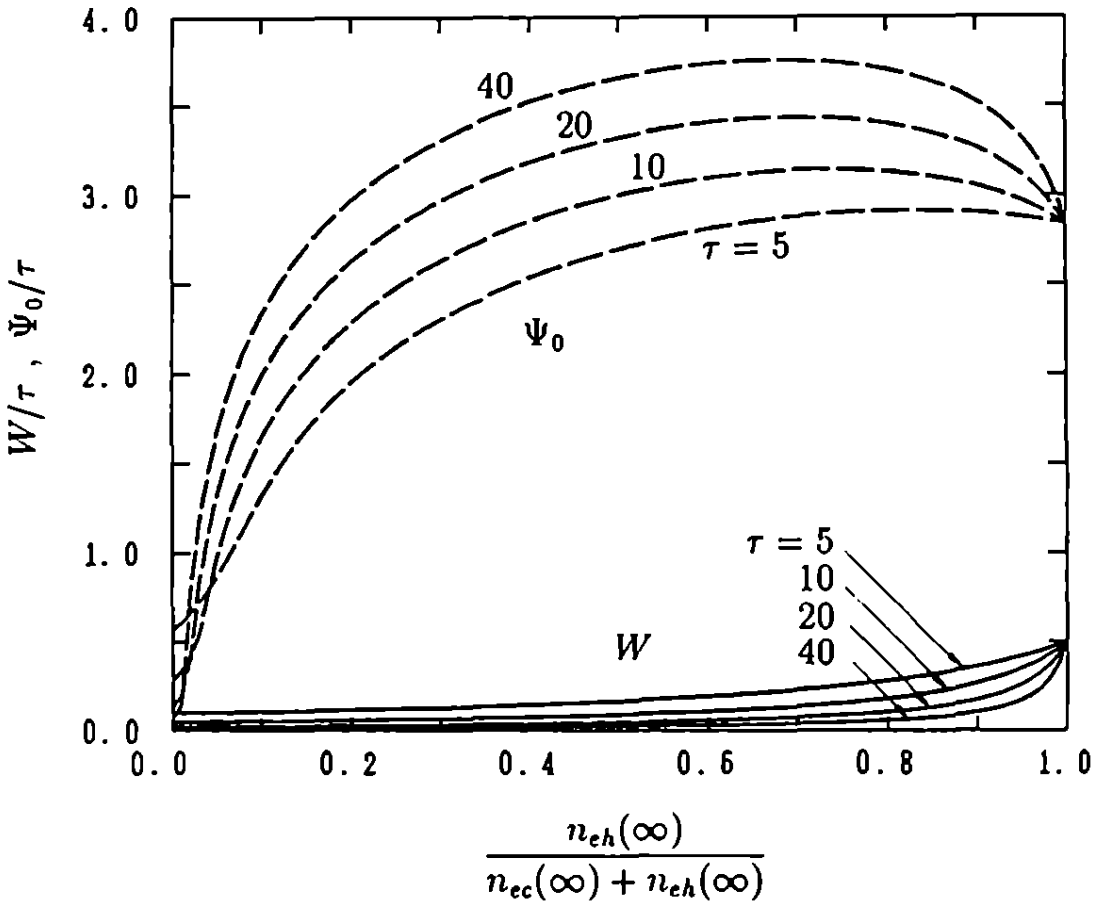

FIG. 6.2. Normalized sheath potential Ψ_0 (broken line) and initial kinetic energy of monoenergetic incident ions, W, (solid lines) in the absence of electron emission as a function of the density ratio $\alpha \equiv n_{eh}(\infty)/[n_{ec}(\infty)+n_{eh}(\infty)]$ for various values of the temperature ratio $\tau \equiv T_h/T_c$.

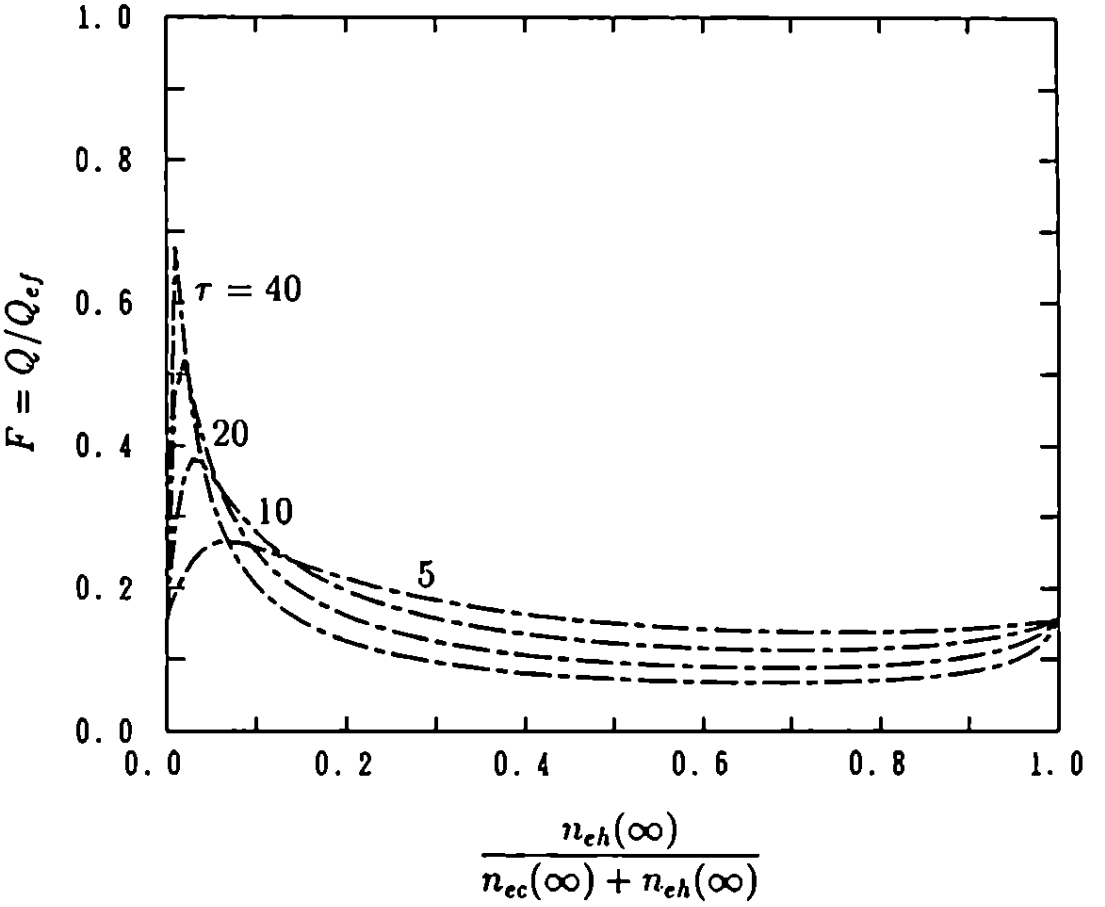

FIG. 6.3. Ratio of the energy flux to the electron free-flow energy flux, $F \equiv Q/Q_{ef}$, in the absence of electron emission as a function of the density ratio for various values of the temperature ratio τ.

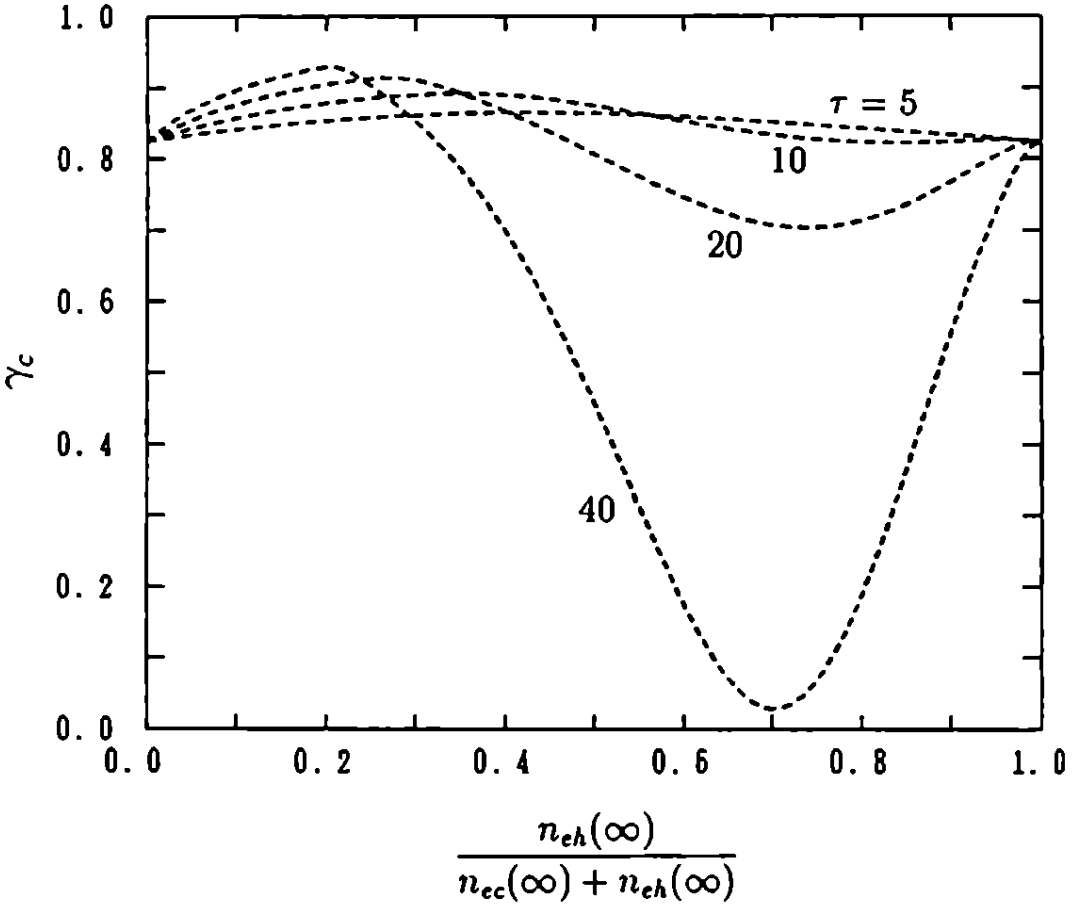

FIG. 6.4. Limiting values of the secondary electron emission coefficient γ_c as a function of the density ratio for various values of the temperature ratio τ.

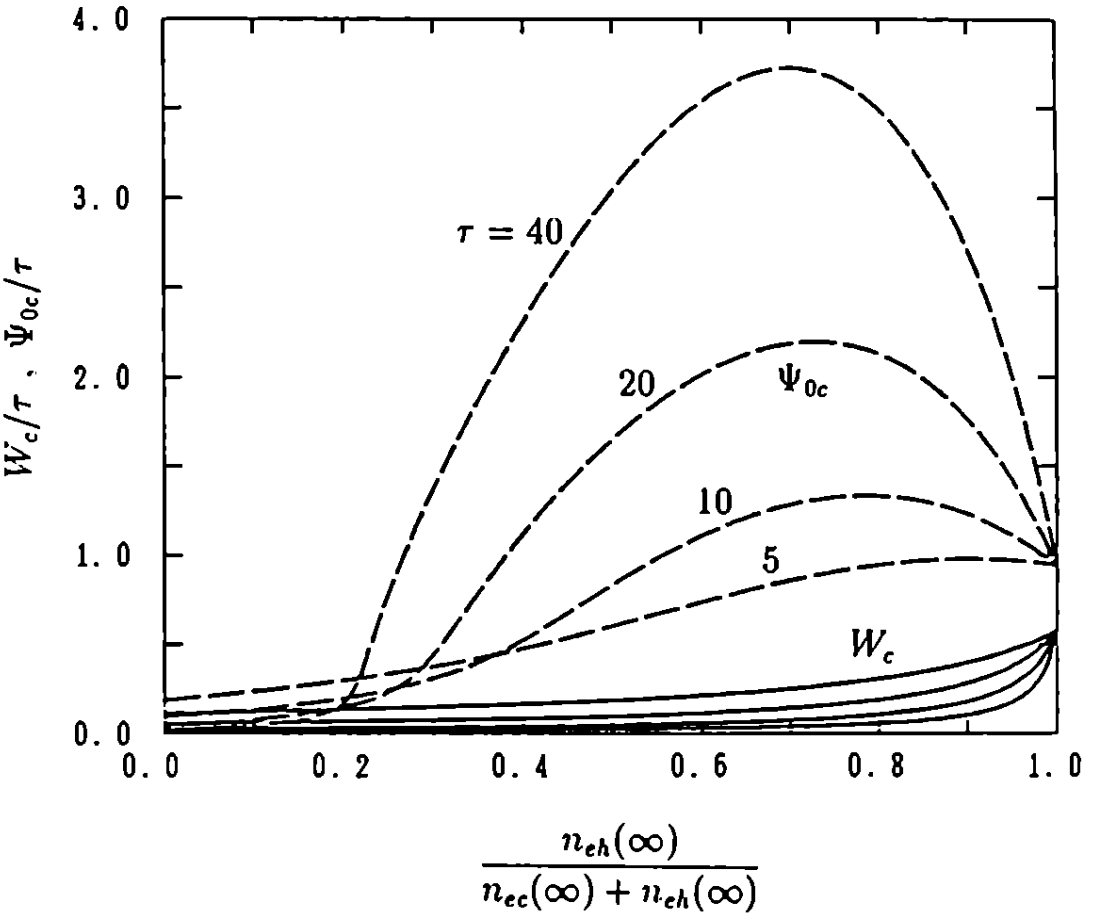

FIG. 6.5. Normalized sheath potential and initial incident energy of ions, Ψ_{0c} and W_c, under conditions of space-charge limitation as a function of the density ratio for various values of the temperature ratio.

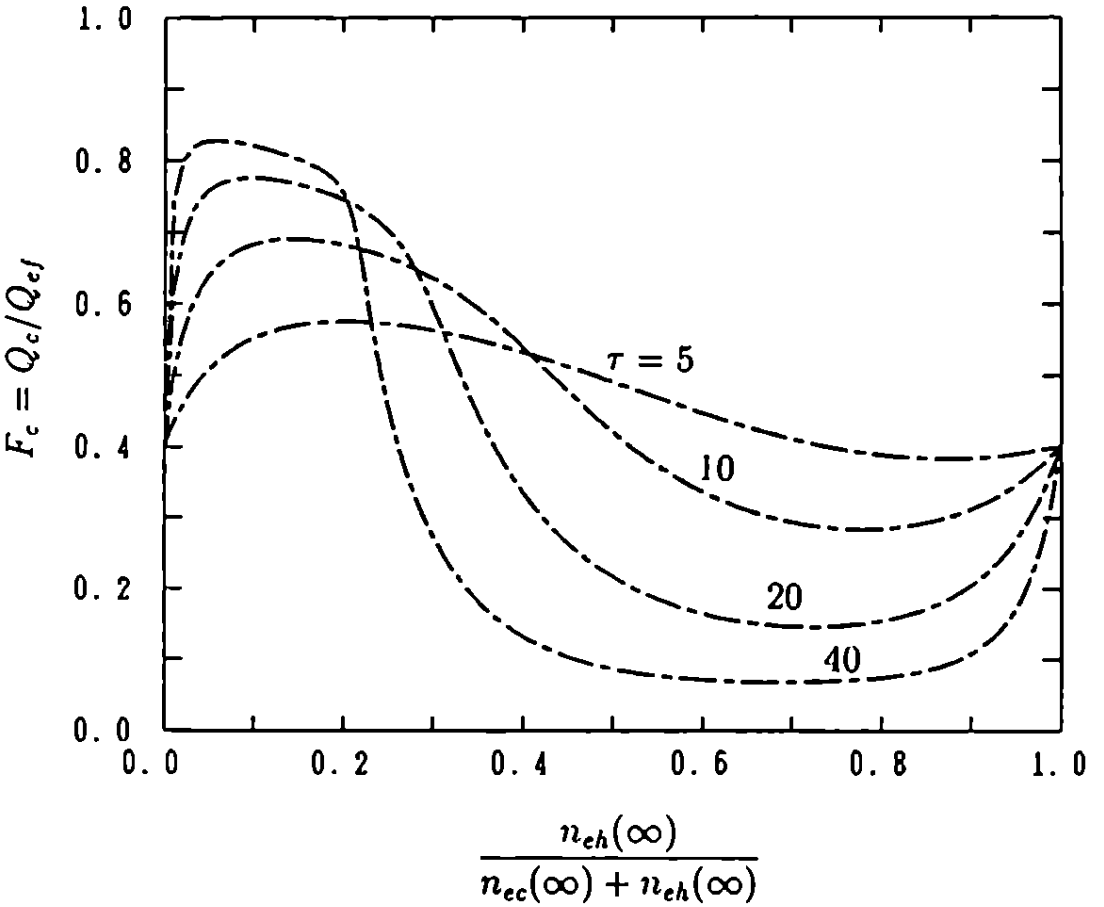

FIG. 6.6. Ratio of the energy flux to the electron free-flow energy flux, F_c, under conditions of space-charge limitation as a function of the density ratio.

electron emission has a negligibly small influence on the normalized incident energy of ions.

It should be noted that the electron emission is suppressed due to the space-charge effect of hot electrons in the range $\alpha > (1-\gamma)^{-1}(2\pi m/\tau M)^{1/2}$ if the temperature ratio is of the order of 10. The sheath potential of the order of τ is set up and the action of the sheath as a thermal insulator is improved as a result of the suppression of electron emission as shown in Figs. 6.5 and 6.6. The formation of the large sheath potential due to the existence of hot electrons has beneficial and detrimental effects with regard to plasma-wall interactions. In the presence of a large sheath potential, ion sputtering is increased owing to the higher ion impact energy resulting from the sheath potential drop, but the total energy flux is decreased owing to the thermal insulation effect of the sheath.

6.4 CONCLUSIONS

The effects of secondary electron emission on a plasma sheath and heat flow in a two-electron-temperature plasma are investigated theoretically. It was found that if the particle density of hot electrons at the sheath edge is much smaller than that of cold electrons, electron emission induces a remarkable reduction of the sheath potential. The sheath potential has a value of the order of the cold electron temperature under conditions of space charge limitation, so that the energy flux of the plasma is enhanced

up to a value near to the electron free-flow energy flux. Suppression of the secondary electron emission due to the space-charge effect of hot electrons can be expected if the hot- to cold-electron temperature is of the order of 10 and the hot electron density is comparable with the cold electron density. The sheath potential in such a plasma has a large value characterized by the hot electron temperature and the heat flow of the plasma is improved as a result of suppression of the secondary electron emission.

REFERENCES

[1] B. Lipschultz, B. LaBombard, H. L. Manning, J. L. Terry, S. Knowlton, E. S. Marmar, M. Porkolab, J. Rice, Y. Takase, S. Texter, and A. Wan , Nucl. Fusion **26**, 1463 (1986).

[2] S. Takamura, A. Sato, Y. Shen, and T. Okuda , J. Nucl. Mater. **149**, 212 (1987).

[3] K. Kurihara, T. Saito, Y. Kiwamoto, and S. Miyoshi , J. Phys. Soc. Jpn. **58**, 3453 (1989).

[4] K. Sato and F. Miyawaki , Phys. Fluids B **4**, 1247 (1992).

[5] G. M. McCracken and P. E. Scott , Nucl. Fusion **19**, 889 (1979).

[6] G. D. Hobbs and J. A. Wesson , Plasma Phys. **9**, 85 (1967).

[7] P. J. Harbour and M. F. A. Harrison , Nucl. Fusion **19**, 695 (1976).

[8] K.-U. Riemann , Phys. Fluids B **1**, 961 (1989).

[9] G. Fuchs and A. Nicolai , Nucl. Fusion **20**, 1247 (1980).

[10] D. Bohm , in *The Characteristics of Electrical Discharges in Magnetic Fields*, eds. A. Guthrie and R. K. Wakerling (McGraw-Hill, New York, 1949) p.77.

CHAPTER 7

Concluding Remarks

In the present thesis, the potential formation in quasistationary plasma flow to a wall has been analyzed by a kinetic treatment ; Spatial variation of the magnetic field, ionization of neutral atoms, energetic electron population, and/or the secondary electron emission are considered in analyses. Results obtained in the preceding chapters are summarized, and the subjects to be investigated in future are suggested in this chapter.

In chapter 2, the plasma-sheath equation has been formulated for a collisionless plasma originating in an expanding open magnetic field. This equation is approximately reduced Abel's integral equation in the plasma except for the sheath, and then it can be solved analytically. The wall potential, the ion distribution function, and the particle and energy fluxes are explicitly calculated. Results have shown that the magnetic profile remarkably affects the potential profile in the plasma. The generalized Bohm criterion for the sheath formation is always satisfied at the plasma-sheath boundary when the magnetic field monotonically decreases in the outside direction.

The plasma-sheath equation with small but finite values of the Debye length has also

been solved numerically for various profiles of the magnetic field. The sheath is formed near the wall with width about ten times as long as the Debye length. The analytic solution agrees well with the numerical one in the presheath when the Debye length is a small fraction ($\leq 10^{-3}$) of the plasma length.

In chapter 3, the presheath potential in an expanding magnetic field has been investigated by numerically solving the plasma equation for the collisionless plasma. Numerical calculations confirm availability of the analytic solution obtained in chapter 2 over a wide range of the magnetic field mirror ratio ($R_1 = 1 \sim 10$). Accuracy of the simulation result obtained by Hussein and Emmert is also checked. A particle source profile has a considerable effect on the potential drop in the presence of the nonuniform magnetic field. For a plasma source localized near the center of the plasma, the increase of the presheath potential drop $\Delta\phi$ due to the expanding magnetic field is roughly estimated by $\Delta\phi \geq kT_e(lnR_1)/e$, where T_e is the electron temperature. This suggests controllability of the presheath potential by applying the nonuniform magnetic field with a proper field strength profile. The plasma flow along the expanding magnetic field satisfies the generalized Bohm criterion with the inequality sign if the sheath edge does not exhibit the singularity.

In chapter 4, development of the potential due to spatial variation of the magnetic field in a collisionless plasma flowing out through the magnetic throat has been investigated. A particle source in a plasma is ignored in this analysis. The plasma flow must exceed the acoustic speed at the throat to avoid the discontinuity of the potential just beyond the magnetic throat. A monotonically falling potential to accelerate the escaping

ions build up in the inner region near the throat only if the generalized Bohm criterion is marginally satisfied at the throat.

Electrons trapped between the magnetic throat and the wall affect on the potential profile in the plasma remarkably. For very small trapped-electron densities, the presheath potential drop is localized near the throat, and it approaches asymptotically to a constant small value at a point apart from the throat. For large trapped-particle densities, the presheath potential drop continuously increases with decreasing the magnetic field strength. These results suggest the possibility of effective potential control in the open region by the combination of an expanding magnetic field and the ECRH heating.

In chapter 5, an electrostatic potential owing to ionization of neutral atoms in a two-electron-temperature plasma has been investigated. The plasma equation is analytically solved to show the possibility of steady-state potential formation, and to evaluate the potential drop in such a plasma. The potential drop in the presheath is allowed to have either a small value characterized by the cold electron temperature T_c or a large one characterized by the hot electron temperature T_h if $T_h/T_c > 10$: the potential drop discontinuously changes from the small value to the large one at a critical value for the hot- to total electron density ratio ($n_{h0}/n_0 \sim 0.2$). A monotonically decreasing potential structure with a current-free double layer is steadily formed in a plasma with such a high temperature ratio in a lower range of the density ratio around the critical value. The double layer marks the transition between the first and second presheathes with different potential levels. It is formed due to self-consistent separation of two electron species with different temperatures and due to generation of cold ions at the presheathes.

The formation mechanism of the present current-free double layer seems to be the same as that of the double layer recently observed in the laboratory experiment.

In chapter 6, influences of secondary electron emission on a plasma sheath and on heat flow of a two-electron-temperature plasma have been investigated theoretically. For particle density of hot electrons very smaller than that of cold electrons at the sheath edge, electron emission induces a remarkable reduction of the sheath potential to a value of the order of the cold electron temperature. The energy flux of the plasma is enhanced up to a value near to the electron free-flow energy flux. Suppression of the secondary electron emission due to the space-charge effect of hotter electrons can be expected if the hot- to cold-electron temperature is of the order of 10 and the hot electron density is comparable with the cold electron density at the sheath edge. The heat flow of the plasma is improved as a result of suppression of the secondary electron emission.

Finally, several interesting subjects to be extended in future from the present analyses are mentioned here. Concerning the potential formation in a spatially varying magnetic field, it is an open problem as to whether the static potential is formed or not in a plasma flowing along a convergent magnetic field. The calculation of a potential profile over the entire region including the inside of the magnetic throat is practically meaningful for the study of plasma transport and plasma-wall interactions, but, it has also been left unsolved. One must take the existence of trapped ions into consideration to treat these problems, which require kinetic treatment. Moreover, a precise calculation considering the power balance of a bounded plasma is necessary to make sure of the possibility of potential control by the combination of an expanding magnetic field and

the ECRH heating. To give problems related to this work, plasma-wall transition in an oblique magnetic field where the presheath mechanism is provided by the Lorenzt force is physically interesting. Unfortunately there are only few investigations on this problem, and these give no understandable picture. Characteristics of the magnetic presheath remains poorly understood. Potential control in a bounded plasma by plate biassing, by electron beam injection, or by rf heating is important from the engineering point of view ; Impurity influxes into a main plasma and ion sputtering at the wall will be controlled through the potential formed in a bounded plasma. The study of these subjects require development of a self-consistent fully kinetic model including particle collisions, charged/neutral interactions or particle injection from a wall.